AD-A137 019 A STUDY OF ANNULAR DIFFUSER FLOW USING A PHOTON-CORRELATING LASER DOPPLER..(U) AIR FORCE INST OF TECH WRIGHT-PATTERSON AFB OH SCHOOL OF ENGI.. 1/2

UNCLASSIFIED J M DIERKSEN DEC 83 AFIT/GAE/AA/83D-6 F/G 20/4 NL

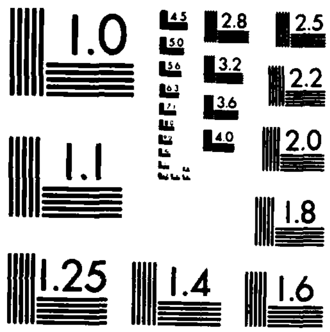

MICROCOPY RESOLUTION TEST CHART
NATIONAL BUREAU OF STANDARDS-1963-A

AF INSTITUTE OF TECHNOLOGY

A STUDY OF ANNULAR DIFFUSER FLOW USING A PHOTON-CORRELATING LASER DOPPLER ANEMOMETER

THESIS

Jeffrey M. Dierksen
Captain, USAF

AFIT/GAE/AA/83D-6

DEPARTMENT OF THE AIR FORCE
AIR UNIVERSITY
AIR FORCE INSTITUTE OF TECHNOLOGY

Wright-Patterson Air Force Base, Ohio

(1)

AFIT/GAE/AA/83D-6

A STUDY OF ANNULAR DIFFUSER FLOW
USING
A PHOTON-CORRELATING LASER DOPPLER ANEMOMETER

THESIS

Jeffrey M. Dierksen
Captain, USAF

AFIT/GAE/AA/83D-6

Approved for public release; distribution unlimited

AFIT/GAE/AA/83D-6

A STUDY OF ANNULAR DIFFUSER FLOW

USING

A PHOTON-CORRELATING LASER DOPPLER ANEMOMETER

THESIS

Presented to the Faculty of the School of Engineering
of the Air Force Institute of Technology
Air University
In Partial Fulfillment of the
Requirements for the Degree of
Master of Science in Aeronautical Engineering

Jeffrey M. Dierksen, B.S.
Captain, USAF

December 1983

Approved for public release; distribution unlimited

Acknowledgements

My study of annular diffuser flow has been a challenging one. Over the past year, a number of people have made important contributions to my project for which they will always have my deepest appreciation. Dr. William C. Elrod, my thesis advisor, was an immense help in this study and the most important contributor to my educational endeavors at AFIT. I also wish to thank the other members of my thesis committee, Major Michael Wallace and Captain Wesley Cox, for their assistance. The people at the AFIT Fabrication Shop were indispensible. The hardware they made for me worked beautifully and was an invaluable aid in my research. I especially wish to thank Carl Shortt, Dave Paine, Ron Ruley, John Brohas, and Jack Tiffany. I also extend my thanks to the AFIT Aero Lab technicians: Nick Yardich, Leroy Cannon, Steve Coates, and Harley Linville. Always willing to help, their assistance made the project run smoothly. I thank Mr. Joe Ferguson of the Air Force Aero Propulsion Laboratory, who helped me obtain the cable to connect the laser anemometer and mini-computer. While it may seem like a small contribution, its benefits were enormous.

There were a number of ups and downs during the course of my studies at AFIT. My wife, Kate, deserves all my love for her understanding and help through the rough times. I couldn't have made it without her.

Jeffrey M. Dierksen

Table of Contents

List of Figures

Figure | Page

Figure		Page

List of Symbols

A	area	(m^2)
ADRF	Annular Diffuser Research Facility	
AFIT	Air Foce Institute of Technology	
D	laser beam separation	(mm)
d	pipe diameter	(cm)
d_a	aperture diameter	(μm)
d_f	fringe spacing	(μm)
d_m	measuring volume diameter	(μm)
d_m'	effective measuring volume height	(μm)
d_m''	effective measuring volume width	(μm)
F	scattered light frequency	(Hz)
ΔF	phase modulator frequency shift	(Hz)
f	focusing lens focal length	(mm)
f'	collecting lens focal length	(mm)
$G^{(2)}(\tau)$	intensity autocorrelation function	
g_1	value of the correlation function at the first valley	
g_2	value of the correlation function at the second peak	
g_3	value of the correlation function at the second valley	
HP	Hewlett-Packard	
$I(t)$	intensity function	
IGV	inlet guide vane	
$\overline{K}_0$	vector sum of two incident light vectors	
$\overline{k}_0$, $\overline{k}_{01}$, $\overline{k}_{02}$	incident light vector	
$\overline{k}_s$	scattered light vector	
L	pipe length	(m)
LDA	Laser Doppler Anemometer	
LDV	Laser Doppler Velocimeter	
l_i	inlet length	(m)
l_m	measuring volume length	(μm)

l_m'	effective measuring volume length	(μm)
$\dot{m}$	mass flow rate	(Kg/sec)
N	number of fringes in the measuring volume	
n	number of velocity samples	
Pk2	channel number of the peak after the first valley of the correlation function	
p	lens reference plane-to-image distance	(mm)
PM	photomultiplier	
Δp	static pressure change	(N/m^2)
q	lens reference plane-to-source distance	(mm)
$\bar{q}$	average dynamic pressure	(N/m^2)
R	correlation function damping ratio	
Re	Reynolds number	
RMS	root-mean-square	
r_h	hydraulic radius	(m)
r_o	unfocused laser beam radius	(mm)
T	experiment or correlation time	(sec)
t	time	(sec)
t_s	correlator sample time	(nsec)
U_∞	free-stream velocity	(m/sec)
u	average velocity component perpendicular to the measuring volume fringes	(m/sec)
u_i	instantaneous velocity component perpendicular to the measuring volume fringes	(m/sec)
u^*	average velocity relative to the measuring volume fringes	(m/sec)
u_i^*	instantaneous velocity relative to the measuring volume fringes	(m/sec)
V	velocity	(m/sec)
$\bar{V}$	velocity vector	
x	linear distance	(m)
α	angle between the optical and collecting axes	(deg)

β	angle between the parallel laser beam plane and the collecting axis	(deg)
δ	boundary layer thickness	(mm)
η	turbulence intensity	
η^*	turbulence intensity relative to the measuring volume fringes	
θ	included angle between the incident laser beams or light vectors	(deg)
λ	laser light wavelength	(Angstroms)
μ	absolute viscosity	($N\text{-}sec/m^2$)
μ_0	refractive index	
ν	kinematic viscosity	(m^2/sec)
$\Delta\nu$	Doppler frequency shift	(Hz)
ρ	density	(Kg/m^3)
τ	correlator delay time	(nsec)

Abstract

An experimental investigation of air flow in an annular inlet and diffuser was conducted using a photon-correlating Laser Doppler Anemometer. The inlet has an inside wall radius of 22.9 Centimeters (9.0 in.) and a cross-sectional area of 0.0426 sq meters (0.4583 sq ft). The diffuser walls have a divergence half-angle of seven degrees. Flow rates in the vicinity of 0.25 kg/sec (0.55 lbm/sec) were studied. The Reynolds number in the annular inlet was 18300. The flow in the annulus was turbulent and the boundary layer growth was approximately 20% less than that predicted using flat plate boundary layer assumptions. The laser anemometer measurements are compared to hot film anemometer measurements. Good comparison was obtained except in the annular inlet. The difference is probably due to the differing boundary layer growth rates between the laser and hot film anemometer tests since they were conducted with different mass flow rates. The photon-correlating Laser Doppler Anemometer is evaluated in this application. The flexibility of a laser anemometer system in measuring three-dimensional, internal flows is determined by two factors: the system's frequency shifting capability and the geometry of its optics. Reflected background light is inherent in measuring internal flows. Without a means of reducing the signal caused by this light, long measurement times are necessary for each data point.

A STUDY OF ANNULAR DIFFUSER FLOW

USING

A PHOTON-CORRELATING LASER DOPPLER ANEMOMETER

I. Introduction

Turbine engine designers are constantly striving to achieve more efficient engines. To realize higher performance, improvements must be made in the engine components themselves. One of these components is the pre-diffuser between the compressor and combustor. It accomplishes the important task of diffusing high velocity discharge air from the compressor to low velocities suitable for the combustor. Additionally, the diffusion must occur in as short a length as possible.

A great deal of information is available on the performance of two-dimensional diffusers. While this has some application to three-dimensional geometries, little experimental data on annular diffusers can be found. This research project is intended to increase the base of experimental knowledge of annular diffusers, particularly with regard to velocity profiles and turbulence intensity.

Background

The initial studies in this project were done by Kelley (reference 1) in 1981. An annular flow handling apparatus was designed and pitot and hot wire anemometer probes used to investigate the diffuser flow. The initial data revealed irregular flow in the test sections. The research was continued in 1982 by Moore (reference 2), who modified the flow handling apparatus and incorporated a Laser Doppler Velocimeter (LDV) as the primary instrumentation system. The modified flow handling apparatus became part of the Annular Diffuser Research Facility (ADRF). Preliminary data was collected; however, it only consisted of velocity measurements because of the limited data acquisition capability of the LDV system. Turbulence intensity data could not be obtained.

Objectives

The following are the objectives of the third phase of this study:

(1) Obtain velocity and turbulence intensity profiles in the annular inlet and diffuser of the ADRF flow handling apparatus using a photon-correlating Laser Doppler Anemometer.

(2) Evaluate the capabilities of the photon-correlating Laser Doppler Anemometer to measure internal fluid flows in similar applications.

Overview

The remainder of the report discusses this phase of the research effort. The topics include:

(1) Internal fluid dynamics, boundary layer theory and the principles of the photon-correlating Laser Doppler Anemometer.

(2) A description of the experimental apparatus and instrumentation.

(3) The procedures used to collect the data and reduce it.

(4) The results of the study.

(5) The conclusions drawn and recommendations for further research.

II. Theory

Boundary layer theory and internal fluid dynamics relevant to the annular diffuser will be discussed. Since the Laser Doppler Anemometer (LDA) was a significant element in this research effort, a discussion of its principles of operation is also included.

Internal Fluid Dynamics and Boundary Layer Growth

The flow in a pipe may be laminar or turbulent depending on the Reynolds number and wall roughness. The Reynolds number for a pipe is defined by Eq (1)

$$Re_{pipe} = \frac{4 r_h \rho V}{\mu} \tag{1}$$

where μ is the absolute viscosity of the fluid, ρ is the fluid density, V is the velocity and r_h is the hydraulic radius (3:63). The hydraulic radius is defined by Eq (2)

$$r_h = \frac{A_c L}{A_w} \tag{2}$$

where A_c is the cross-sectional area of the pipe, L is the pipe length, and A_w is the total wetted area (3:64). The critical Reynolds number for the transition from laminar to turbulent flow for a pipe with a sharp-edged entrance is approximately 2300; however, the critical Reynolds number may exceed 10,000 for a system which is exceptionally free from disturbances (4:39). It is also a fact that at Reynolds numbers below 2000, flow in a pipe will remain laminar even in the presence of strong disturbances (4:451).

Boundary layer growth in a pipe begins at the entrance. This is also true of an annulus. While this boundary layer may be laminar even though the flow outside of it is turbulent, roughness on the walls and turbulence in the flow outside of the boundary layer would hasten the transition from laminar to turbulent. To approximate the growth of a boundary layer on the wall of an annulus, one may use the results of boundary layer growth on a flat plate in a uniform flow. The thickness of a laminar boundary layer on a flat plate is given by Eq (3)

$$\delta = 5 \left(\frac{\nu x}{U_\infty}\right)^{0.5} \tag{3}$$

where x is the distance from the leading edge of the plate, U_∞ is the free stream velocity and ν is the kinematic viscosity (4:140). On the other hand, the thickness of a turbulent boundary layer on a flat plate is determined by Eq (4) (4:638).

$$\delta = 0.37x \left(\frac{U_\infty x}{\nu}\right)^{-0.2} \tag{4}$$

While the flat plate approximation is very useful for estimating the boundary layer growth in an annulus, the three-dimensional nature of the flow channel will also affect boundary layer growth. The boundary layer on the inner wall will be thinner than on the outer wall because the shear work from the inner wall to the flow is diffused over an increasing area as the distance from the wall increases. On the outer wall, the shear work is diffused over a decreasing area (2:5). The smaller the ratio of inner wall to outer wall radius, the smaller the ratio of inner wall boundary layer thickness to outer wall thickness.

As the boundary layer in a pipe, or annulus, grows, it will eventually cover the entire flow channel. Even after this occurs, the velocity profile will continue to develop until it reaches a point downstream where there is no further change. The flow is then called "fully-developed" and the distance from the entrance of the pipe to this point is the inlet length. Experiments have been conducted to determine the inlet length of a circular pipe. For laminar flow, the inlet length is approximately

$$l_i = (0.03d)\, Re_{pipe} \tag{5}$$

where d is the pipe diameter (4:596). For Reynolds numbers from 1500 to 2000, it ranges from 45 to 60 pipe diameters. The inlet length for turbulent flows is typically shorter than for laminar flows. Kirsten measured its length to be about 50 to 100 diameters while Nikuradse measured an inlet length of 25 to 40 diameters (4:596).

Laser Velocimetry

Over the last two decades, several types of laser velocimeters and various methods of signal processing have been developed. One combination, and the system used for this research, is a Laser Doppler Anemometer (LDA) using a photon-correlating signal processor. It is this particular system which will be discussed here.

The Laser Doppler Anemometer (LDA) is based on the principle of the Doppler shift of light scattered by a moving particle. If the velocity of a moving particle is represented by $\bar{V}$, the incident light beam by $\bar{k}_o$, and the scattered light beam by $\bar{k}_s$ where $|\bar{k}_s| = |\bar{k}_o| = 2\pi/\lambda$($\lambda$ is the wavelength of the incident light), then the Doppler shift of the scattered light is given by Eq (6) (5:249).

$$\Delta\nu = (\bar{k}_s - \bar{k}_o) \cdot \bar{V} \tag{6}$$

Thus, measuring the frequency of the scattered light indirectly determines the velocity of the particle which caused the scattering. However, it is impractical, in most situations, to measure the Doppler shifts inherent in low speed flows. This problem can be avoided by using two incident light beams, $\bar{k}_{01}$ and $\bar{k}_{02}$, of the same wavelength (5:250). Now, the Doppler shifts of light, from each beam, scattered by the moving particle are

$$\Delta\nu_1 = (\bar{k}_s - \bar{k}_{01}) \cdot \bar{V} \tag{7}$$

$$\text{and} \quad \Delta\nu_2 = (\bar{k}_s - \bar{k}_{02}) \cdot \bar{V} \tag{8}$$

When the scattered light is detected, the Doppler shift will be

$$\Delta\nu_1 - \Delta\nu_2 = (\bar{k}_{02} - \bar{k}_{01}) \cdot \bar{V} = \bar{K}_o \cdot \bar{V} \tag{9}$$

where the geometry is shown in Figure 1 (5:249). This is known as the Doppler Difference Effect. Eq (9) can be written

$$\Delta\nu_1 - \Delta\nu_2 = \frac{4\pi u}{\lambda} \sin\left(\frac{\theta}{2}\right) \tag{10}$$

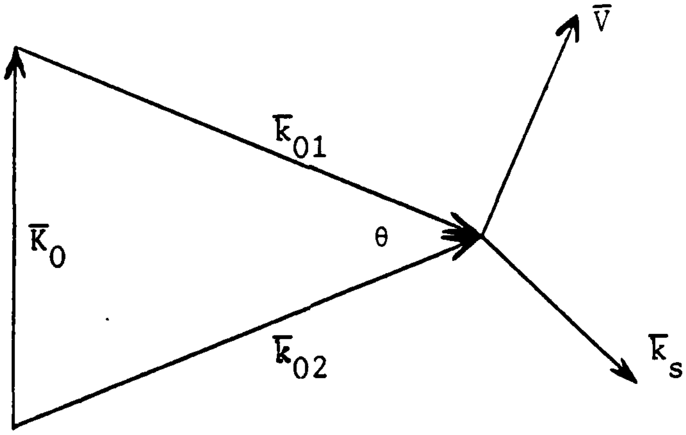

FIG. 1. DOPPLER DIFFERENCE EFFECT

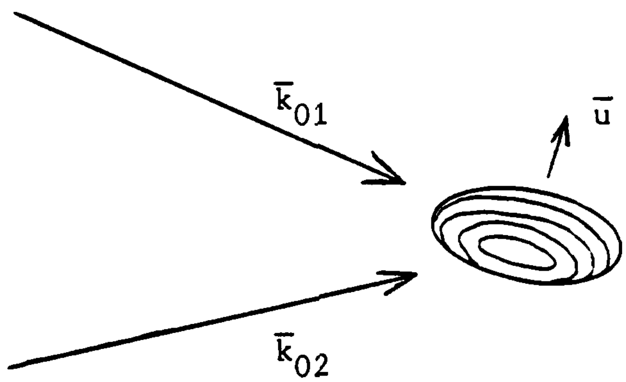

FIG. 2. MEASURING VOLUME FRINGES

where u is the component of $\overline{V}$ in the direction of $\overline{K}_o$. A significant aspect of Eq (10) and the Doppler Difference Effect is that the Doppler-shifted frequency is independent of the scattering direction. So regardless of where the scattered light is detected, the result is the same.

While the theory of the Doppler Difference Effect from the classical physics standpoint is important in understanding the LDA, the theory can also be explained using a model commonly referred to as the "fringe model". Even though it is not technically appropriate in all respects, it does yield identical velocity and turbulence intensity results.

In the Doppler difference laser anemometer, the incident laser beams cross at some point in space. The intersection of the two, finite-size beams forms an ellipsoidal volume termed the <u>measuring volume</u>, the region in which the fluid flow is measured. With the fringe model, the intersection of the monochromatic, coherent laser beams forms a classical interference pattern of bright and dark, planar fringes in the measuring volume. These fringe planes are perpendicular to the plane formed by the two incident beams as depicted in Figure 2. The distance between like fringes can be calculated using Eq (11) (6:6-1).

$$d_f = \frac{\lambda}{2 \sin\left(\frac{\theta}{2}\right)} \tag{11}$$

As a particle, moving with the fluid, passes through the measuring volume, it scatters a "burst" of light every time it moves through a bright fringe so the frequency of the light bursts is related to the particle's velocity by Eq (12).

$$F = \frac{u}{d_f} \tag{12}$$

The frequency of light bursts from the interference pattern is identical to the Doppler-shifted frequency ($\Delta\nu_1 - \Delta\nu_2$) of photons scattered by the particle as it moves through the "classical" measuring volume (7:97). Hence, each light "burst" scattered by a particle in the fringe model is similar to a photon scattered in the classical sense. The fringe model is also useful in understanding the principles of the remaining LDA components.

Photon correlation was used in this study to analyze the scattered light from the measuring volume. The particles, moving with the fluid, will have an ordered motion which causes the scattered light to have an order about it. The scattered light intensity varies with time as the particles move through the fringes. By determining the time correlation of the intensity, the velocity and turbulence of the flow can be calculated.

The time correlation of the light is represented by the intensity autocorrelation function defined by Eq (13)

$$G^{(2)}(\tau) = \lim_{T\to\infty} \frac{1}{T}\int_0^T I(t)I(t+\tau)\,dt \tag{13}$$

where I is the light intensity, t is time, T is the time interval over which the intensity is monitored (experiment time), and τ is the correlator delay time (8:16). The autocorrelation function is determined as a function of τ after the intensity is determined in the time domain. Light intensities of a random nature will result in a constant autocorrelation function as T approaches infinity. However, intensities of an ordered, periodic nature will result in a periodic autocorrelation function due to the multiplication of the intensity function and time-delayed intensity function. As a result, this method of signal processing can separate the signal of interest from large amounts of background noise. Additionally, the nature of the method makes photon correlation sensitive at low scattering particle densities (9:439).

III. Apparatus and Instrumentation

This research included the integration of a photon-correlating LDA system to the Annular Diffuser Research Facility (ADRF) flow handling apparatus designed and fabricated by Kelley (reference 1) and Moore (reference 2). A Hewlett-Packard data acquisition system was used to control the LDA system and process the data. A hot-film anemometer was also used with the ADRF flow handling apparatus. The following is a discussion of this equipment.

ADRF Flow Handling Apparatus

The ADRF Flow Handling Apparatus (Figure 3) consists of a stilling chamber, a particle seeder, an annular interface, an inlet guide vane section, an annular inlet test section, an annular diffuser test section, and a dump section. Air is supplied to the stilling chamber by two Worthington Corporation compressors through a 7.6 centimeter (3 in) diameter pipe. These compressors are capable of steadily supplying 0.36 kg/sec (0.80 lbm/sec) of air to the flow handling apparatus. As the air enters the stilling chamber, it passes through two paper filters held in place by an aluminum holder. This filter is a recent addition to the flow handling apparatus due to the contamination of the air supply by particulate matter. The contaminate mostly consists of rust particles from the inner surfaces of the pipes. The filter allows better control over the size and types of particles in the air

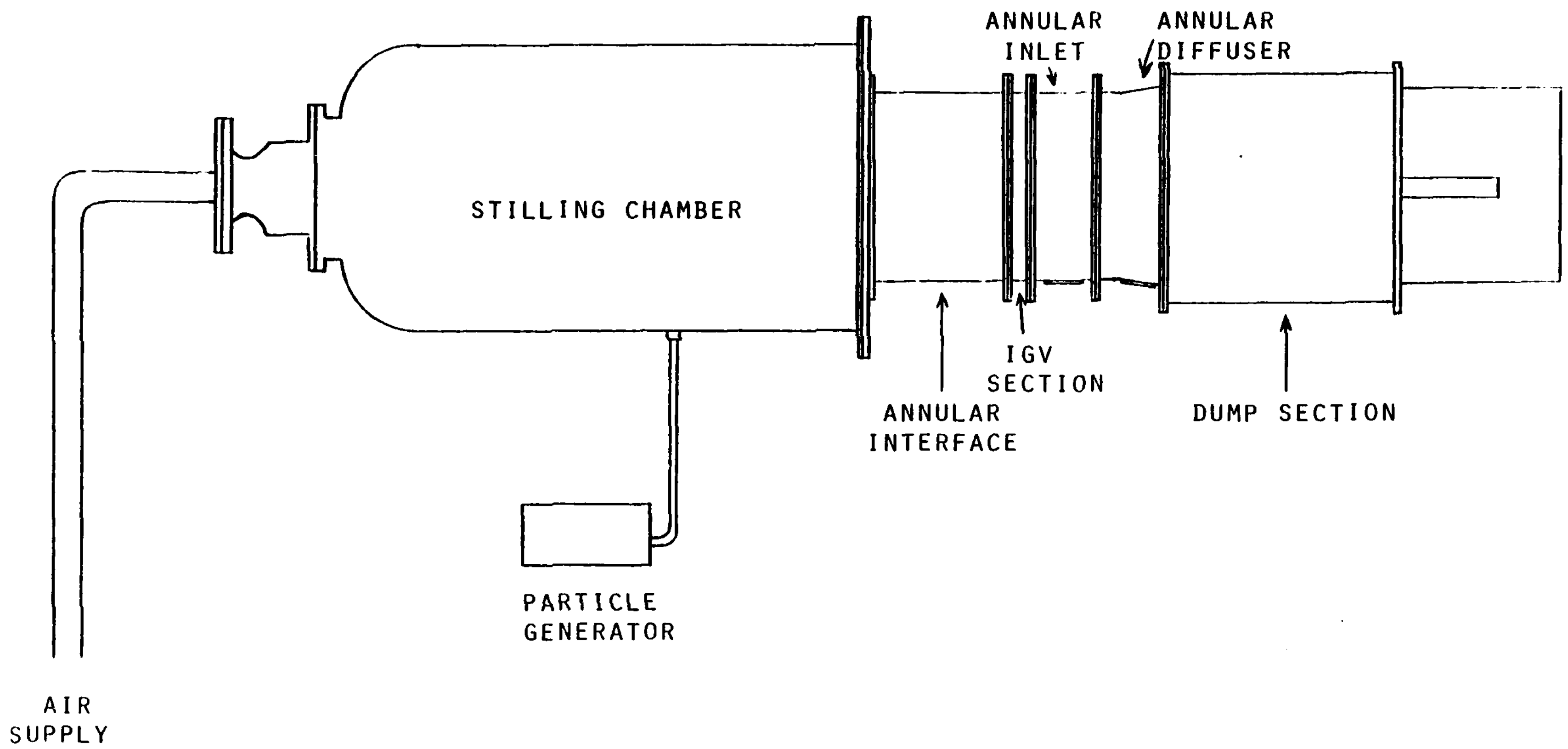

FIG. 3. ADRF FLOW HANDLING APPARATUS

flow since this is the basis for LDA measurements. The filter also prevents abrasion of the test section windows by the contaminates suspended in the flow.

The filtered air next enters a perforated cylinder which allows the air to exit radially through eighty-one, three millimeter (0.125 in) diameter holes while also reducing the pressure. The air is turned back to the axial direction and passed through four smoothing screens. After the screens, seed particles are introduced into the flow through two, six millimeter (0.25 in) diameter tubes supplied by a 9.5 millimeter (0.375 in) diameter tube which protrudes through the stilling chamber wall. A particle generator is connected to the supply tube which is contained inside a streamlined shroud to minimize flow disturbances. The particles are injected in the direction of the flow.

A TSI Model 9306 Six Jet Atomizer was used to provide a glycerin (propylene glycol) aerosol for flow seeding. The volume output of the atomizer can be varied by using from one to six of the available jets and by adjusting the input pressure of the unit. The particle concentration of the glycerin aerosol is constant at $2(10^8)$ particles per liter. The sizes of the particles vary from 0.5 to 4.0 μm (.00002 to .00016 in).

The seeded air is accelerated in an annular nozzle contained within the stilling chamber. The nozzle leads to a constant area annular interface (see Figure 3). The inner and outer radii of the annulus are nominally 22.9 centimeters (9.0 in) and 25.4 centimeters (10.0 in) respectively. At the end of the annular interface is a row of sixty-six equally spaced inlet guide vanes (IGV) mounted radially between the inner and outer walls of the annulus. The IGVs are NACA 0012 airfoils with a chord of 19.1 millimeters (0.75 in) giving them an aspect ratio of 1.33.

The annular inlet test section which follows the inlet guide vanes allows flow studies in a constant area annulus (see Figure 4). Optical access for flow measurements is gained through a glass window. It measures 102 millimeters (4.0 in) in the axial direction and 19.1 millimeters (0.75 in) in the circumferential direction. The inner wall of the annulus is a wooden centerbody which is painted flat black. On the portion of the centerbody opposite the outer access window, another optical glass window is installed. It measures 8.0 millimeters (0.32 in) in the circumferential direction and 105 millimeters (4.1 in) in the axial direction. This window, as well as a similar one in the annular diffuser test section, allows the laser beams to pass through the inner wall of the annulus to the inside of the centerbody. This greatly reduces the amount of laser light reflected from the wall. LDA measurements can then be made at points closer to the wall than would be possible against the centerbody's black surface. More about the effects of the centerbody windows will be discussed in a later section.

The annular diffuser test section follows the annular inlet (see Figure 4). The flow from the inlet is diffused in this 10.2 centimeter (4.0 in) long section by walls which are set at a nominal diffusion half-angle of seven degrees. Like the inlet test

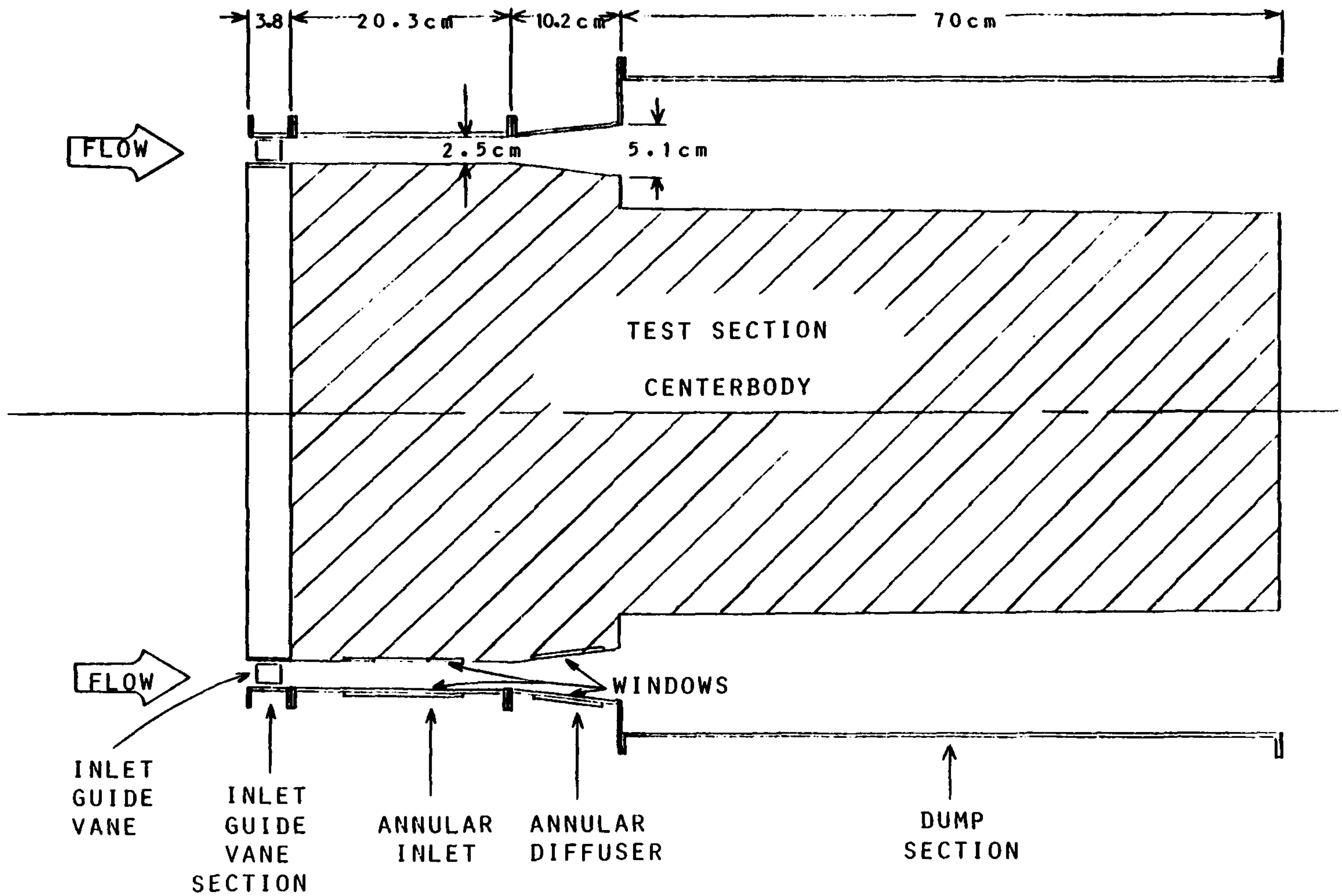

FIG. 4. ANNULAR TEST SECTIONS

section, optical access to the diffuser is gained through a glass window. This window measures 76 millimeters (3.0 in) axially by 19.1 millimeters (0.75 in) circumferentially. Another window which measures 8.0 millimeters (0.32 in) circumferentially and 76 millimeters (3.0 in) axially is installed in the test section centerbody to accomplish the same purpose as the centerbody window in the inlet test section.

The flow enters an annular dump section after exiting the diffuser. This section is designed to minimize laboratory effects on the flow in the test sections. More detailed information on any section of the ADRF Flow Handling Apparatus may be found in references 1 and 2.

Instrumentation

Two systems, a Laser Doppler Anemometer and a hot-film anemometer, were used to make flow measurements in the test sections. The LDA system is supported by a mini-computer (primarily used for data acquisition and reduction), an oscilliscope, and a universal counter. The hot-film anemometer system is supported by a micro-computer, an analog-to-digital converter and a root-mean-square (RMS) voltmeter. Both anemometer systems are supported by a square-edged orifice plate and mercury manometer flow measuring system. A static pressure probe was used to make pressure measurements in the inlet and diffuser.

Laser Doppler Anemometer. The LDA system consists of four major components:

1) A helium-neon laser.

2) Transmitting optics.

3) Collecting optics.

4) A photon-correlating signal processor.

Laser. The first component is a Spectra Physics Model 124A fifteen milliwatt, helium-neon laser which emits a single, monochromatic beam of 6328 Angstroms wavelength. The beam has a $1/e^2$ radius of 0.55 mm (0.022 in) and a divergence angle of 1.0 milliradians. The laser is powered by a Spectra Physics Model 255 power supply which operates on 115 volt, single-phase current.

Transmitting Optics. The first element of the transmitting optics is a Malvern Instruments, Ltd. Type RF307 beamsplitter which is attached directly to the laser exit. Through a combination of partially and totally reflective mirrors, the beamsplitter divides the single beam into two, equal-intensity beams. It can be adjusted to alter the divergence or convergence angle between the two beams and their separation.

The two laser beams are directed into a Malvern Type K9023 phase modulator. The unit is designed to accept parallel beams with a separation of twenty millimeters (0.79 in). The beams pass through a pair of crystals which, when excited, modulate the phase of the beams through the Pöckels electro-optic effect, changing the frequency of one beam relative to the other (10:L36). The result is a change in the Doppler-shifted frequency of light scattered by particles moving through the measuring volume. In terms of the fringe model, phase modulation imparts a uniform translation to the fringes in a direction perpendicular to the fringe planes. The phase modulator crystals are excited by a separate drive unit which uses a sawtooth waveform for the driving function. The drive unit can be set to shift the Doppler frequency by fixed amounts of 20, 50, 100, 200, 500, or 1,000 KHz, or continuously between 50 KHz and 1 MHz. The "fringe velocity" imparted by the phase modulator can be determined by using Eq (12) and replacing F with ΔF, the phase modulator frequency shift. The result is Eq (14).

$$\text{Fringe Velocity} = \Delta F \times d_f \tag{14}$$

The sense of the fringe motion can be changed by the DRIVE/INVERT switch on the drive unit, thus increasing or decreasing the Doppler-shifted frequency by the set amount. The output of the drive unit was monitored with a Hewlett-Packard (HP) 5325B Universal Counter.

The use of a phase modulator in a LDA system increases its flexibility. Frequency shifting is used to aid in determining the direction of flow, making measurements in highly turbulent or high speed flows, and in increasing the velocity resolution of the system. Velocity resolution will be discussed later.

The laser/beamsplitter and phase modulator are mounted on a 12.7 centimeter (5.0 in) wide steel channel which allows these units to be used as a single assembly. Once they are aligned with respect to each other on the channel, the entire assembly can be moved to align the laser beams with the remaining optics.

The two laser beams which exit the phase modulator are directed by two, front-silvered plane mirrors through a periscope to a lens which focuses and crosses the beams to form the measuring volume (see Figure 5). The fringe spacing can be determined using Eq (11) and the focusing geometry. When parallel beams are transmitted through the focusing lens in the configuration shown in Figure 6, Eq (15) can be used to calculate the fringe spacing.

$$d_f = \frac{f\lambda}{D\mu_0} \tag{15}$$

In the above equation, f is the focal length of the focusing lens, D is the parallel beam separation, and μ_0 is the refractive index of the medium where the measuring volume is located (μ_0 = 1.0 for air) (6:6-2). In all of the tests conducted with the LDA system, a 250 mm focal length focusing lens and 20 mm beam separation were used. The resulting fringe spacing is 7.91 μm (0.00031 in).

Collecting Optics. The velocity and turbulence intensity of the flow are measured by analyzing the frequency content of the light scattered from the measuring volume. This is done by converting the light, through the photomultiplier effect, into an electrical signal to be analyzed by a signal processor. In using the fringe model, each light "burst" (instead of a photon in the classical sense) absorbed by the photosensitive material causes the emission of an electron or electrons which comprise the electrical signal.

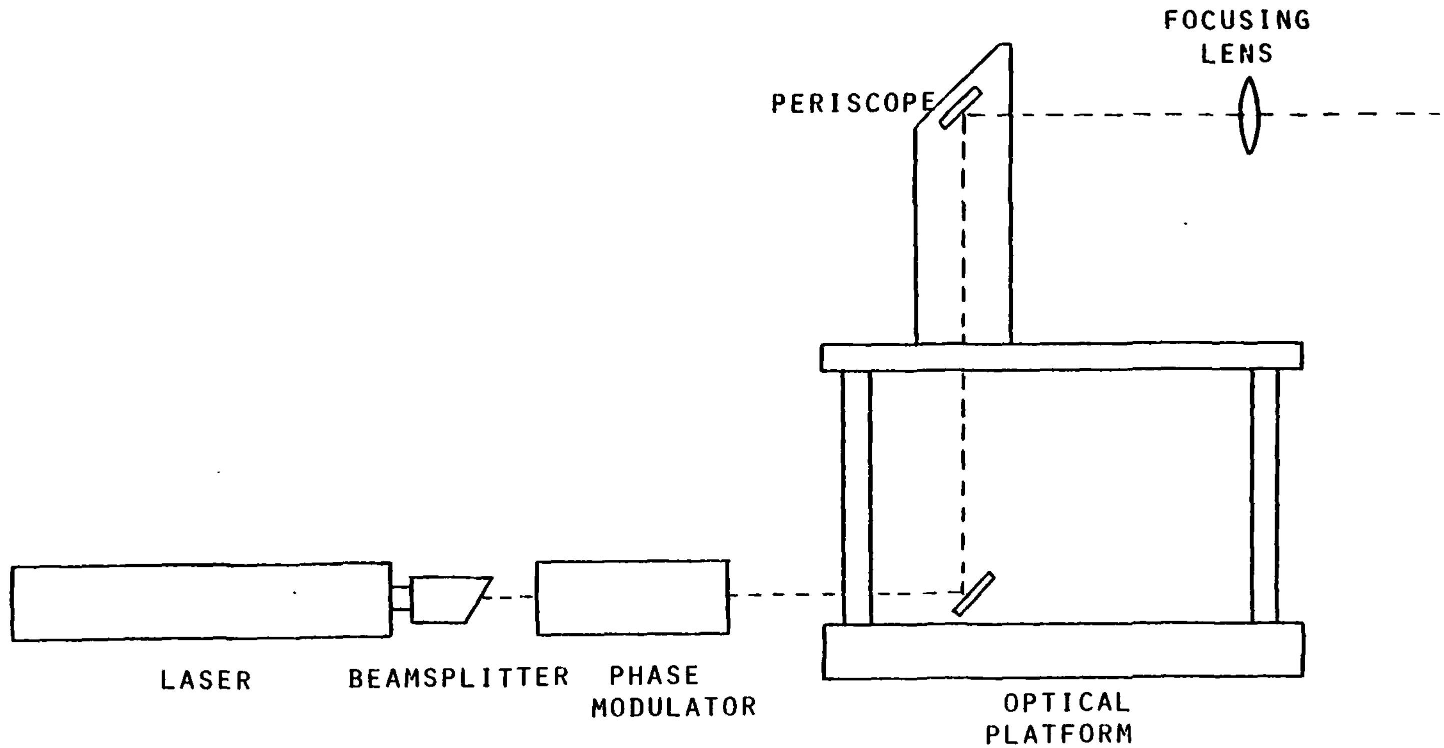

FIG. 5. TRANSMITTING OPTICS CONFIGURATION

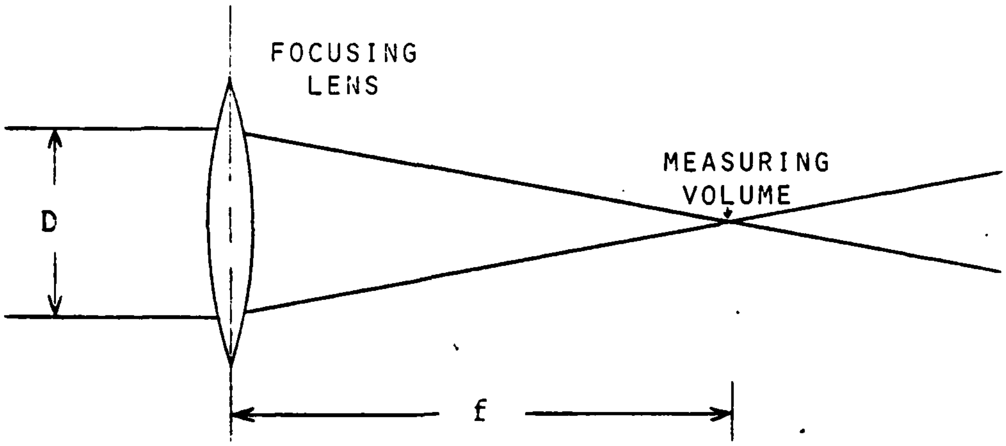

FIG. 6. FOCUSING GEOMETRY

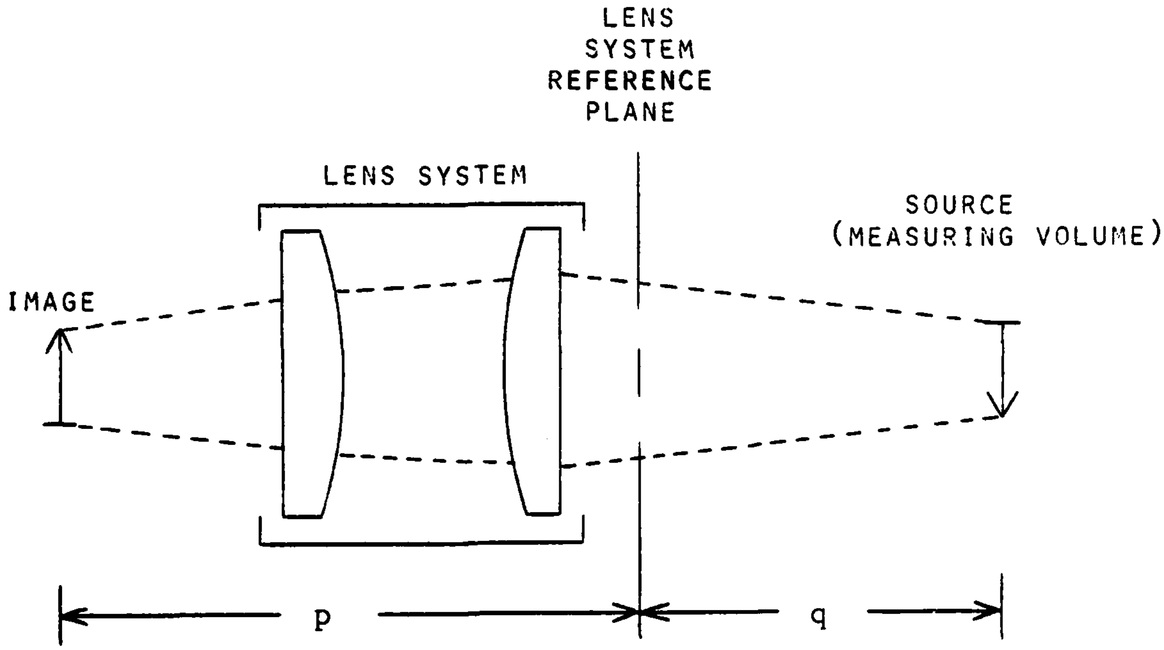

FIG. 7. LENS EQUATION DIMENSIONS

The collecting optics consist of a Tamron 105 mm telephoto lens and a Malvern Type RF313 photomultiplier (PM) assembly using an EMI 9863 KB/100 type photomultiplier tube. The laser light collected by the telephoto lens is focused on a 100 μm (0.00394 in) aperture just before the light enters the photon detection portion of the PM assembly. A 2.5, 6.5, or 9.0 cm spacer may be placed between the PM assembly and telephoto lens to allow light gathering at various distances from the measuring volume. The lens equation, Eq (16), governs the distance from the measuring volume at which the collecting optics must be set to focus the scattered light on the aperture.

$$\frac{1}{f'} = \frac{1}{p} + \frac{1}{q} \tag{16}$$

In the lens equation, f' is the focal length of the collecting lens, p is the distance from the lens system reference plane to the image on the aperture, and q is the distance from the reference plane to the measuring volume (see Figure 7).

The PM assembly was set to collect the scattered light, in backscatter, at an angle of 16.9 degrees off the optical axis defined by the bisector of the crossed laser beams. While the transmitting optics determine the actual measuring volume size (to the $1/e^2$ contour), the collecting optics geometry and aperture size determine the effective measuring volume size since the PM tube may only receive light from a portion of the actual measuring volume. Appendix A contains the actual and effective measuring volume sizes as well as the method used to determine them.

The periscope, focusing lens, and PM assembly are mounted on an optical platform which can be raised or lowered (see Figure 8). This platform can also be translated along an axis perpendicular to the test section centerbody axis. The optical platform was originally designed and used by Walterick (reference 11). With proper optical alignment, the two axis system allows the measuring volume to be positioned in the test section and traverse the annulus in the radial direction. A vernier scale is attached to the translating base to determine the measuring volume's radial position to within 0.25 mm (0.01 in). The laser and optics are mounted on a laboratory bench which rests on rollers guided by two parallel rails. A chain-and-sprocket drive system, attached to the rails and bench, turns two 3/4 x 10 threaded rods which move the bench along the rails. A mechanical counter is connected to a gear on one of the drive rods. Through the gear ratio in the counter itself, angular displacement of the drive rods is displayed to within 0.1 revolutions. Thus, the measuring volume can be moved in the axial direction and its position determined to within 0.25 mm (0.01 in).

<u>Signal Processor</u>. The heart of the LDA system is the Malvern Type K7023 digital correlator which analyzes the signal from the PM assembly. The correlator monitors the signal for a predetermined sample time (t_s), which can be set from 50 nsec to 0.995 sec, and counts the number of pulses caused by light "bursts" (fringe model) or photon detections (classical). This results in a digitized version of the intensity function I(t) discussed in

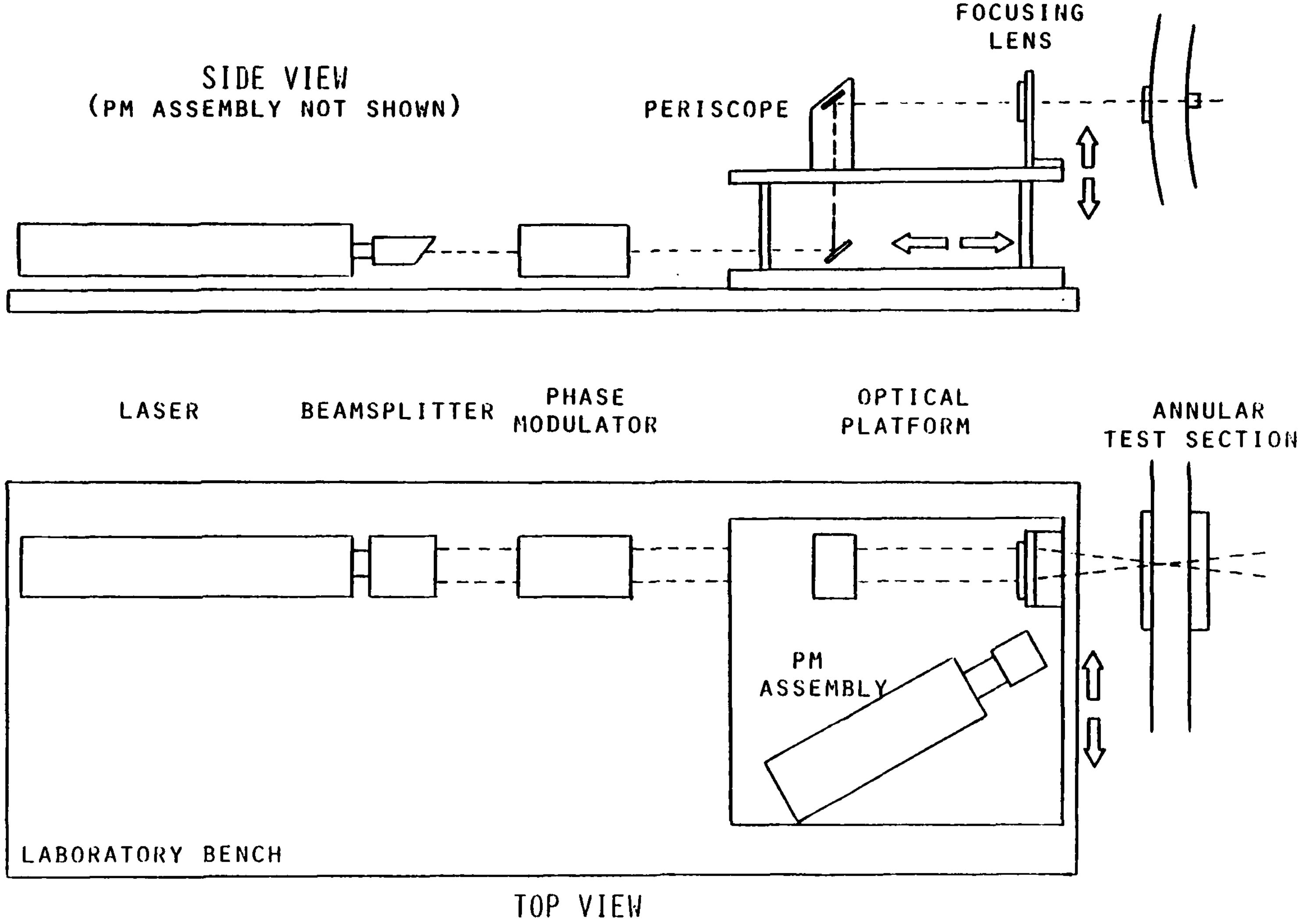

FIG. 8. LASER AND OPTICS CONFIGURATION

Laser Velocimetry Theory. Electronically, the correlator also takes the function $I(t + \tau)$, where τ varies from zero to 95 times t_s in integer increments, to develop the intensity autocorrelation function. The experiment time (T) can be set for 10 to 10^9 samples, in powers of 10, or for any time interval by simply starting and stopping the correlator when desired. The autocorrelation function, $G^{(2)}(\tau)$, is in a digital form represented by 96 channels (the 96 values of τ mentioned earlier). The correlator will display the entire function on an X-Y display or the numeric value of each channel on a digital display.

Oscilloscope. A Tektronix 465 M oscilloscope was used as an X-Y display to graphically view the correlation function on a real-time basis.

Mini-computer. A HP 3052A data acquisition system was used to control the digital correlator and process the data received from it. The interfaces and software were developed by Neyland (reference 12) in 1981 for his Master's thesis. The system was originally used with the Air Force Institute of Technology Smoke Tunnel; however, the interfaces and software were modified to satisfy the needs of this research. A summary of the interfacing and software is contained below. A more detailed description may be found in reference 12.

The LDA and data acquisition systems were not collocated so cables had to be run to connect them. Two 22.9 meter (75 ft) lengths of Belden 8773 cable were used. Each cable contains 27 twisted, shielded pairs of conductors. Forty pairs were used for signal transmission: six computer-to-correlator control lines and thirty-four correlator-to-computer data lines. The second conductor in each pair was connected to ground; however, the shields were not grounded. The unused, twisted pairs were left unconnected.

The software used to control the correlator and process the data is contained in a program titled DARLA MOD1. A program titled DARLA (Data Acquisition And Reduction of Laser Anemometry), which was written by Neyland, is the basis of DARLA MOD1. The software performs the following functions:

1) Run the correlator for a specified period of time to develop the intensity autocorrelation function.
2) Transfer the correlation function values to the HP 3052A.
3) Store the correlation function and other test information on a flexible disk.
4) Process the data to calculate velocities and turbulence intensities.
5) Plot the velocity and turbulence intensity profiles on a HP 9872S plotter.
6) Print a summary of the data in tabular form on a HP 9871A printer.

Both DARLA and DARLA MOD1 may be found at the Air Force Institute of Technology, School of Engineering, Wright-Patterson AFB, Ohio 45433.

Hot-film Anemometer. A TSI Model 1050 Constant Temperature Anemometer and TSI Model 1051-6 Monitor and Power Supply were used with a TSI Model 1214-20 hot-film sensor to gather additional velocity and turbulence information in the annular inlet and diffuser. The probe was mounted to the dump section sidewall and inserted upstream into the inlet and diffuser test sections. It is adjustable in both the radial and axial directions. The anemometer bridge output was connected to a HP 3400A RMS voltmeter and an Alpha Product Co. eight bit, analog-to-digital converter. The RMS voltage was read from the voltmeter to get turbulence intensity information. A Radio Shack TRS-80 Model III micro-computer was used to sample the output of the analog-to-digital converter and average the samples to obtain an average DC voltage. The sampling rate of the TRS-80 is approximately 50 Hertz.

Flow Meter. A Meriam Instrument Co. square-edged orifice plate, a Meriam U-tube mercury manometer, and a Bourdon tube pressure gage were used to measure the air flow rate into the flow handling apparatus. The orifice is 2.5 centimeters (1.0 in) in diameter inside a 7.6 centimeter (3.0 in) pipe. Flange taps were used for the pressure measurements. The pressure measurement upstream of the orifice has an accuracy of ±6890 N/sq meter (1.0 psig). The measurement of the pressure drop across the orifice has an accuracy of ± 1.3 millimeters (0.05 in) of mercury. The air temperature was measured in the dump section with a mercury thermometer to an accuracy of ±0.5 degrees Fahrenheit. Since low velocities are involved, this temperature measurement is representative of the static air temperature at the orifice plate to within 0.75 degrees Fahrenheit.

Static Pressure Probe. A locally-built static pressure probe was used to measure the pressure in the annular inlet and diffuser (see Figure 9). The probe was mounted to the dump section sidewall in the same manner as the hot-film anemometer probe and inserted upstream into the test sections. The pressure was indicated by a Meriam Instrument Co. water micro-manometer. The ambient air pressure was measured with a Fortin-type, mercury barometer.

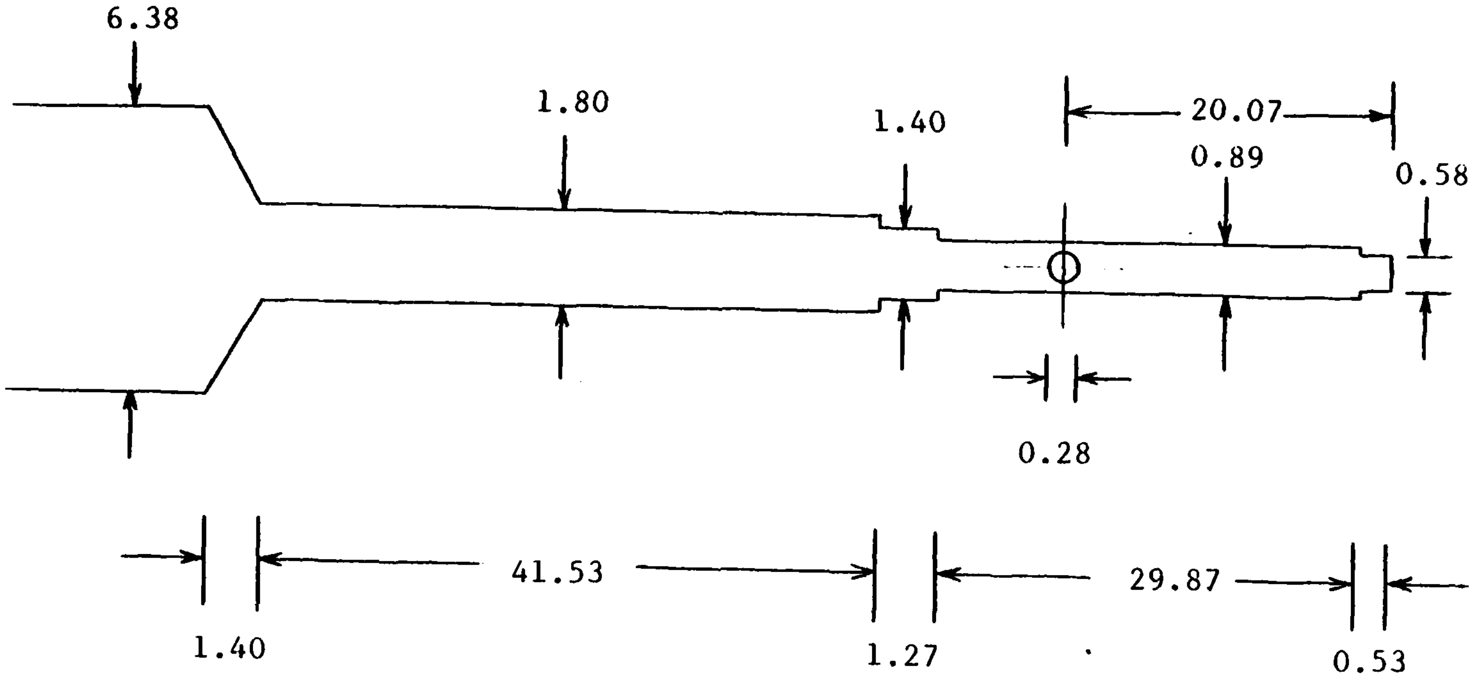

ALL DIMENSIONS ARE IN MILLIMETERS.

FIG.9. STATIC PRESSURE PROBE

IV. Experimental Procedure

The procedure used to collect and reduce the data will be discussed in this section. It can be divided into four segments: laser and optical alignment, LDA measurements and data reduction, hot film anemometer measurements and data reduction, and static pressure measurements.

LDA Optical Alignment

A critical step in making flow measurements with an LDA system is the alignment of the laser and optics. The alignment of the LDA system used in this research meets the following criteria:

1) As the optical platform translates, the measuring volume moves only in the radial direction of the flow handling apparatus.
2) As the laboratory bench translates, the measuring volume moves only in the axial direction.
3) The measuring volume always remains fixed in space with respect to the PM assembly so the two will remain aligned as the optical platform is translated.

The alignment procedure is decribed in Appendix B.

LDA Flow Measurements

LDA measurements were collected with the digital correlator in the single-clipped autocorrelation mode (without clipping). Each test consists of a traverse of the flow channel at one axial position. For each test, all room lighting was extinguished because of its detrimental effect on data collection. The reason for this will be evident later in this section. The air flow through the flow handling apparatus was allowed to reach a steady state before the tests began since there is no active control of the flow rate.

The goal of each LDA measurement is a smooth correlation function with three peaks and valleys, similar to Figure 10, in the shortest possible time. After positioning the measuring volume at the desired point in the flow, the aperture on the collecting lens is set. A smaller aperture requires a longer correlator run time (correlation time) to develop the same correlation function. The frequency shift (ΔF) and sample time (t_s) should be set, based on Eq (17) if the approximate velocity being measured is known.

$$u = \frac{d_f}{(Pk2-3)} + \Delta F(d_f) \qquad (17)$$

If the velocity (u) cannot be estimated, different combinations of ΔF and t_s must be tried to obtain the desired correlation function. Frequency shifts in the INVERT mode reduce the damping of the correlation function and are useful in high turbulence flow regions to obtain more distinct peaks and valleys. In the DRIVE mode, frequency shifts increase damping and are normally used only in laminar and low turbulence flows (η<25%).

The correlator is run for a specified period of time to obtain the correlation function for the flow measurement. If a

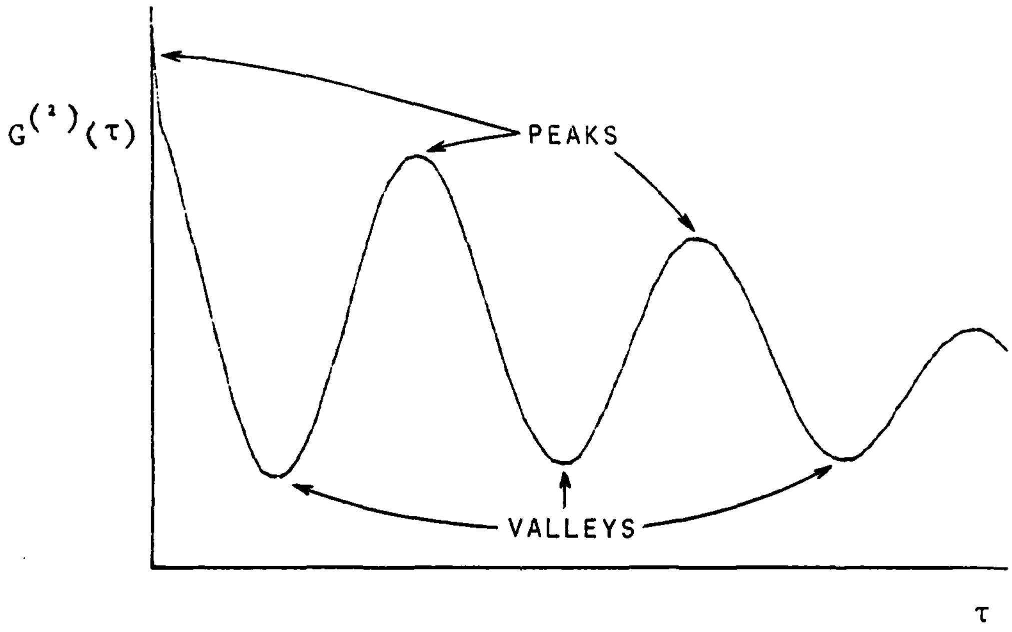

FIG. 10. CORRELATION FUNCTION: PEAKS AND VALLEYS

real-time display on the oscilloscope is desired, the correlator can be operated from the unit itself using the START and STOP buttons. Correlator data cannot be transferred to the HP 3052A while the oscilloscope display is active. If the HP 3052A is used to control the correlator through the program DARLA MOD1, the correlation time is input after which the computer will immediately start the correlator and stop it after the specified time has elapsed. The correlator channel contents are transferred to the computer and the correlation function is displayed on the computer's video display. If the function is smooth and has at least three peaks and valleys, the data is kept in the computer memory for subsequent transfer to flexible disk. If the correlation function is not smooth or has fewer than three peaks and valleys, the data is rejected by the experimenter and a new correlation function obtained.

The most significant factor determining the correlation time needed to obtain a smooth correlation function is the amount of background light which enters the PM assembly. There are two sources of this background light. The phase modulator and periscope mirrors, the first source, diffuse a large amount of laser light and create stray beams which are then transmitted through the focusing lens and projected on the outer surface of the test section access windows (see Figure 11a). This light reflects off the windows into the PM assembly. The second source is the portion of each primary laser beam which is reflected by the test section centerbody window surfaces each time the beam crosses a surface

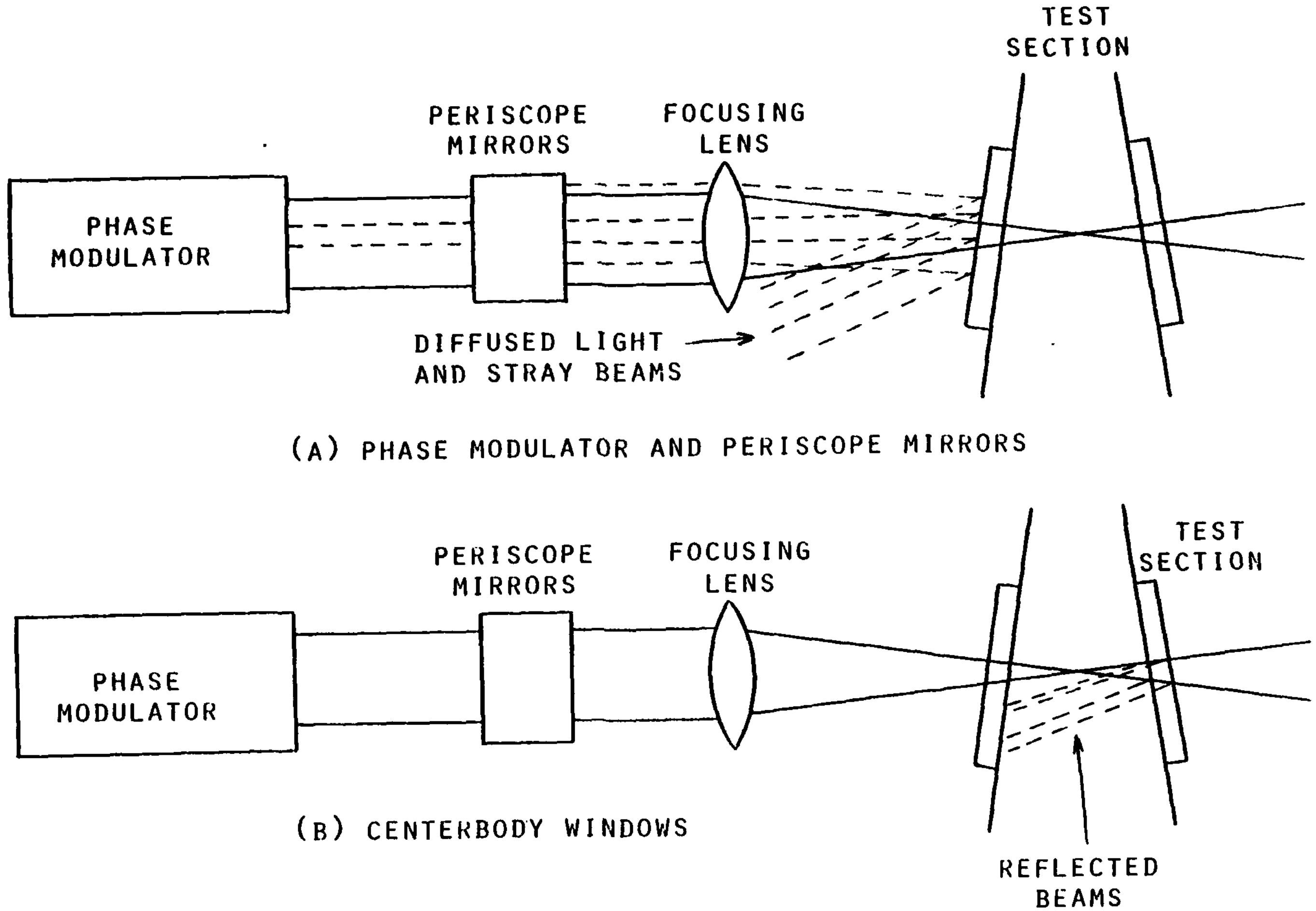

(A) PHASE MODULATOR AND PERISCOPE MIRRORS

(B) CENTERBODY WINDOWS

FIG. 11. SOURCES OF BACKGROUND LIGHT

(see Figure 11b). The reflected beams cross the flow channel. If these beams which reflect into the flow channel are in the vicinity of the collecting axis, the scattered light from them will tend to mask the light from the measuring volume. This results in points in the flow channel, away from the walls, which have large amounts of background light. Because of the centerbody and collecting optics geometry, this is a particular problem in the diffuser test section.

Bright background light has several detrimental effects on LDA flow measurement. It may be so bright that it saturates the PM tube and the correlation function fails to develop at all. Using a smaller collecting lens aperture will normally solve this problem. However, the amount of light may be great enough that even if the correlation function develops, it cannot develop eneugh to distinguish the peaks and valleys. In some situations when the effective measuring volume is near, but not on a wall, the dominant signal may be a reflection of the actual measuring volume which gives a zero velocity measurement. This usually occurs in the diffuser test section as much as 1.0 millimeters (0.04 in) from the inner wall. Flow measurements cannot be made in these situations. On the other hand, if a correlation function develops to a point where peaks and valleys are distinguishable (as in Figure 12), a longer correlation time will improve the function.

The amount of background light reaching the PM assembly is controlled in several ways. A paper mask was placed over the

FIG. 12. UNDER-DEVELOPED CORRELATION FUNCTION

focusing lens which allowed only the two parallel laser beams to pass. When near the inner wall of the annulus, the test section centerbody windows reflect much less light than the black, painted surface. However, when the measuring volume is more than three to five millimeters from the inner wall, the centerbody is rotated to move the windows out of the beam paths. This avoids the problem caused by the reflected beams passing through the flow channel.

Tests were run at the following axial positions (see Figure 13):

34.3 mm (1.35 in)	from	the	IGV	trailing	edges
48.8 mm (1.92 in)	"	"	"	"	"
110.0 mm (4.33 in)	"	"	"	"	"
215.4 mm (8.48 in)	"	"	"	"	"
240.0 mm (9.45 in)	"	"	"	"	"
262.4 mm (10.33 in)	"	"	"	"	"

Data points were taken every 0.5 millimeters (0.02 in) across the flow channel except when prohibited by excessive background light. Points to within 0.5 mm of the inlet walls were obtained. In the diffuser, data points were obtained to within 2.5 mm of the inner wall and 1.0 mm of the outer wall.

For all of the tests, atomized glycerin was used to "seed" the flow. The seeder output ranged from 22.8 to 26.4 liters per minute with $2(10^8)$ particles per liter. The particles varied in size from 0.5 to 4.0 μm (.00002 to .00016 in). Correlation times in the annular inlet ranged from 30-45 sec away from the walls to 90-120 sec near the walls. In the diffuser test section, corre-

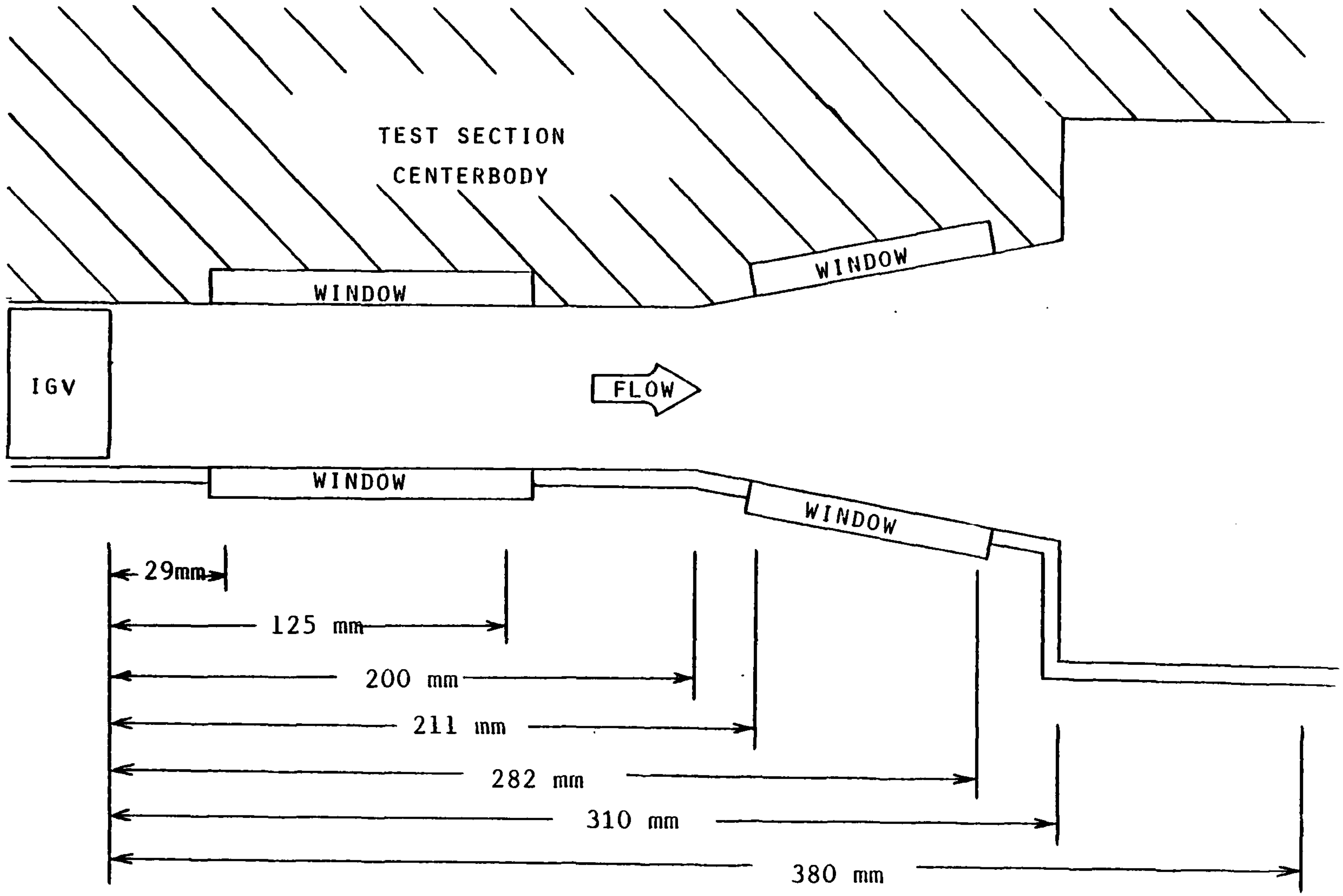

FIG. 13. DATA COLLECTION POSITIONS

lation times were 60-90 sec away from the walls to 180-420 sec near the walls. For the tests on 20 SEP 83 and thereafter, the air supply mass flow was measured at periodic intervals during the tests using the square-edged orifice plate. After reaching a steady-state, the mass flow was constant so only periodic measurements were necessary to ensure gross fluctuations in the flow rate did not occur during a test.

LDA Data Reduction

The data was reduced using the program DARLA MOD1 on the HP 3052A data acquisition system. The method is described in Appendix C. The velocity and turbulence intensity data was plotted to provide a visual representation of the profiles. A separate program was used to integrate the velocity profiles of each test to calculate the mass flow through the annulus. The integration was carried out by estimating the area under the profiles by a series of rectangles whose width is the distance between adjacent data points and height is the average of the velocities at the two points.

Hot Film Anemometer Measurements

Flow measurements were also made with the hot film anemometer. As before, the air flow was allowed to reach a steady state before the test began. These tests were not made in conjunction with the LDA tests because the glycerin particles would alter the heat transfer on the sensor and introduce an unknown amount of error into the data.

The hot film tests were made at the same axial positions as the LDA tests except for the 34.3 mm position. The laser was used to determine the position of the sensor by focusing the beams on the probe and reading the position on the optical platform's vernier scale. Data points were taken at intervals from one to two millimeters across the flow channel. At each point, the TRS-80 computer calculated the average DC voltage of the bridge output by averaging 500 samples. During this time, the RMS voltmeter was visually monitored and the average RMS voltage of the bridge output was estimated.

Hot Film Anemometer Data Reduction

The bridge voltages and sensor calibration curve points were input into the HP 3052A to reduce the data. A program which compared the voltages and calibration curve was used to calculate the average velocity and turbulence intensity. The average velocity is derived from the DC voltage, while the turbulence intensity is derived from the RMS voltage. The hot film data was also plotted to give a visual representation of the profiles. The velocity profiles were integrated, using the method described earlier, to calculate the mass flow.

Static Pressure Measurements

The static pressure in the annular inlet and diffuser was measured at various axial positions with a static pressure probe and water micro-manometer. The air flow was allowed to reach a steady-state before measurements were taken. The laser was used to position the static pressure port in the axial direction by focusing the beams on the pressure port. The position was determined by the reading on the mechanical counter of the laboratory bench translating system. Measurements were taken at 19 mm (0.75 in) intervals in the axial direction in the inlet and at 13 mm (0.50 in) intervals in the diffuser.

V. Results

A total of twelve tests were run with the LDA system. A test was conducted at each of the following axial positions: 34.3, 48.8, 110, 215.4, 240, 262.4 mm. Three additional tests were made at both the 48.8 and 110 mm positions to establish the repeatability of the system. Five tests were run with the hot film anemometer: one at each axial position used with the LDA except the 34.3 mm position. A profile of the static pressure in the axial direction of the annulus was made with pressure measurements in the inlet and diffuser. This section discusses the results of the flow investigation and evaluation of the LDA system.

Flow Characteristics

The velocity profiles acquired with the LDA at each of the six axial positions used for testing are shown in Figures 14 through 19. The dotted lines on the plots represent the test section walls with the channel width indicated on the abscissa. The mass flows were obtained by integrating the profiles over the annulus using the method described in the previous section. The calculated mass flows were within 5% of the values measured with the orifice plate flow meter. As expected, the profiles in Figures 16 through 19 show a thinner boundary layer on the inner annulus wall than on the outer wall. This effect is more pronounced in the annular diffuser where the ratio of the inner to outer wall radii is smaller (see Figures 17 through 19). The turbulence in-

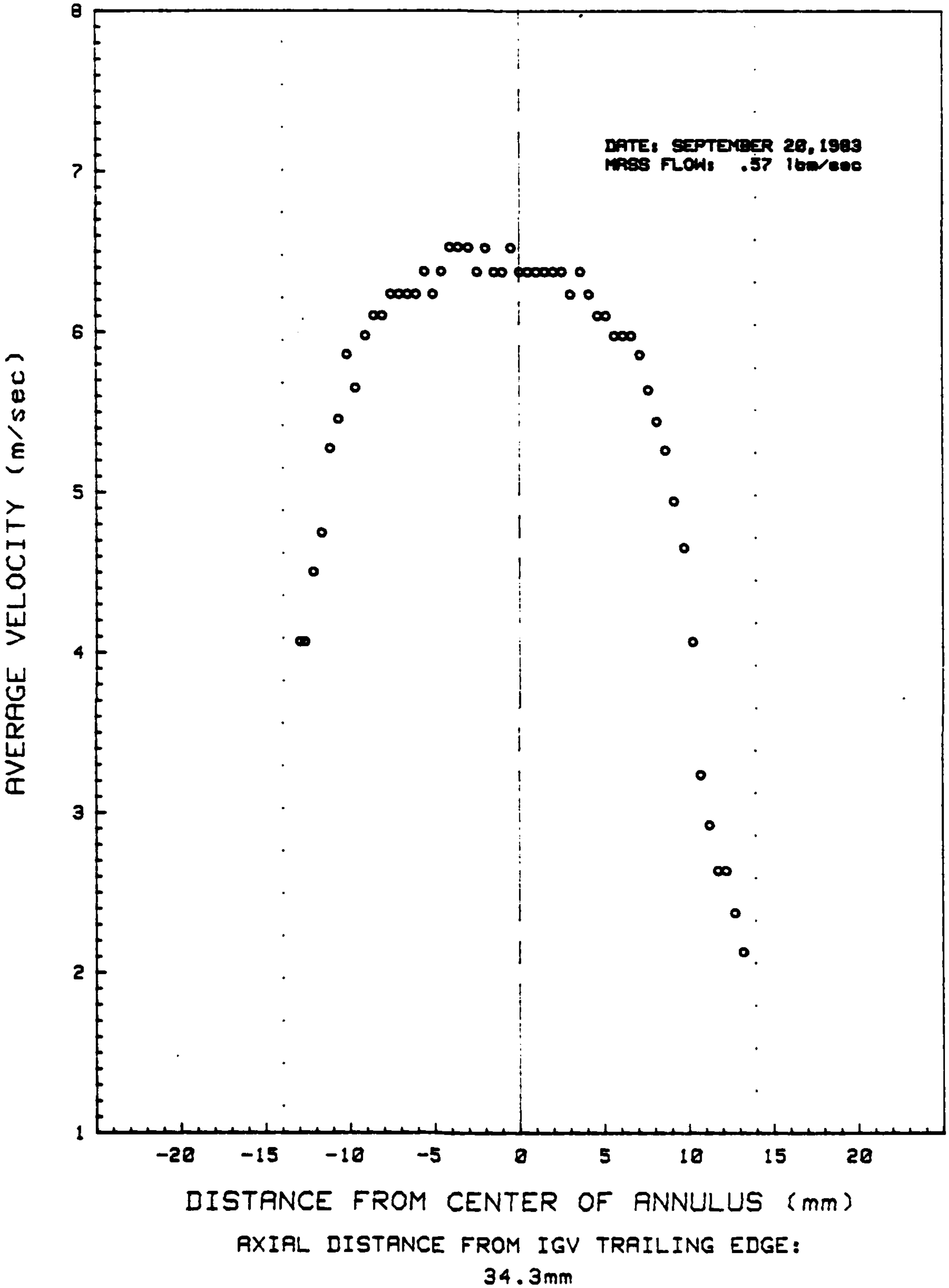

FIG. 14. AVERAGE VELOCITY PROFILE

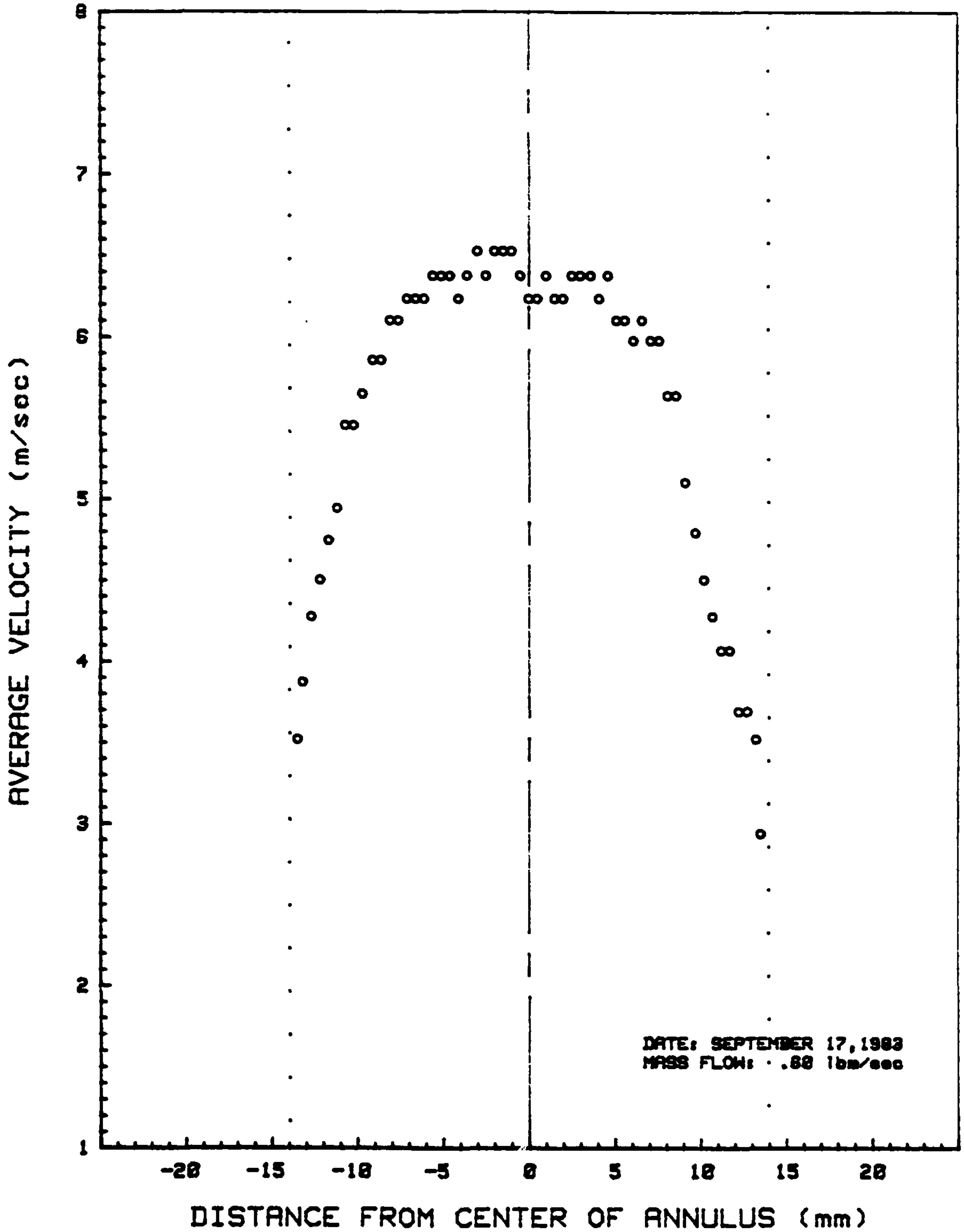

AXIAL DISTANCE FROM IGV TRAILING EDGE:
48.8mm

FIG. 15. AVERAGE VELOCITY PROFILE

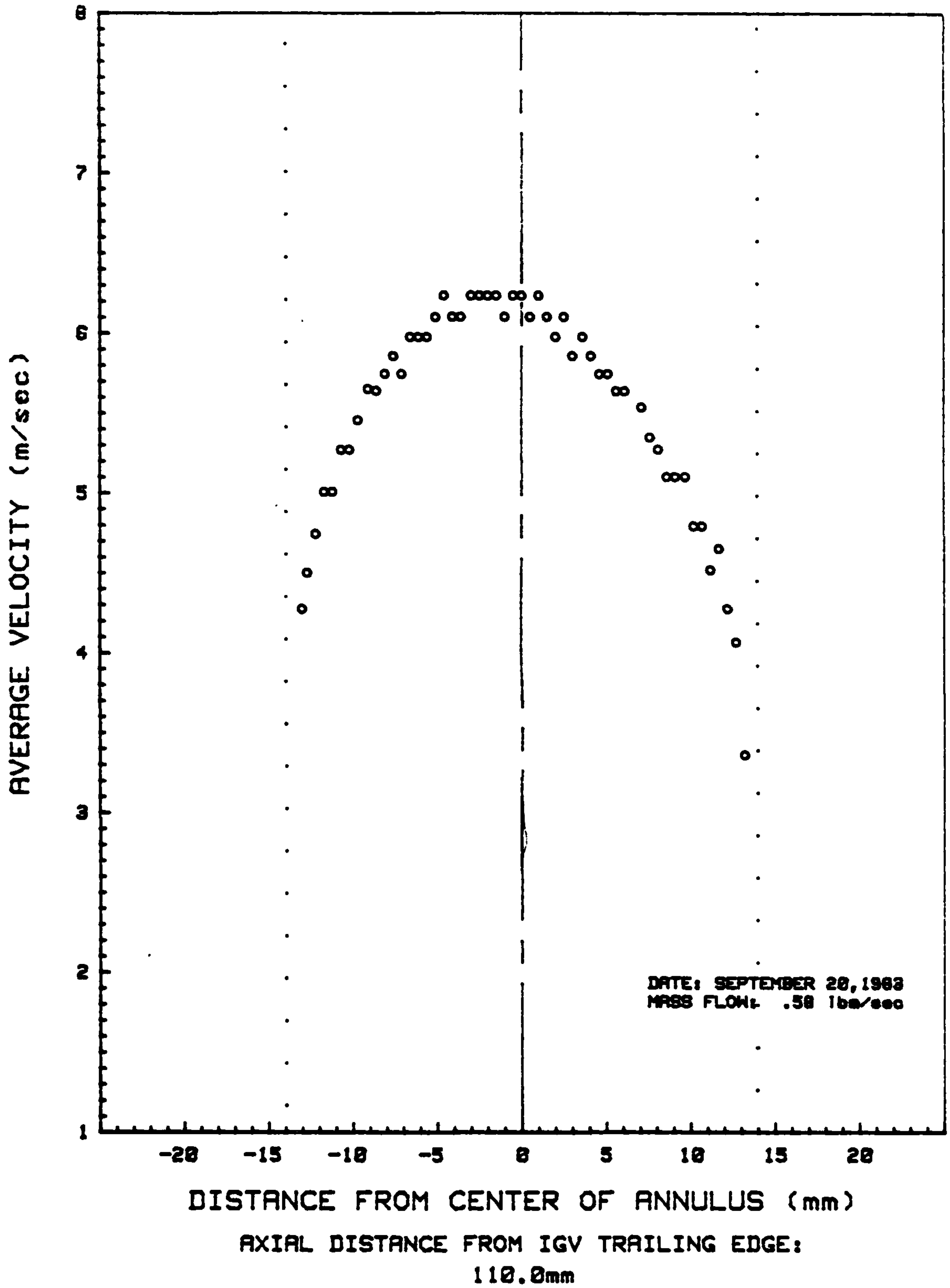

FIG. 16. AVERAGE VELOCITY PROFILE

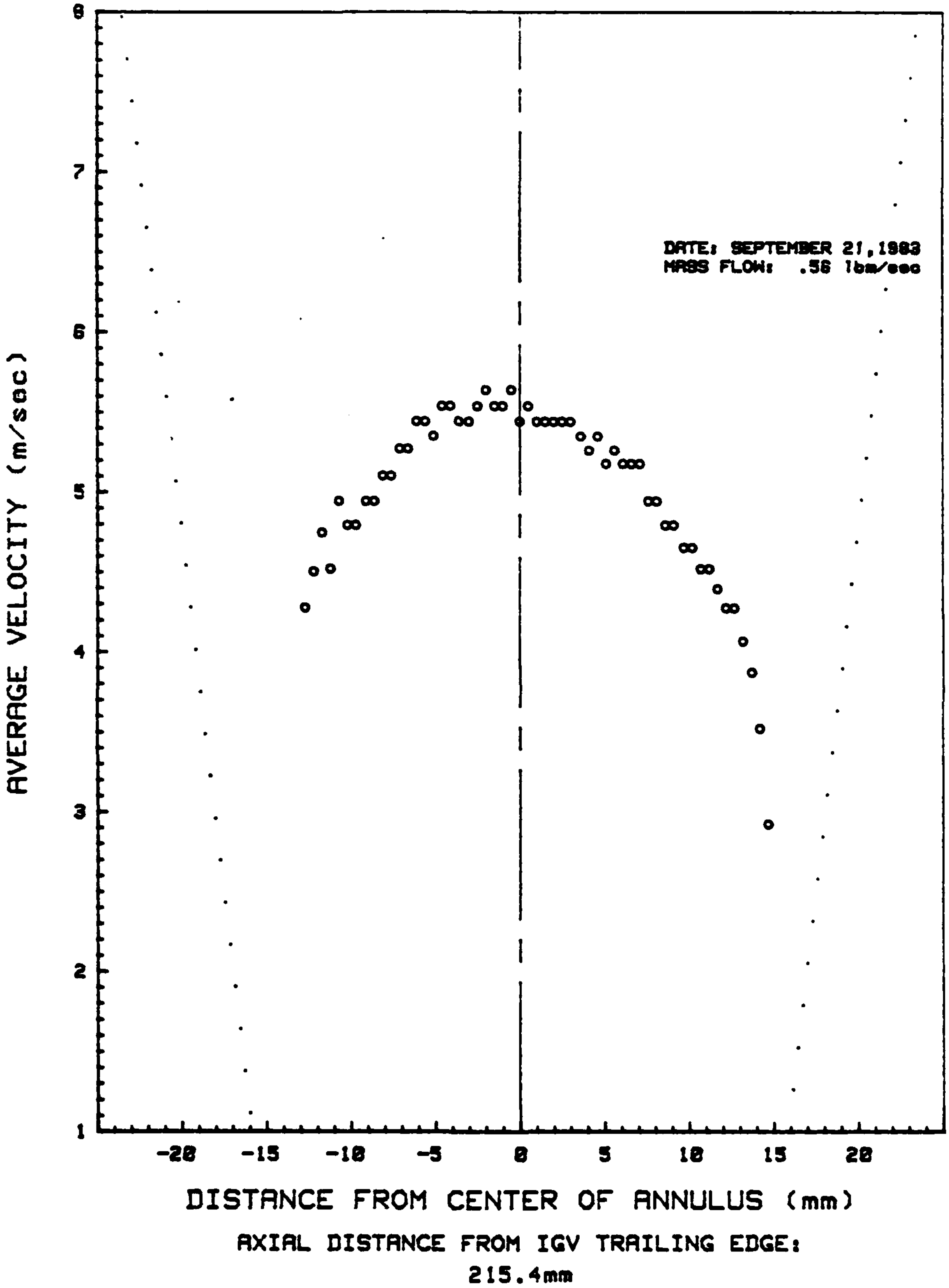

FIG. 17. AVERAGE VELOCITY PROFILE

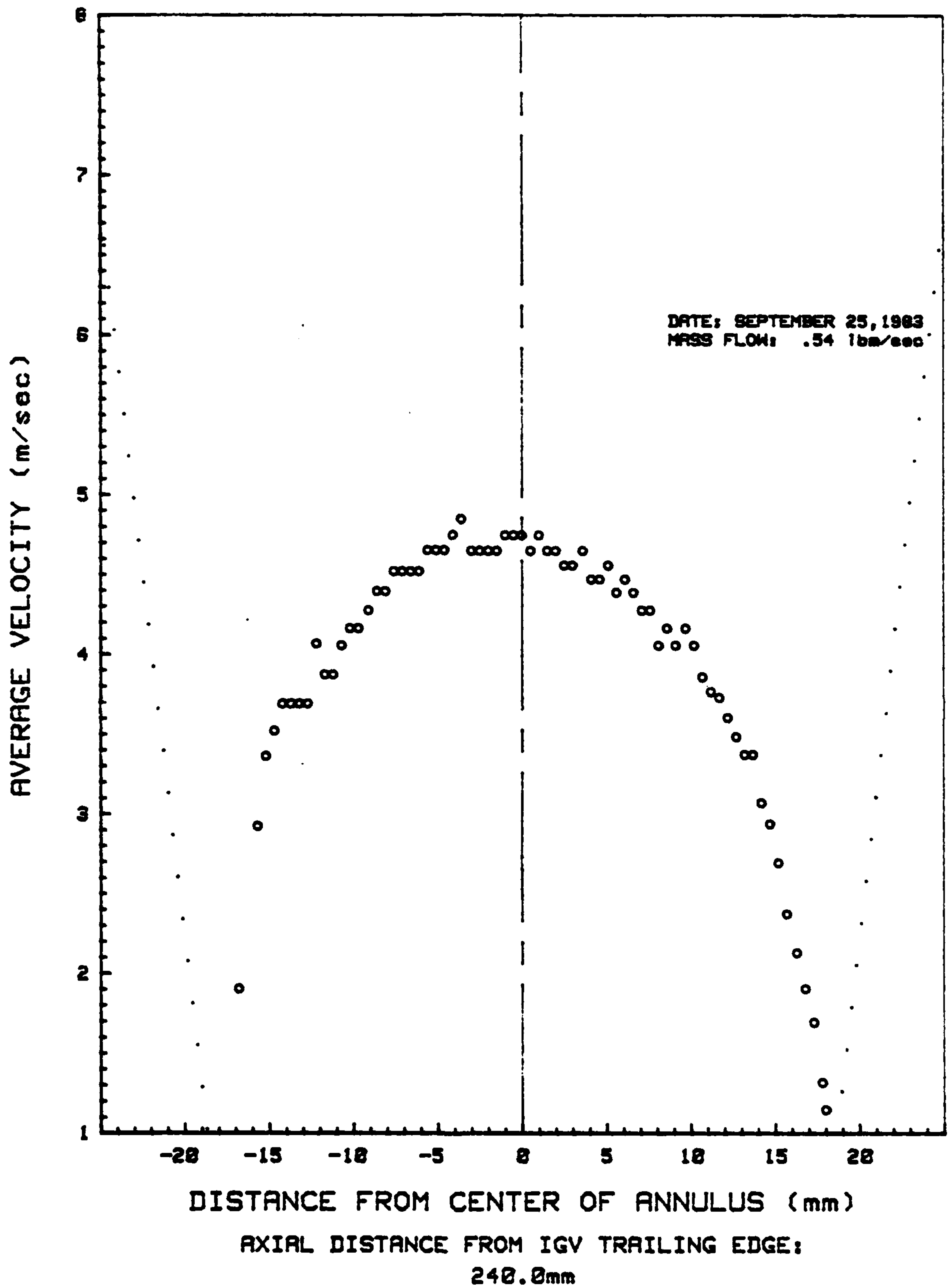

FIG. 18. AVERAGE VELOCITY PROFILE

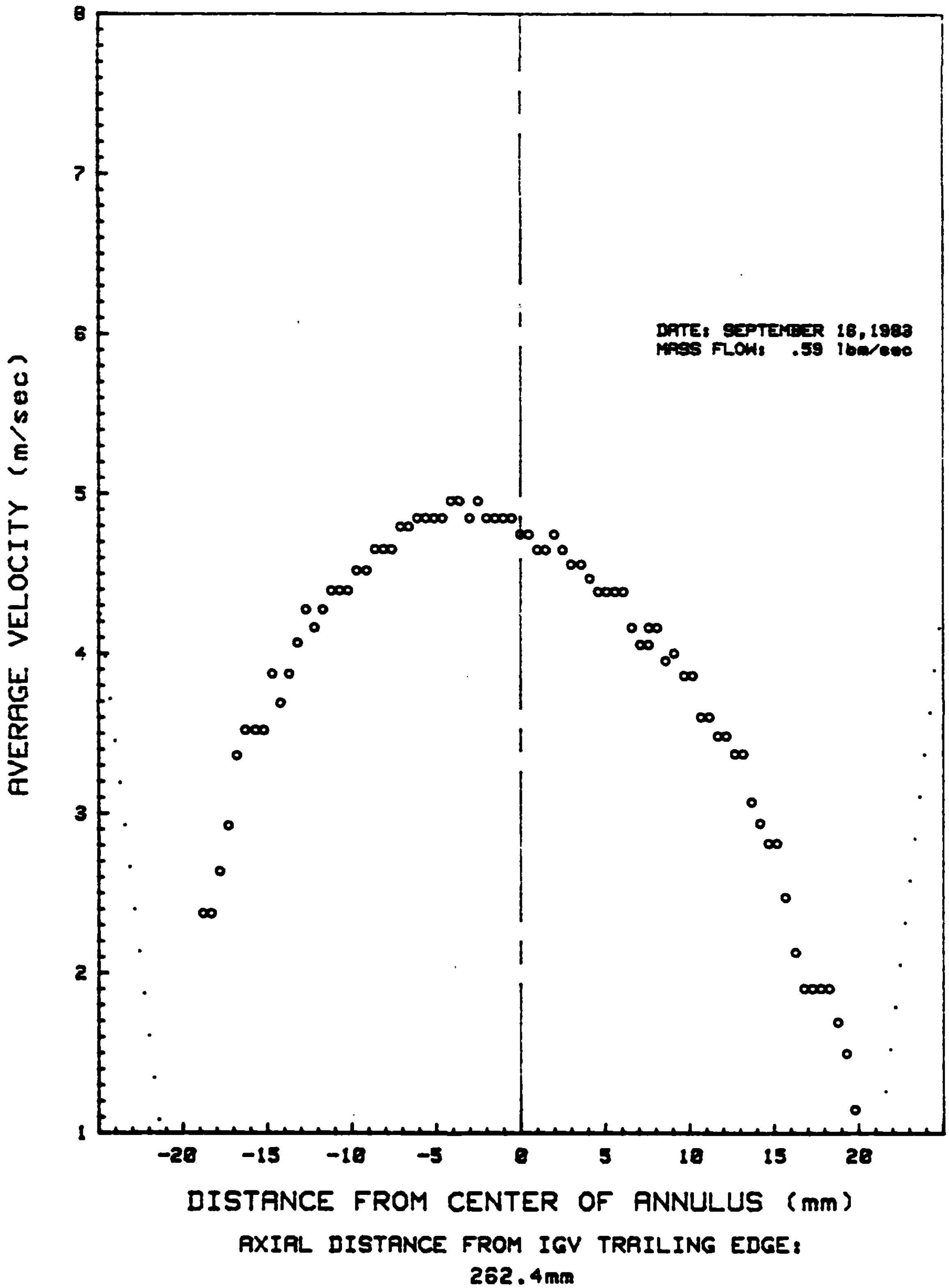

FIG. 19. AVERAGE VELOCITY PROFILE

tensity profiles corresponding to these velocity profiles are shown in Figures 20 through 25. The turbulence intensity is defined as the standard deviation of the velocity at each radial position divided by the average velocity at that position. The flow in the annulus, outside the boundary layers, is turbulent. This is consistent with the pipe Reynolds number of 18300 calculated with Eq (1). The turbulence intensity is approximately 8% in the inlet and 10% in the diffuser. The boundary layers are also turbulent. This is consistent with the theoretical predictions using a Reynolds number in the annular inlet of 3.42 (10^5) and the fact that the freestream flow is turbulent throughout the annular interface. A disturbance along the outer wall in the annular inlet is noticeable in the turbulence intensity profiles of Figures 20 through 22. This is caused by a step discontinuity in the outer wall between the IGV section and annular inlet test section. The step increases the width of the flow channel in this region by about two millimeters (0.08 inches). A summary of the data for these velocity and turbulence profiles is contained in Appendix D.

Flow Development

The development of the velocity and turbulence intensity profiles in the annular inlet are shown in Figures 26 and 27 respectively. The velocity profiles are nondimensionalized using a reference velocity determined with Eq (18)

$$V_{ref} = \frac{\dot{m}}{\rho A_{inlet}} \tag{18}$$

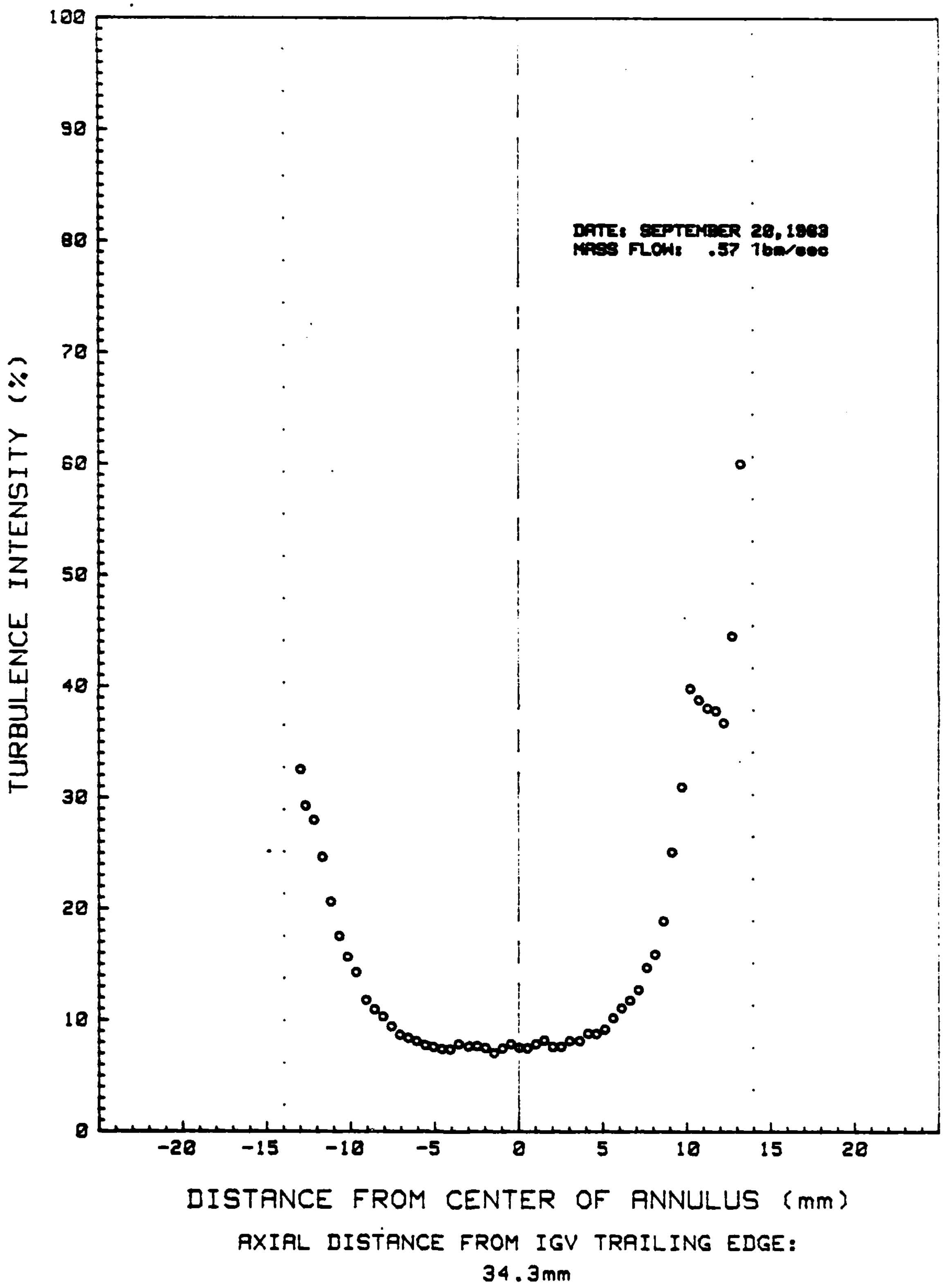

FIG. 20. TURBULENCE INTENSITY PROFILE

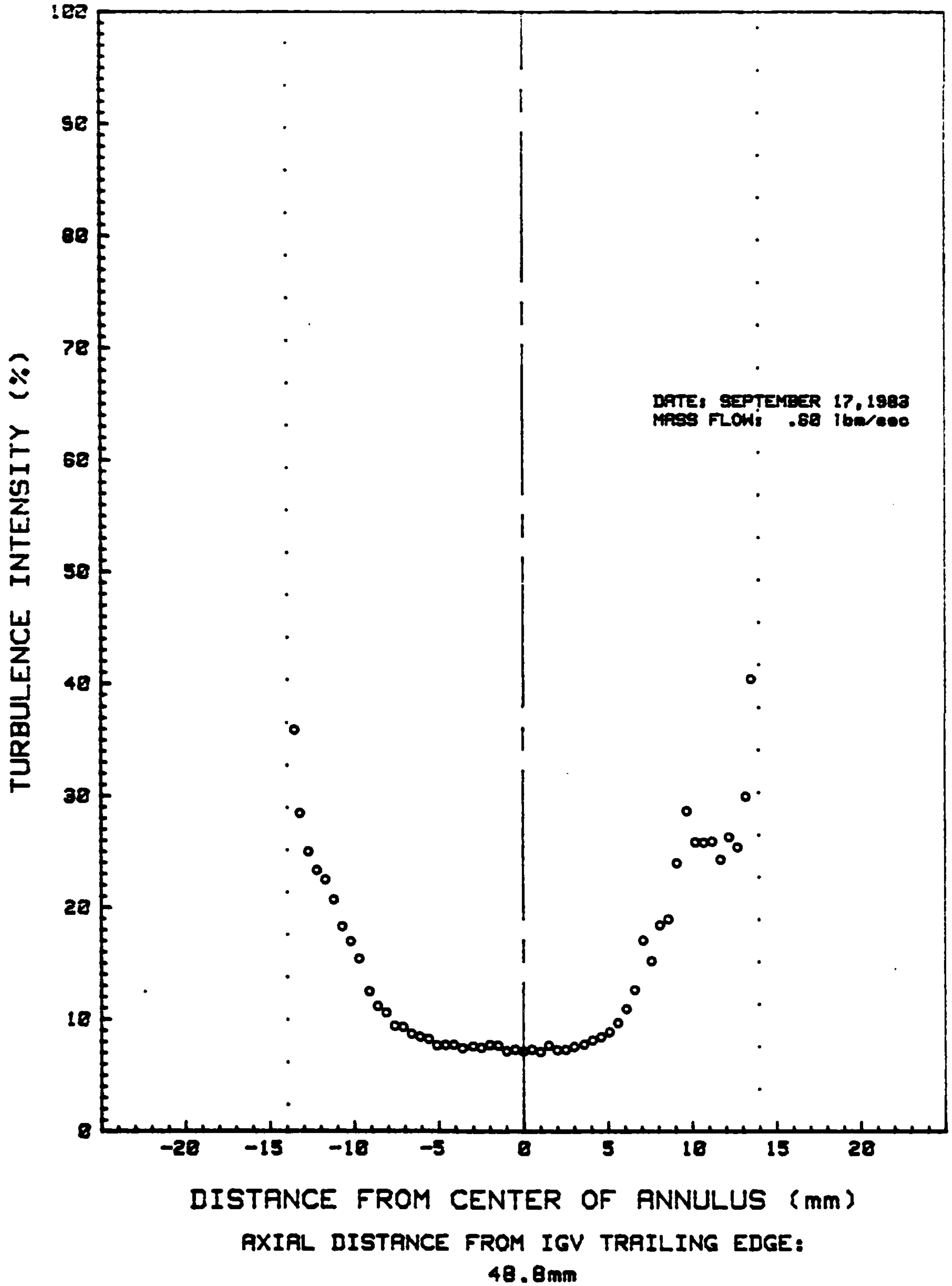

FIG. 21. TURBULENCE INTENSITY PROFILE

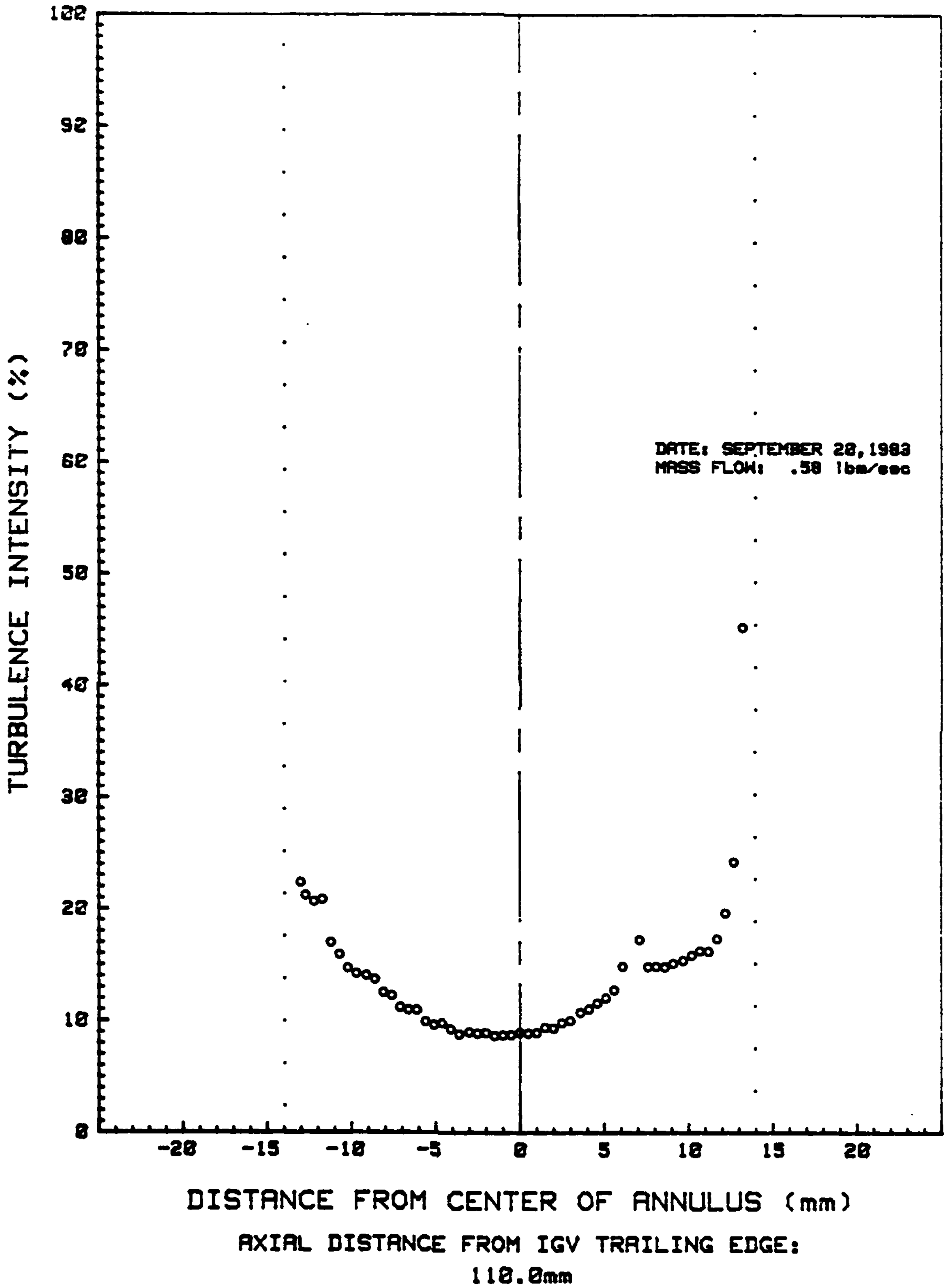

FIG. 22. TURBULENCE INTENSITY PROFILE

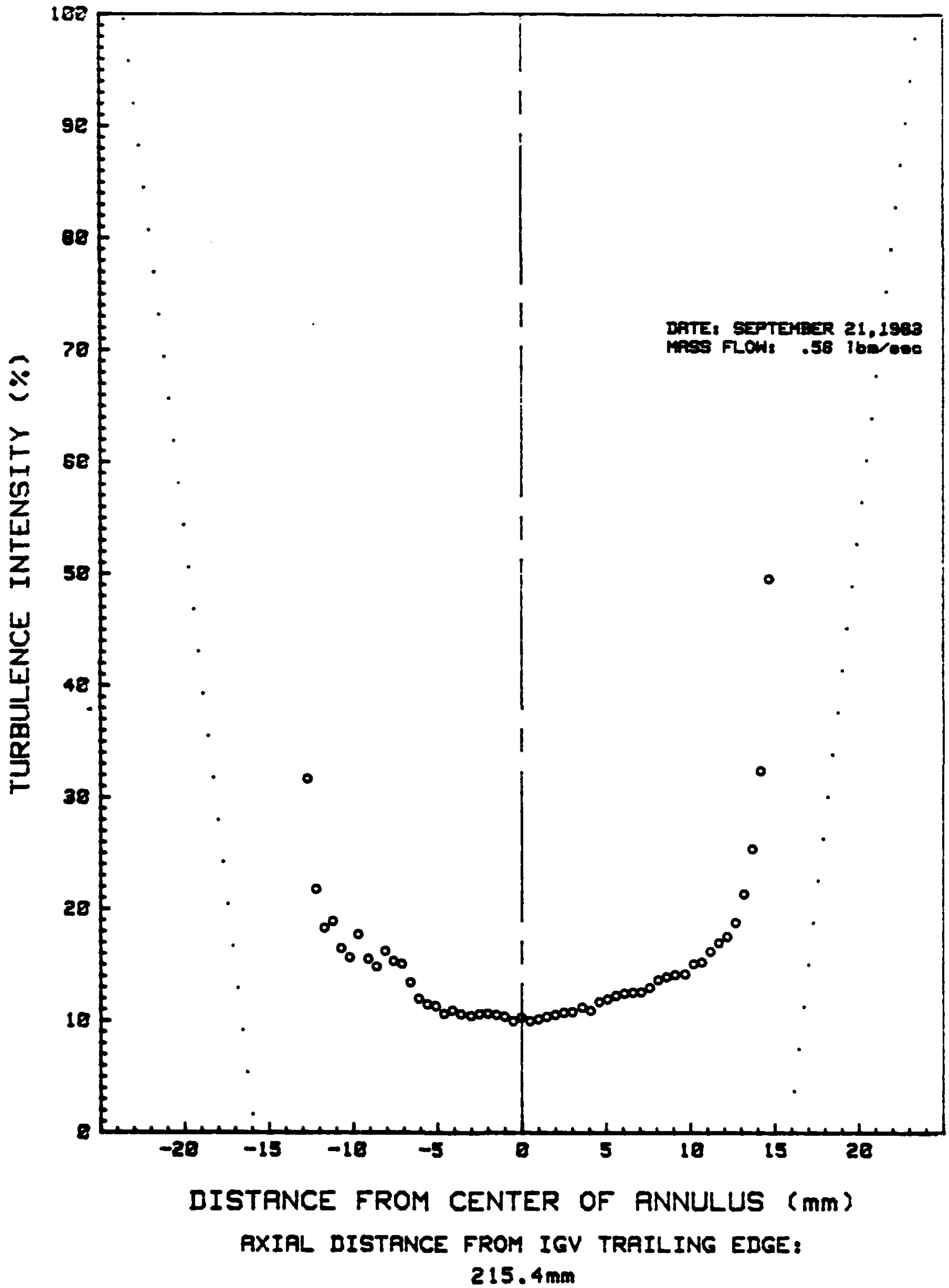

FIG. 23. TURBULENCE INTENSITY PROFILE

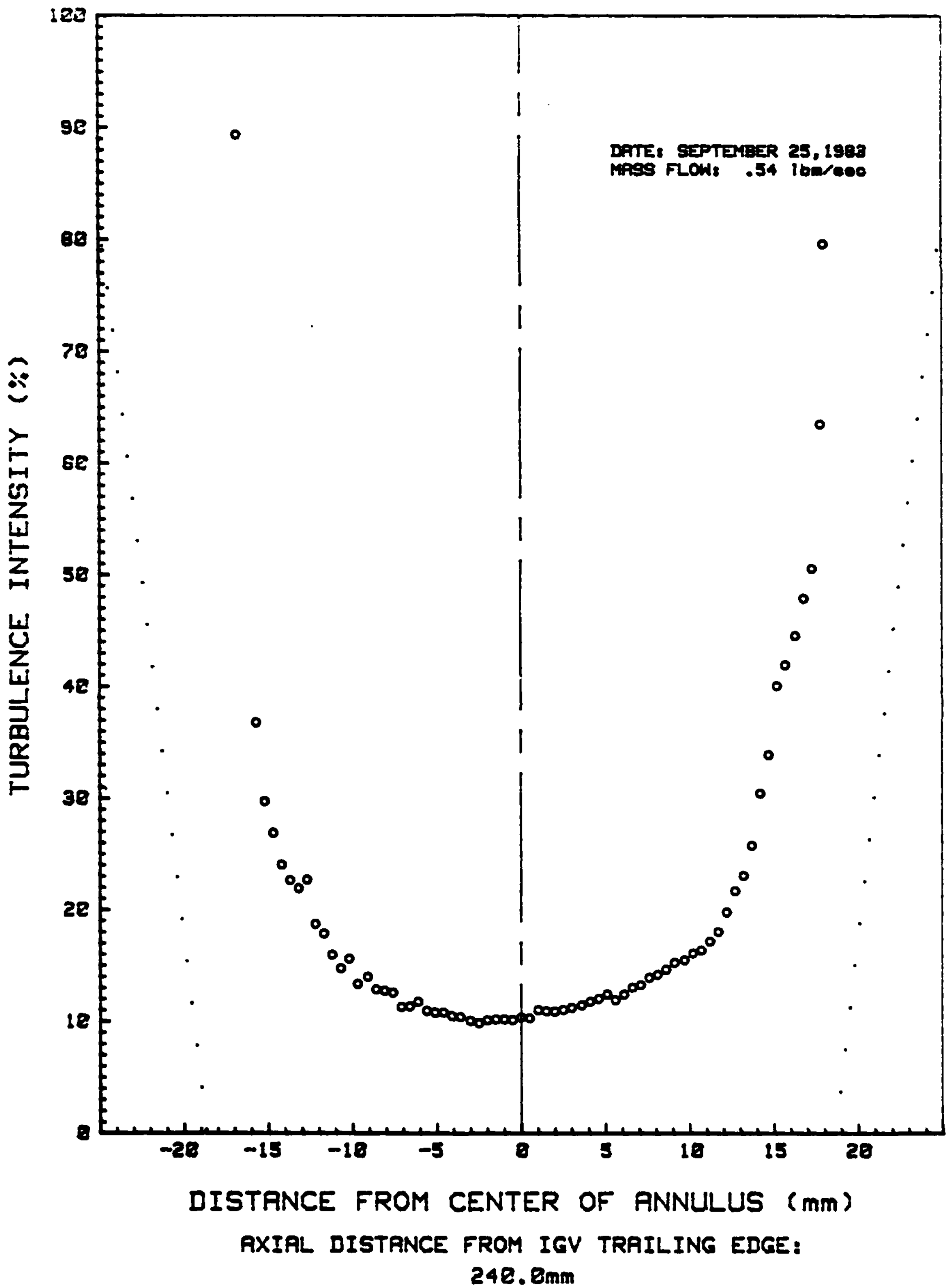

FIG. 24. TURBULENCE INTENSITY PROFILE

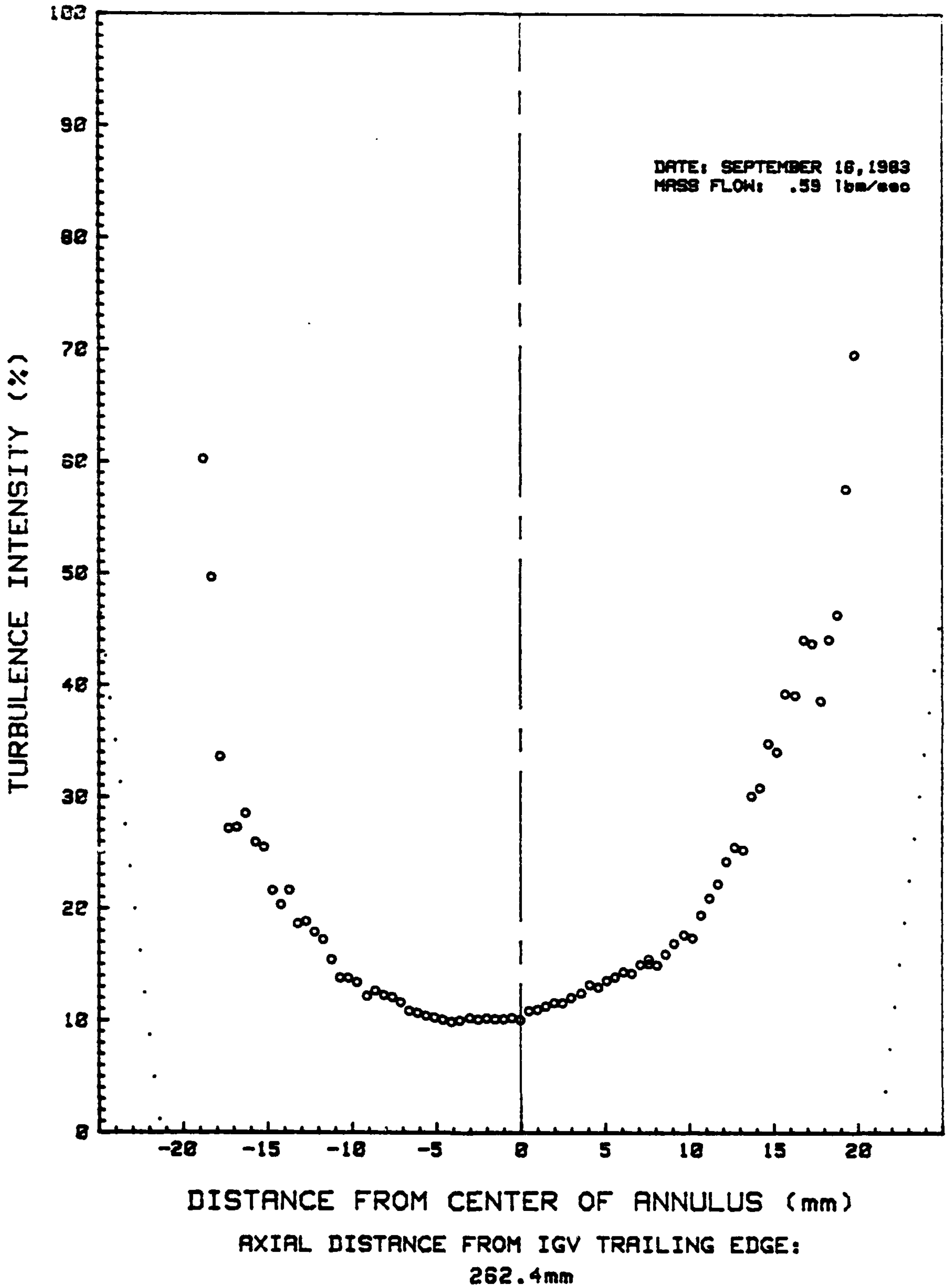

FIG. 25. TURBULENCE INTENSITY PROFILE

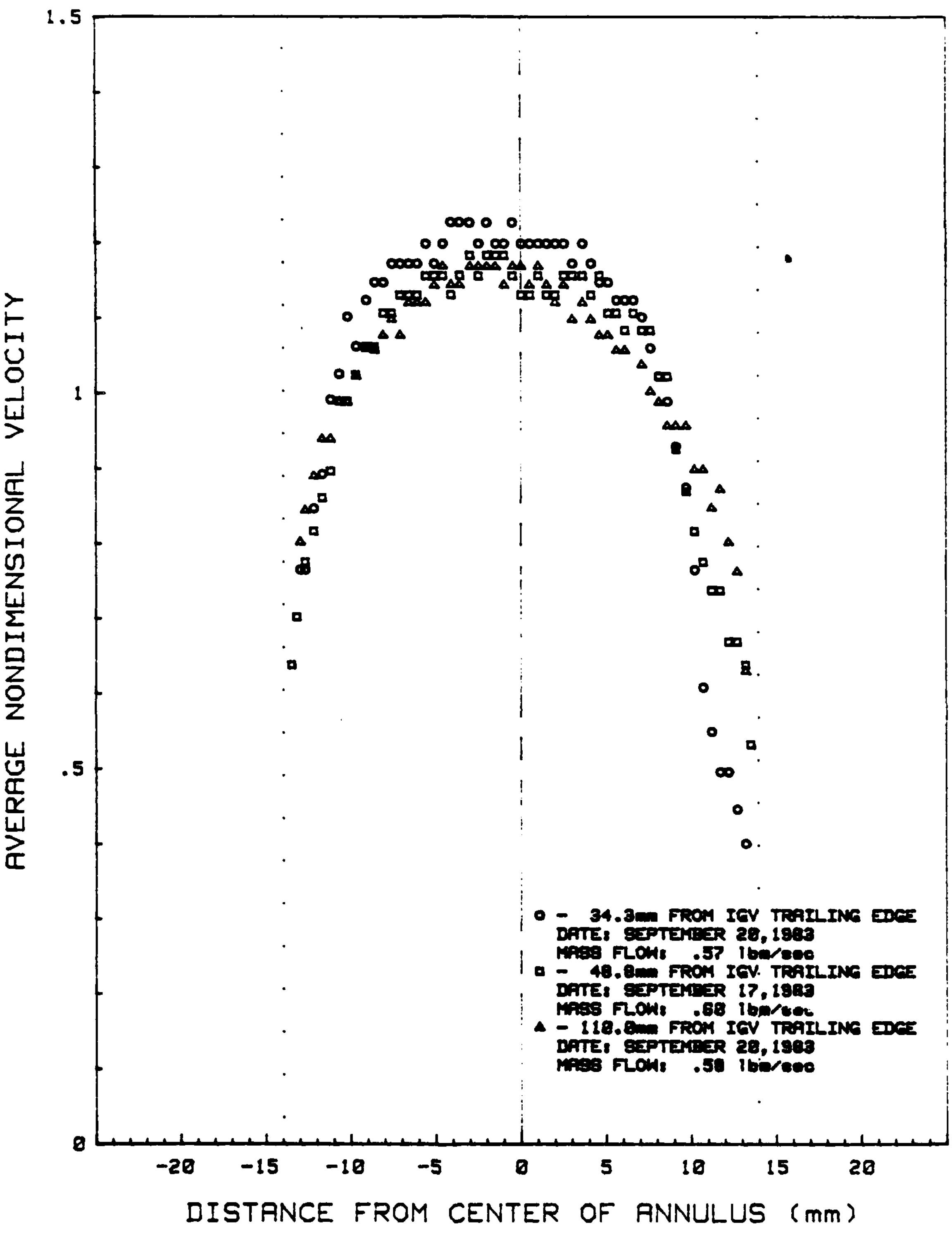

FIG. 26. ANNULAR INLET VELOCITY PROFILE DEVELOPMENT

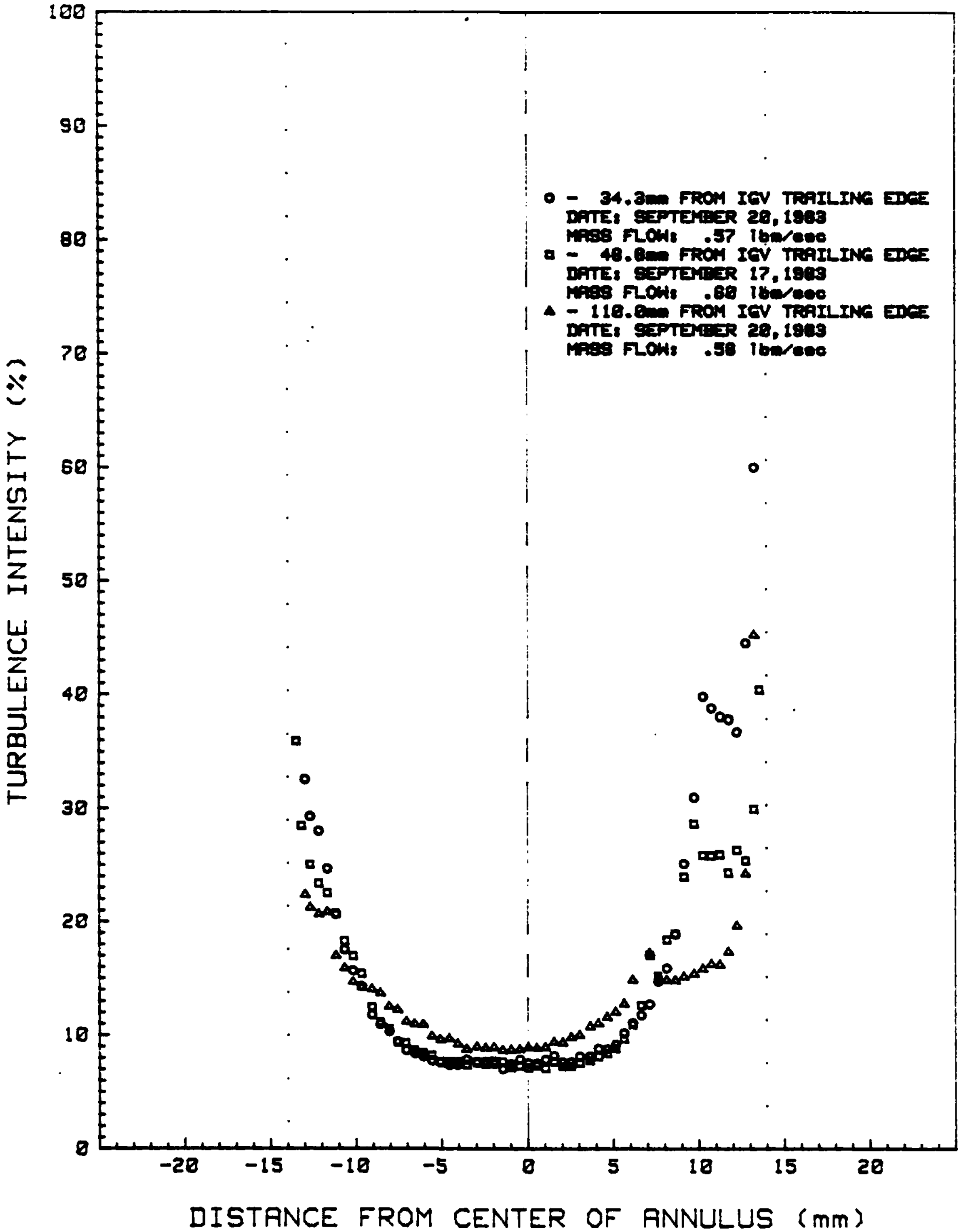

FIG. 27. ANNULAR INLET TURBULENCE INTENSITY PROFILE DEVELOPMENT

where $\dot{m}$ is the mass flow calculated from the integrated velocity profile, ρ is the density of the air, and A_{inlet} is the annular inlet area of 0.0426 sq meters (0.4583 sq ft) based on the measured flow channel width of 27.9 millimeters (1.10 in). From Figure 26, it appears that the inner and outer wall boundary layers have not merged until the vicinity of the 110 mm axial position. Near the centerline of the flow channel at the 110 mm axial position, the velocity profile has a more parabolic shape representative of merged boundary layers. On the other hand, the velocity profile at the 48.8 mm position shows a region of uniform flow near the center of the channel. Flat plate boundary layer predictions of a turbulent boundary layer growing from the beginning of the annular interface estimate the thickness to be 15.2 mm (0.60 in) at the 34.3 mm axial position. The calculation is based on the reference velocity and the distance from the start of the annular interface to the axial position of interest. This would indicate the boundary layers should just cover the entire flow channel. Due to differences in the flow over a flat plate and internal flow, this estimate is only an approximation. Additionally, scatter in the data points and insufficient velocity resolution (0.15 m/sec) near the center of the flow do not allow a conclusive determination of whether or not the boundary layers have merged at the 34.3 or 48.8 mm axial positions. At the 110 mm position, however, the velocity profile shows the effects of merged boundary layers (see Figure 26). As the flow velocities near the centerline have decreased from the values upstream, the velocities in the boundary layers have increased in order to satisfy continuity. Figure 27 shows that the turbulence in the annular inlet gradually increases in the center of the flow but decreases near the walls. Also, the disturbance caused by the wall discontinuity is seen to decrease as well as move away from the outer wall.

The boundary layers cover the entire flow channel at the 110 mm position but the velocity profile continues to develop as the flow moves downstream. The inlet length may be estimated using the results of Kirsten or Nikuradse discussed in the Theory section. In the case of an annulus, the channel width would be an appropriate characteristic dimension to use in determining the inlet length, since it is analogous to the diameter of a circular pipe when considering boundary layer growth. Based on Kirsten's work, the inlet length is at least 127 cm (50 inches) from the entrance to the annular interface. The minimum inlet length based on Nikuradse's results is 63 cm (25 inches). The entrance to the annular diffuser is 60 cm (23.5 inches) from the annular interface entrance.

The velocity profile development in the annular diffuser is shown in Figure 28. It shows the degree to which the velocities decrease as the flow channel increases in area. The movement of the peak velocities toward the inner wall due to its smaller boundary layer is also evident. Figure 29 shows the development of the turbulence intensity profile. There is no marked change in turbulence intensities although they are slightly less near the walls as the flow travels through the diffuser. These profiles, like

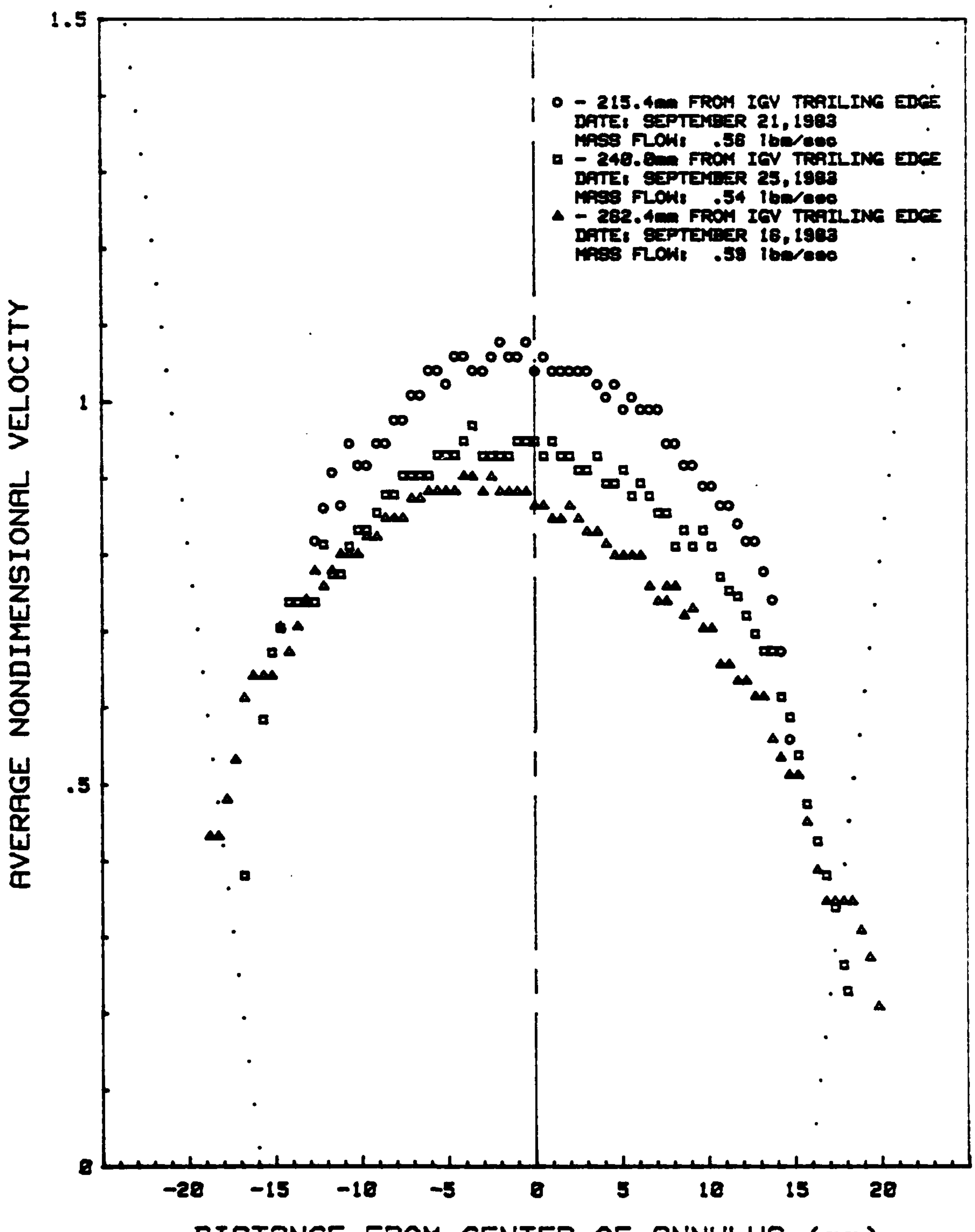

FIG. 28. ANNULAR DIFFUSER VELOCITY PROFILE DEVELOPMENT

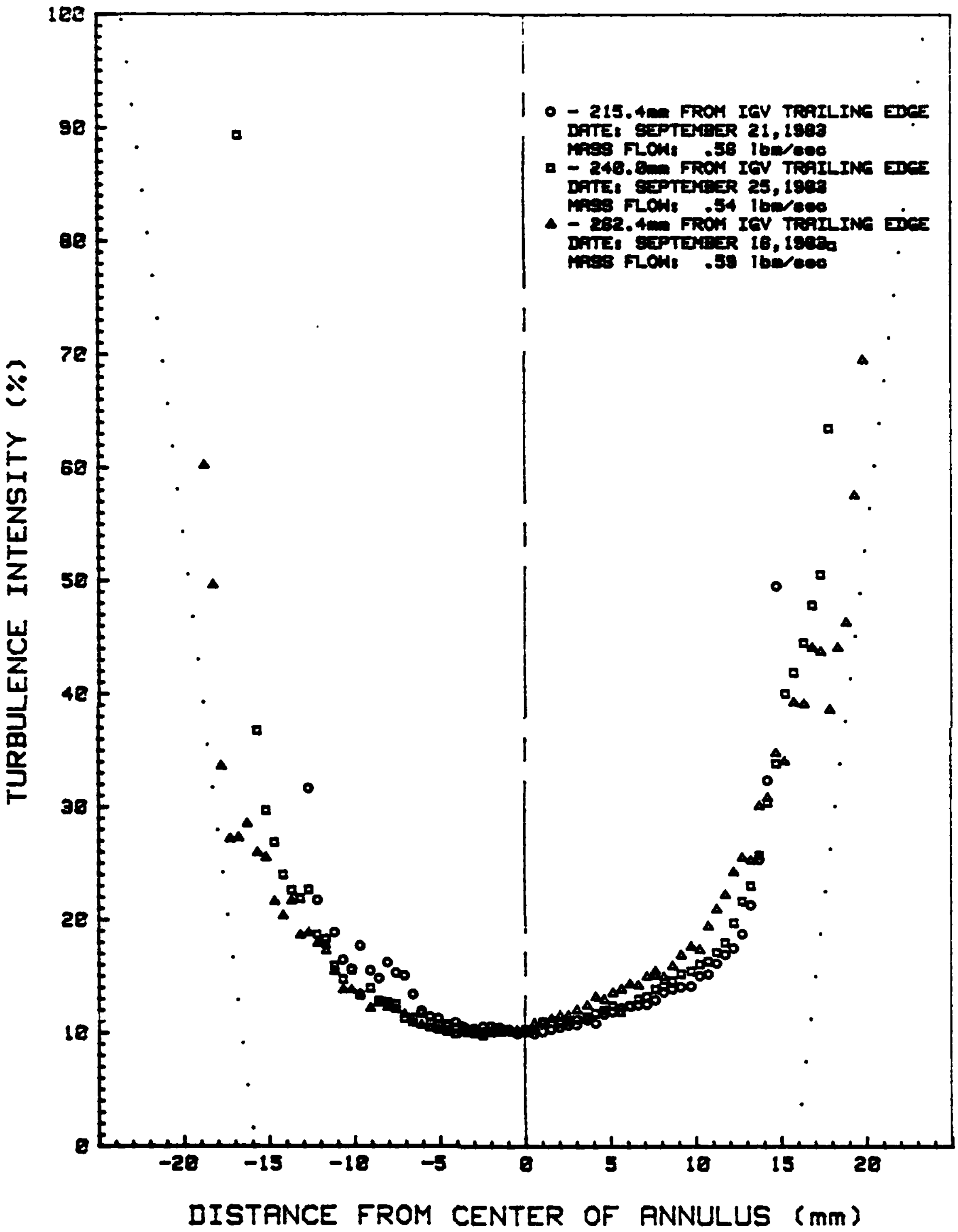

FIG. 29. ANNULAR DIFFUSER TURBULENCE INTENSITY PROFILE DEVELOPMENT

the velocity profiles, are skewed toward the inner wall because the turbulence intensity is calculated using the average velocity at each point.

LDA Repeatability

Figures 30 through 33 show the results of multiple tests at the 48.8 and 110 mm axial positions. The repeatability of the LDA measurements in the flow handling apparatus is quite good. Scatter in the data points on the velocity profiles can be due to the finite correlation time used to measure the flow. The resultant average velocity may be different than the true average obtained if the correlation time were allowed to approach infinity. Another cause for velocity point scatter, particularly near the center of the flow, is a velocity resolution which is approximately the same value as the velocity change between adjacent data points. Due to the digital nature of the correlation function, a velocity change of this amount may or may not be detected by the LDA system. For a development of the velocity resolution for this LDA system, see Appendix E.

The single biggest reason for scatter in turbulence intensity measurements is inadequate correlation times in high background light environments. Large amounts of background light and short correlation times at points in the outer half of the annulus at the 110 mm position caused the scatter in the points of Figure 33 between the 2.0 and 9.0 mm radial positions. A highly skewed and damped correlation function will also cause inaccurate, scattered

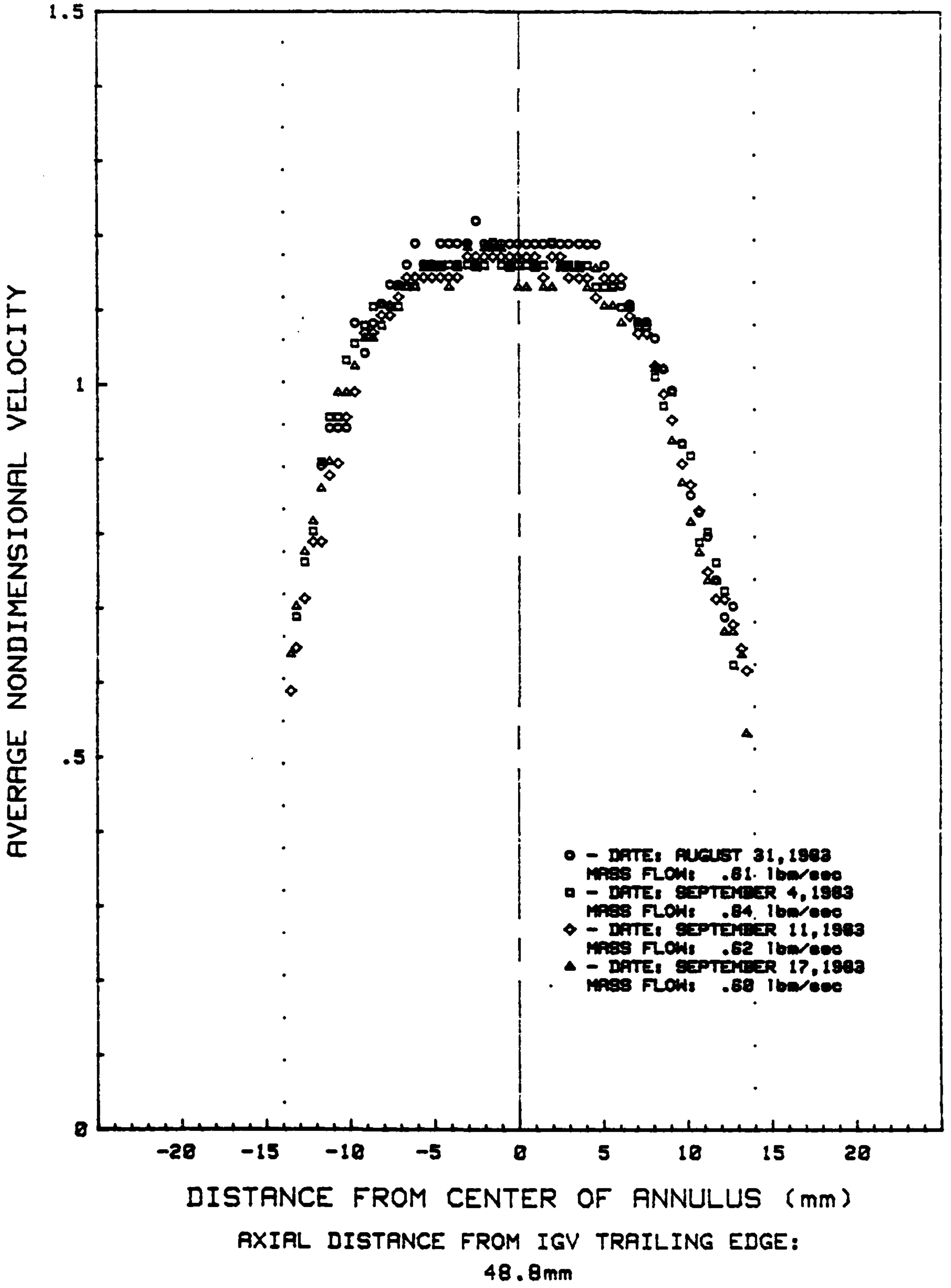

FIG. 30. LDA REPEATABILITY: VELOCITY PROFILE

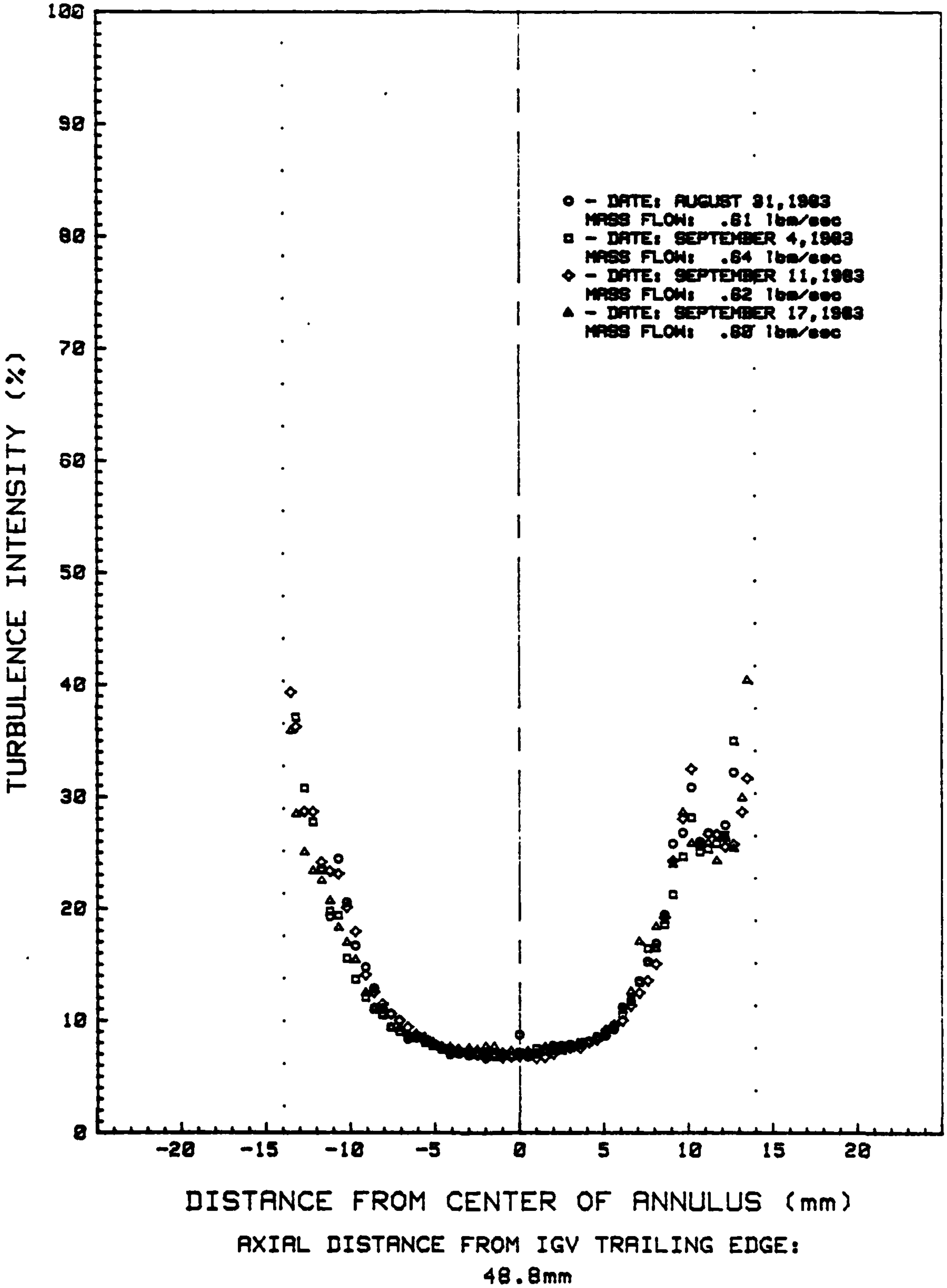

FIG. 31. LDA REPEATABILITY: TURBULENCE INTENSITY PROFILE

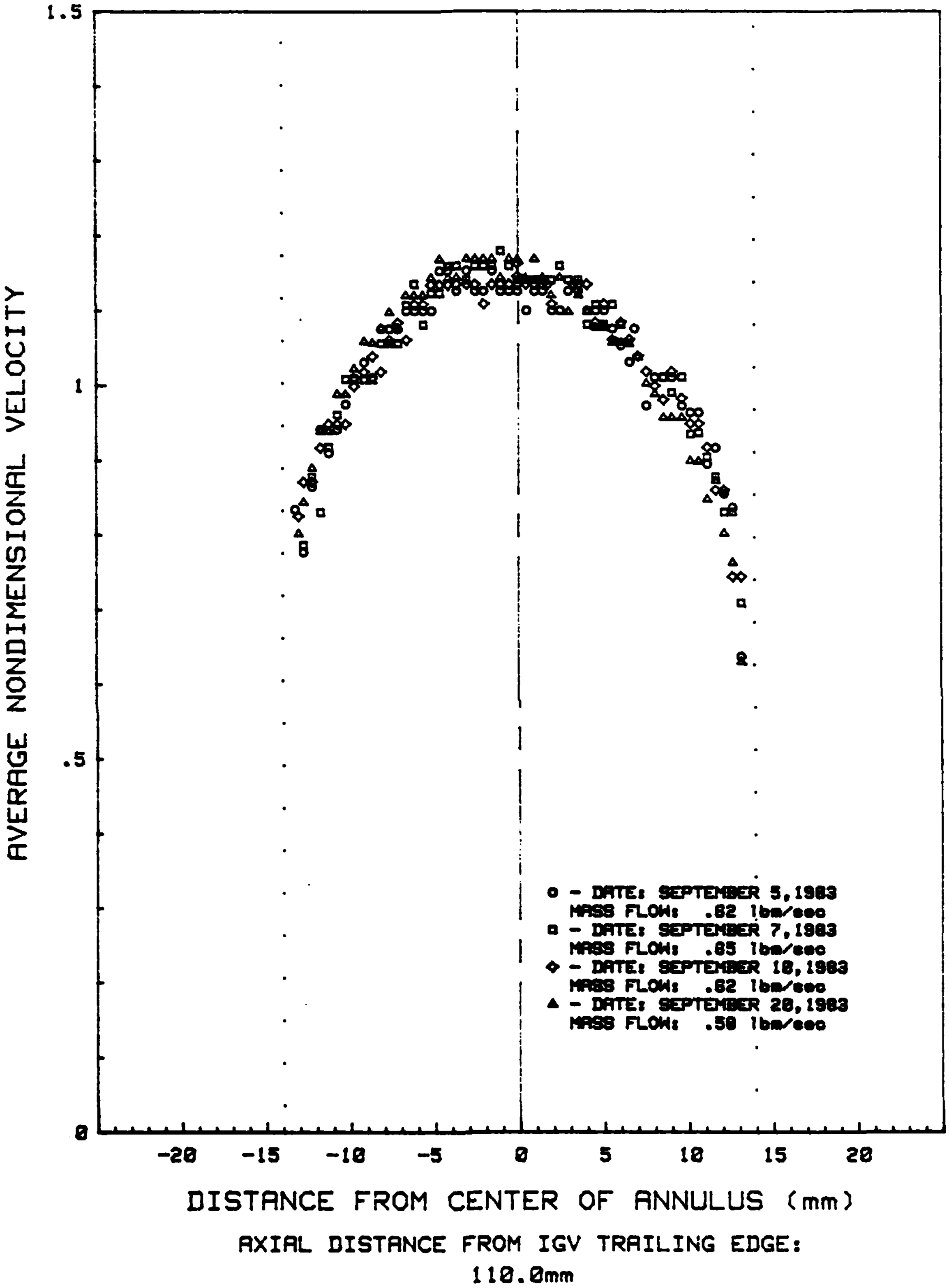

FIG. 32. LDA REPEATABILITY: VELOCITY PROFILE

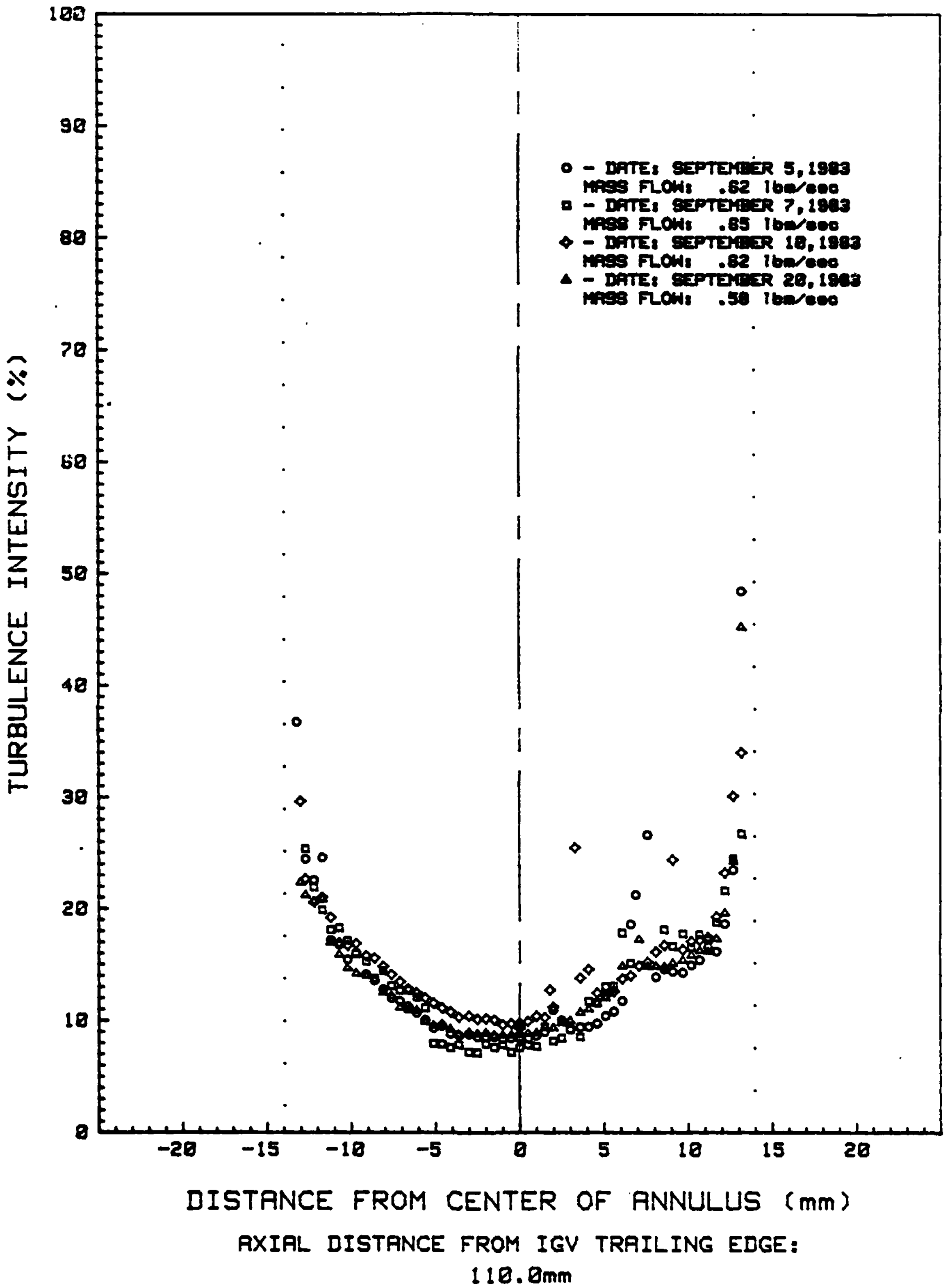

FIG. 33. LDA REPEATABILITY: TURBULENCE INTENSITY PROFILE

turbulence measurements because the data reduction method to unskew the function cannot do it as accurately as if an unskewed or slightly skewed function were generated from the start.

LDA and Hot Film Anemometer Comparison

The velocity measurements with the hot film anemometer are compared to the LDA measurements in Figures 34 through 38. The profiles agree closely except in the annular inlet test section (see Figures 34 and 35). The hot film velocities are higher near the center of the channel but close to the LDA measurements near the walls. A possible cause for this is the growth of thicker boundary layers in the hot film anemometer tests. The mass flow for the hot film tests was significantly lower than that of the LDA tests. This would result in more rapid boundary layer growth and a more rapid acceleration of the flow in the center of the channel as the flow progresses axially. After the boundary layers merge and the flow continues to develop in the inlet, the air enters the diffuser where the effect of the more rapid boundary layer growth is unnoticeable (see Figures 36 through 38).

The turbulence intensity profiles taken with the hot film anemometer are compared to the LDA data in Figures 39 through 43. The shapes of the hot film profiles are similar to the LDA profiles except in the annular inlet (see Figures 39 and 40). This difference seems to be related to the wall discontinuity. The turbulence from the discontinuity could move away from the wall more rapidly because of the quicker growth of the boundary layer in the hot film tests as compared to the LDA tests. Not including the wall

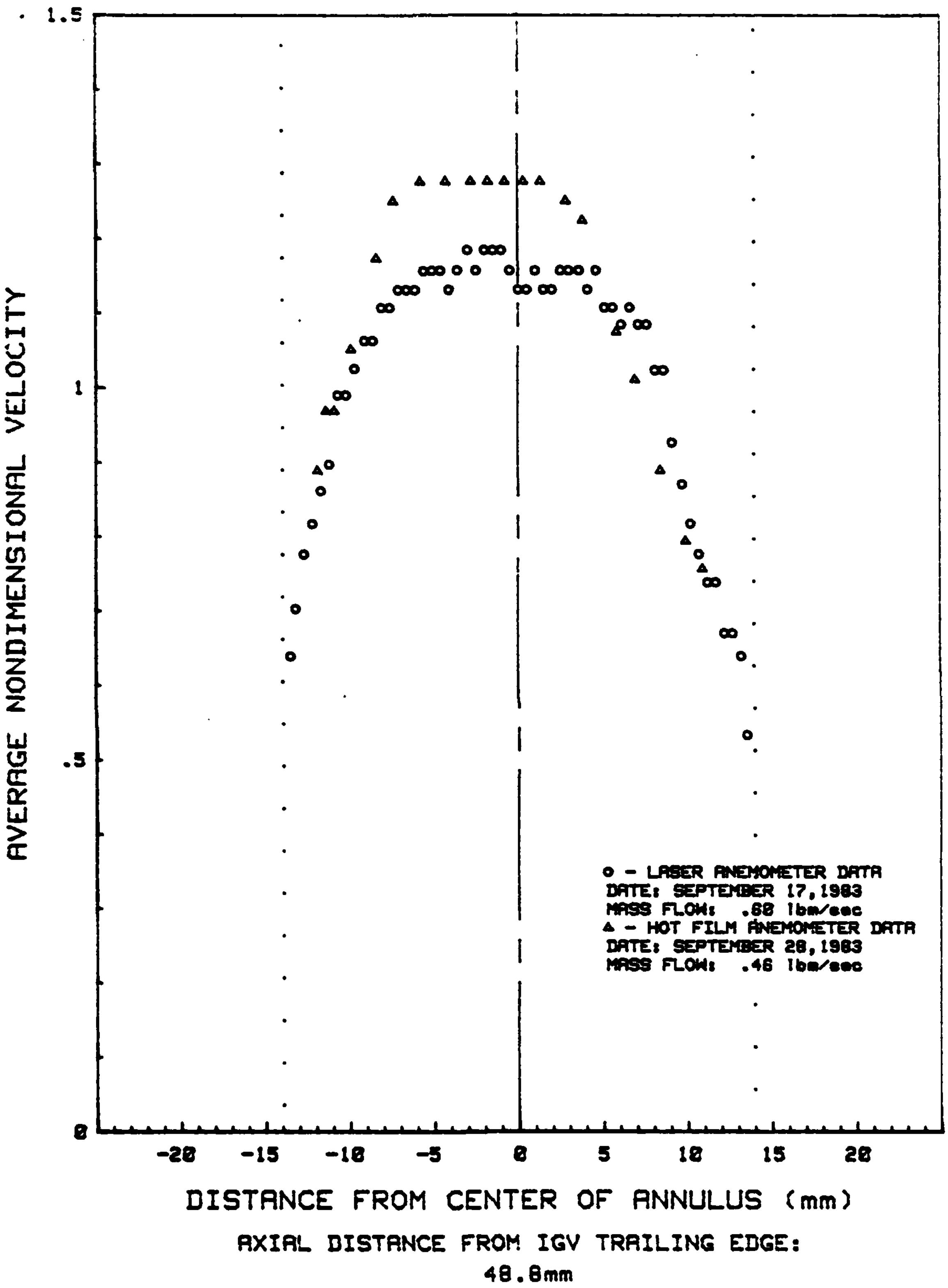

FIG. 34. LDA/HOT FILM ANEMOMETER VELOCITY PROFILE COMPARISON

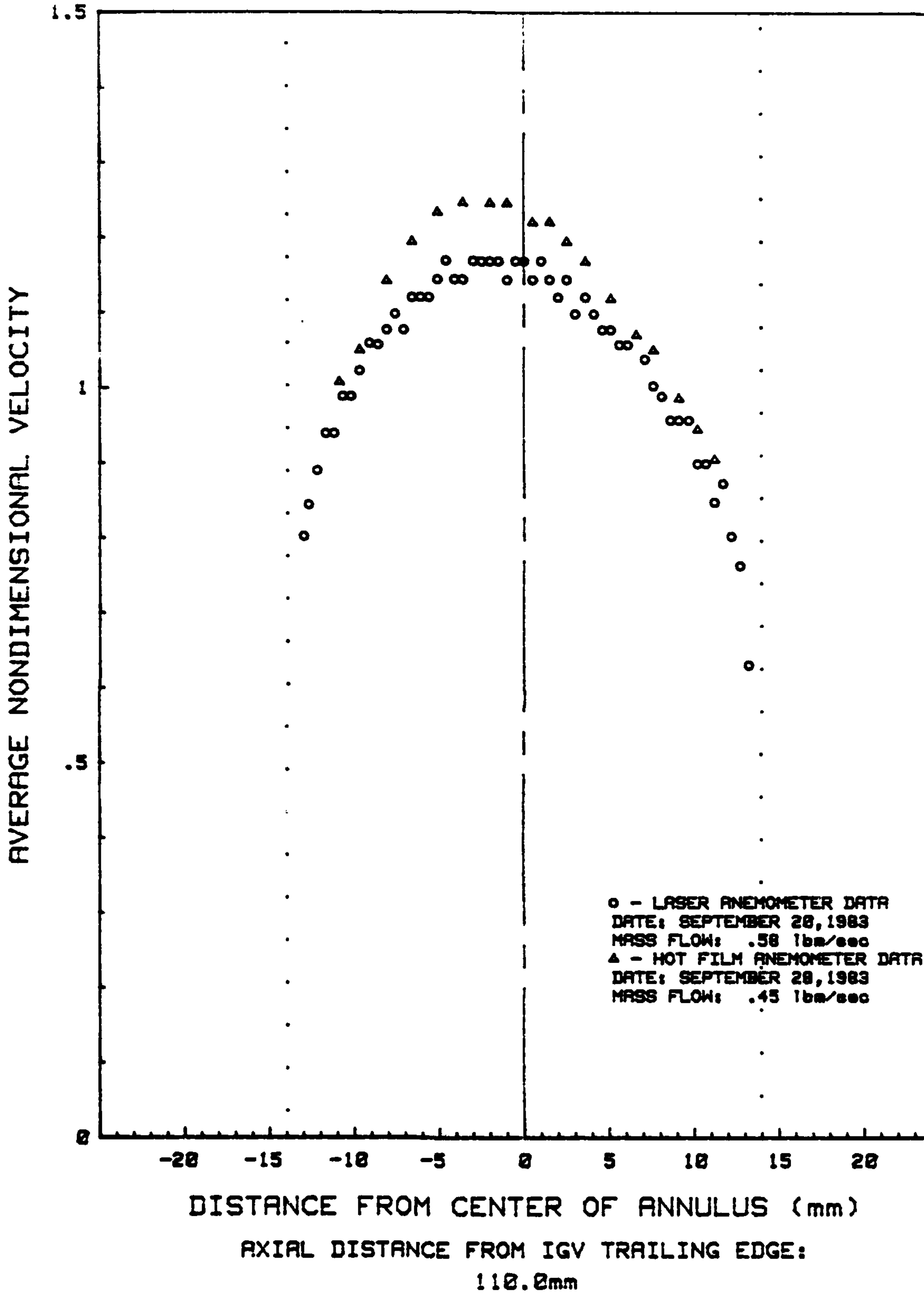

FIG. 35. LDA/HOT FILM ANEMOMETER VELOCITY PROFILE COMPARISON

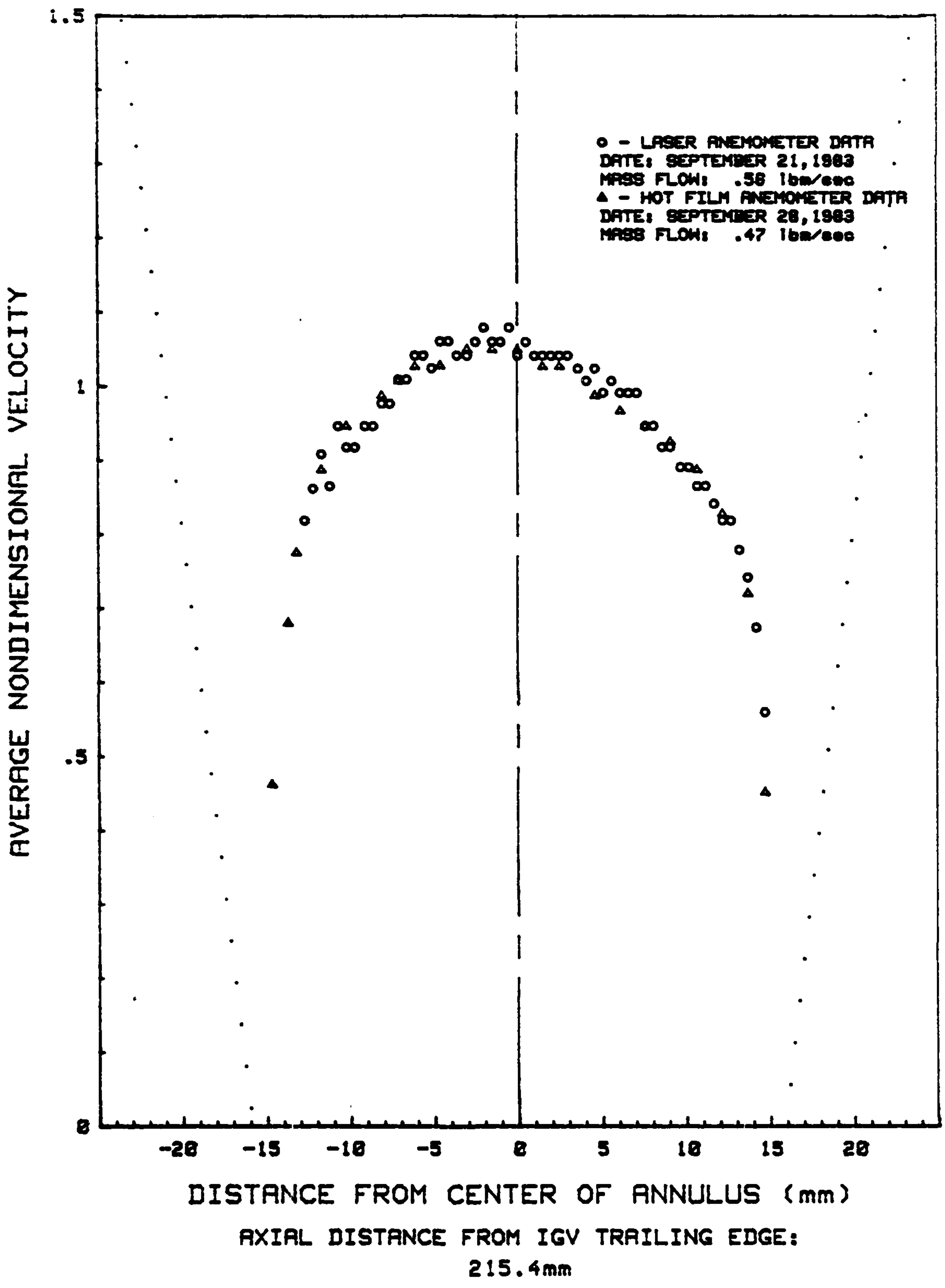

FIG. 36. LDA/HOT FILM ANEMOMETER VELOCITY PROFILE COMPARISON

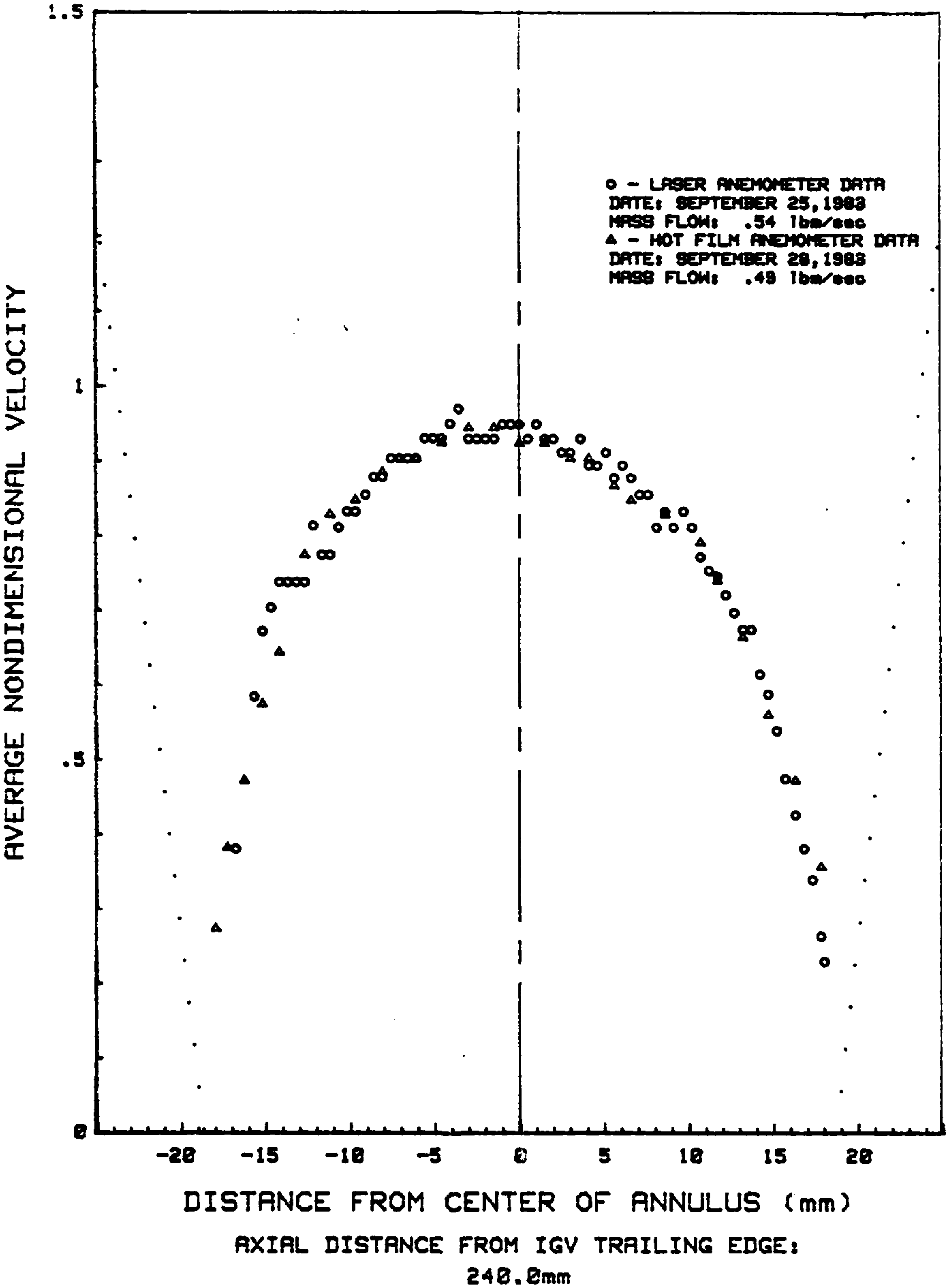

FIG. 37. LDA/HOT FILM ANEMOMETER VELOCITY PROFILE COMPARISON

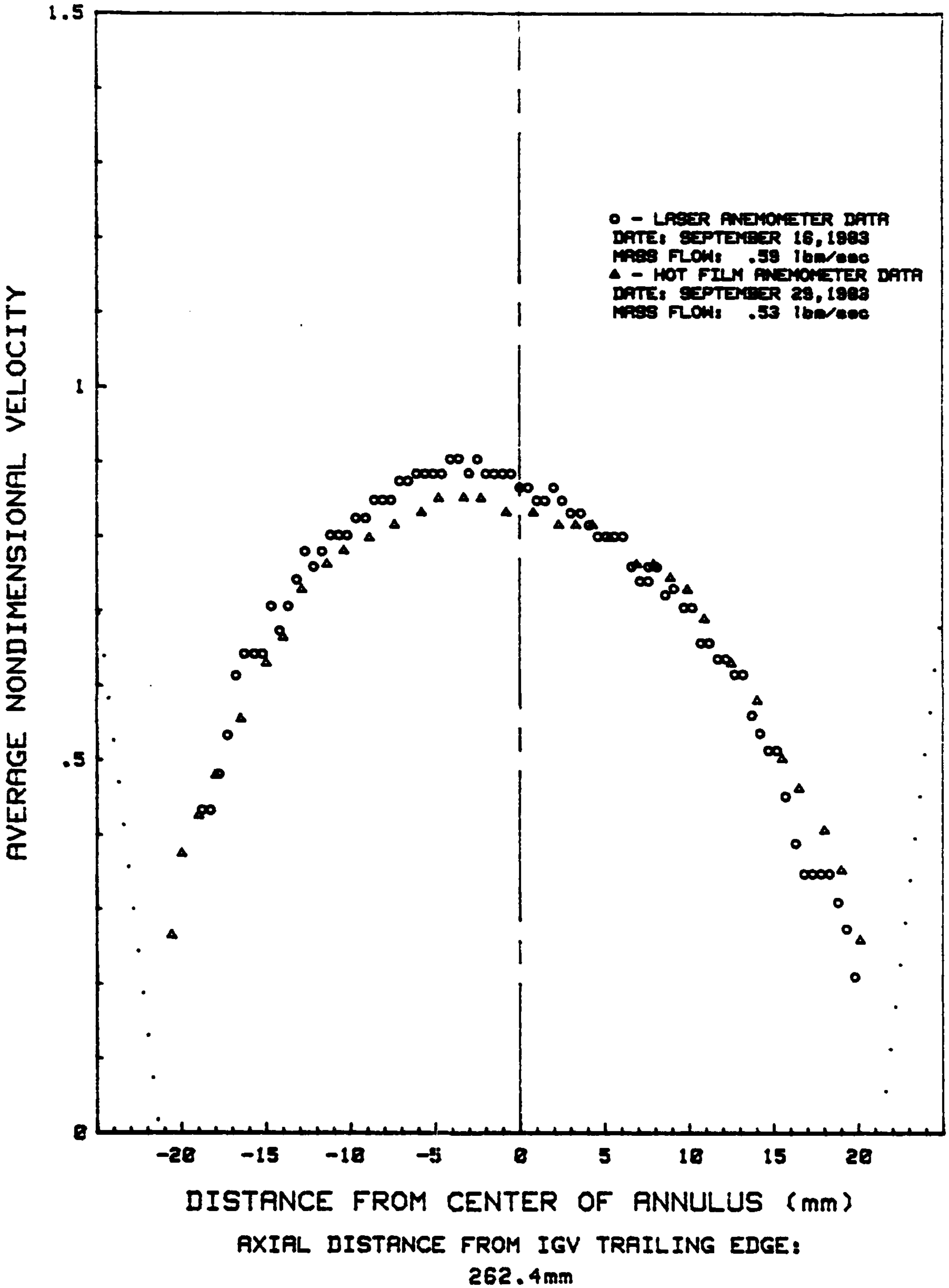

FIG. 38. LDA/HOT FILM ANEMOMETER VELOCITY PROFILE COMPARISON

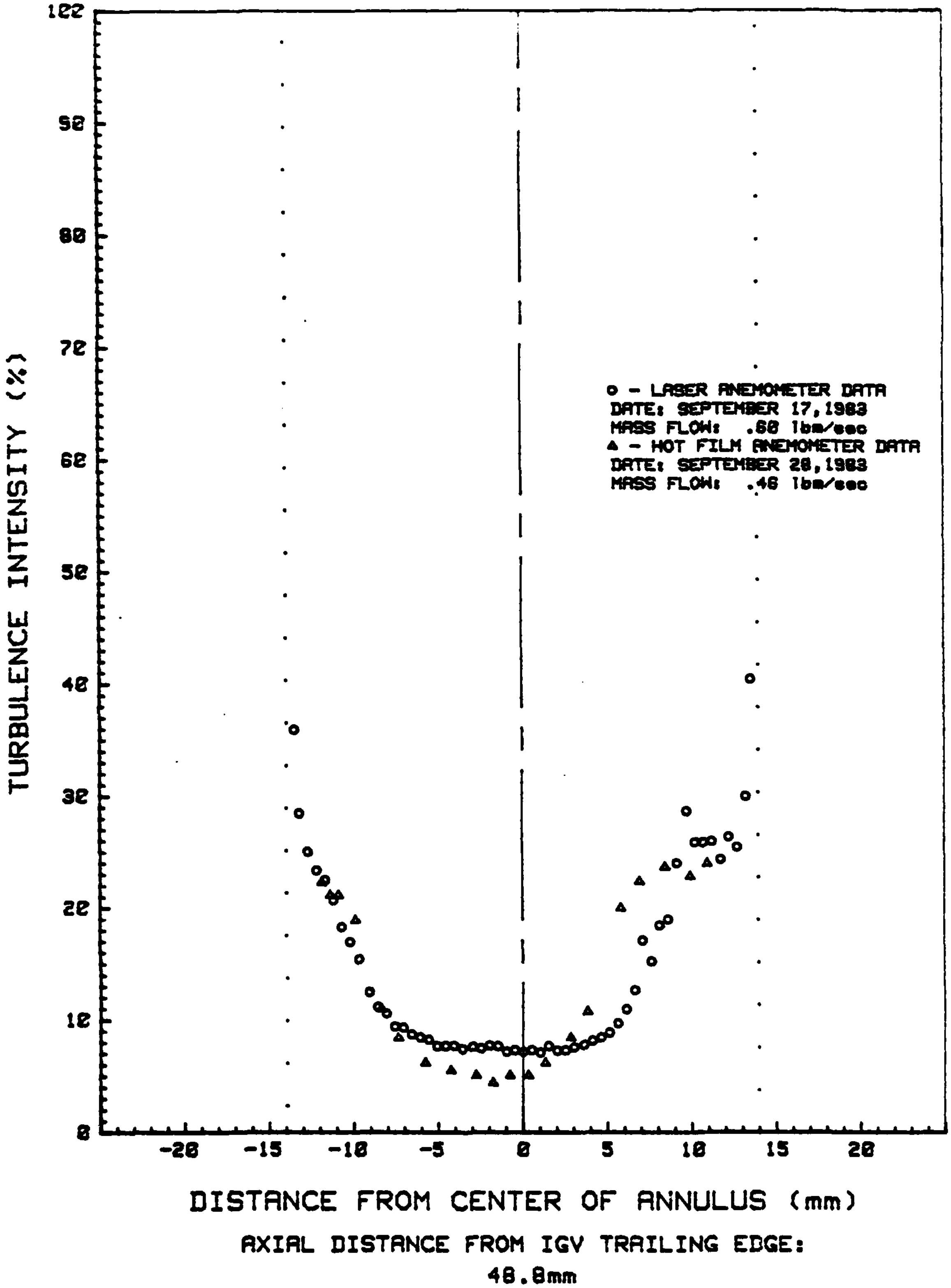

FIG. 39. LDA/HOT FILM ANEMOMETER TURBULENCE INTENSITY PROFILE COMPARISON

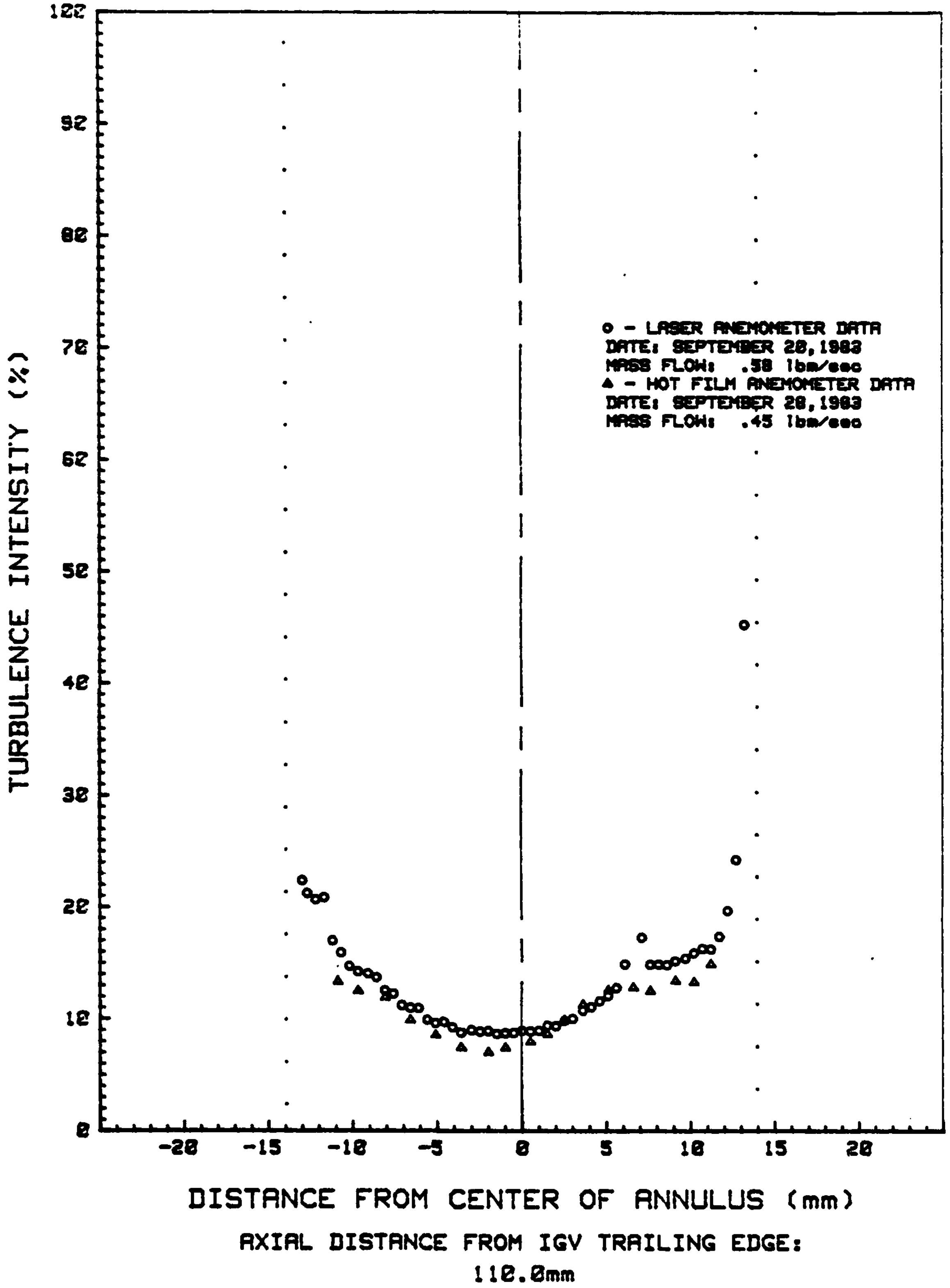

FIG. 40. LDA/HOT FILM ANEMOMETER TURBULENCE INTENSITY PROFILE COMPARISON

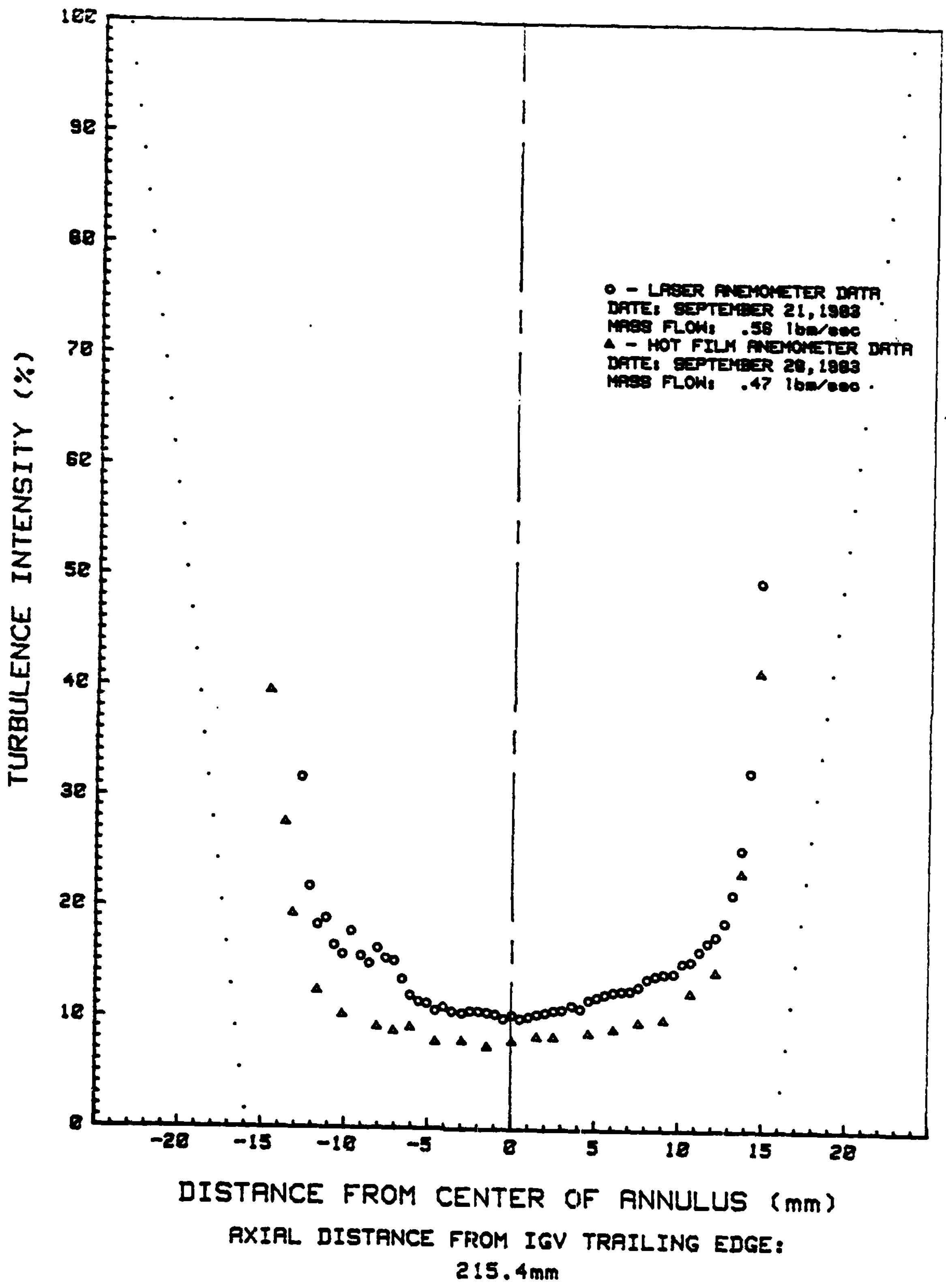

FIG. 41. LDA/HOT FILM ANEMOMETER TURBULENCE INTENSITY PROFILE COMPARISON

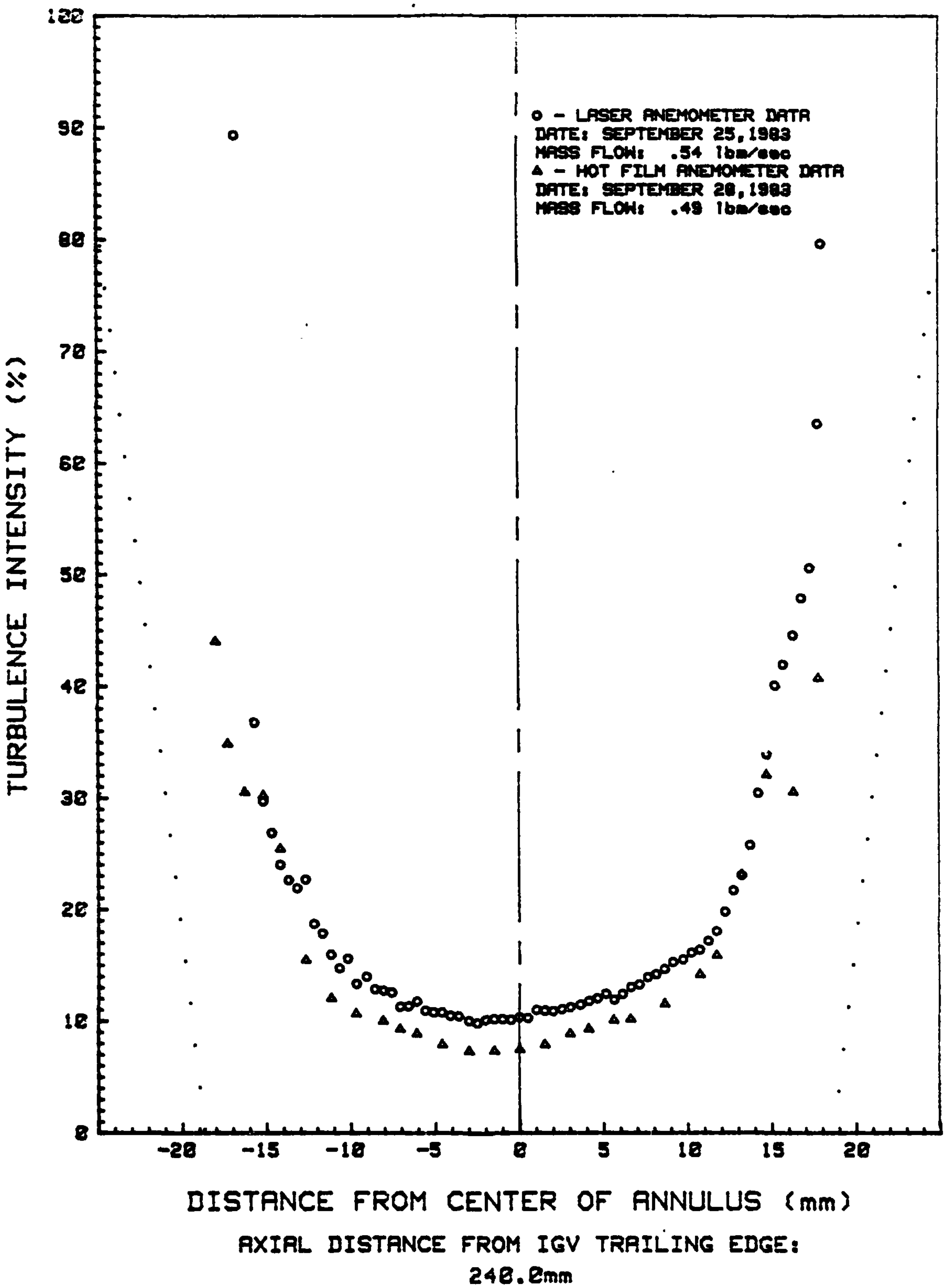

FIG. 42. LDA/HOT FILM ANEMOMETER TURBULENCE INTENSITY PROFILE COMPARISON

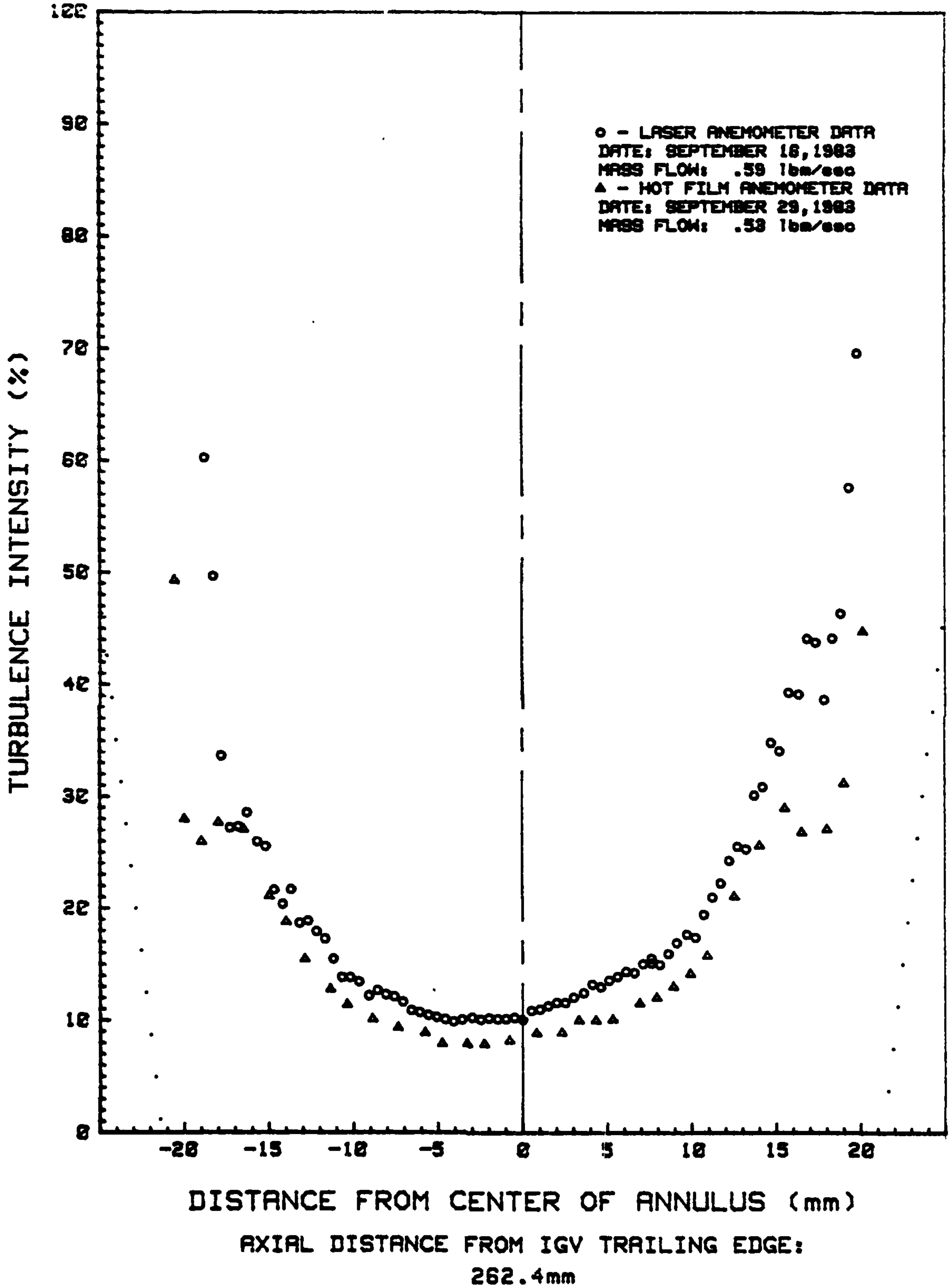

FIG. 43. LDA/HOT FILM ANEMOMETER TURBULENCE INTENSITY PROFILE COMPARISON

discontinuity disturbance, the turbulence intensities of the hot film tests are consistently lower than the LDA tests. This difference is probably due to the fact that seed particles were injected into the flow during the LDA measurements, but not during the hot film measurements. When the particle generator is operating, it injects the particles into the flow through the two 6.3 millimeter diameter orifices at jet velocities from 6.00 m/sec (19.7 ft/sec) to 6.94 m/sec (22.8 ft/sec), depending on the volume output of the unit. The local velocity of the main air flow is approximately 0.6 m/sec (2 ft/sec) at the point where the seed particles are introduced. The turbulence created by the mixing of these two streams would be carried downstream through the annular inlet and diffuser test sections.

Static Pressure Profile

The results of the static pressure measurements are contained in Table 1. The mass flow through the annulus was measured with the orifice plate flow meter and was 0.23 kg/sec (0.50 lbm/sec). The pressure recovery coefficient, $\Delta p/\overline{q}$, is defined as the static pressure rise from the pressure measured at the 29 mm axial position divided by the average dynamic pressure at the 29 mm position. (Figure 13 shows the relative positions of the data points in the test sections.) The average dynamic pressure was calculated using the air density at the 29 mm position and the continuity equation, $\dot{m} = \rho A \overline{V}$. The pressure recovery coefficient, as expected, is constant in the annular inlet. In the diffuser, it steadily in-

Table I

Static Pressure Profile

Axial Position (mm)	Static Pressure Rise from 29mm position (N/sq m)	Pressure Recovery Coefficient
29 (INLET)	0	0
48 "	0.479	.039
67 "	0.479	.039
86 "	0.479	.039
105 "	0.479	.039
200 "	0.479	.039
211 (DIFFUSER)	0.958	.078
224 "	2.394	.196
237 "	3.830	.314
249 "	5.267	.431
262 "	5.746	.471
275 "	6.224	.510
295 "	6.703	.549
380 (DUMP SECTION)	7.182	.588

creases, although most of the pressure recovery occurs in the first half of the diffuser. This data indicates a well-behaved diffuser with no separated regions causing jet flow.

Photon-correlating LDA Evaluation

The above discussions have alluded to some of the advantages and disadvantages of the photon-correlating LDA system. These will now be covered in more detail.

The photon-correlating LDA provides a non-intrusive means of measuring fluid flow in small flow channels and regions close to boundary surfaces. With good optical access, the LDA can measure internal flows where it would be difficult or impossible to insert a pitot or hot film probe. Good resolution is possible in low velocity flows as is evident in the velocity and turbulence profiles discussed earlier. The low light capabilities of the photon-correlating LDA make it ideal for low scattering particle densities and low-power lasers.

Laser anemometer systems also have their drawbacks. Without a method of filtering the signal caused by high background light levels, the long correlation times of a photon-correlating LDA mean long test times to obtain the same amount of data when compared with other flow measuring systems. Long correlation times eliminate any capability to make measurements of a dynamic fluid flow. Good optical access is an absolute requirement. Additionally, the laser light reflections inherent in measuring internal flows must be controlled or avoided so they do not mask the data completely or cause unnecessarily long correlation times. In high background light caused by these reflections, the correlation time necessary to acquire an accurate measurement cannot be predetermined. This requires a high degree of monitoring and control by the experimenter if correlation times are to be kept as short as possible. Thus, it becomes difficult to automate the flow measuring process.

The particular LDA system used in this research has limited flexibility in measuring the flow through the ADRF flow handling apparatus. The reason is a lack of phase modulator frequency shifts above one megahertz (positive or negative). Two advantages of frequency shifting are the capabilities it provides to measure flows with high turbulence intensity and to measure with high velocity resolution. While frequency shifts for the low velocities (1 to 7 m/sec) encountered in this research were adequate, they become inadequate at higher velocities. At velocities of 20 m/sec, the system can measure the flow with 0.94 m/sec resolution and turbulence intensities up to 46%. At velocities of 50 m/sec, these numbers change to 11.25 m/sec and 35%. These two figures can be improved by using larger fringe spacing with a longer focal length lens. However, the collecting optics now become the critical factor. If they are kept on the same platform as the focusing lens, the effective measuring volume becomes so large that the LDA no longer makes measurements at a "point". In this case, the effective length would be 2 mm (0.08 in) for a 500 mm focal length focusing lens and 7 mm (0.28 in) for a 1000 mm lens. The effective measuring volume length can be reduced by larger off-axis collection angles or by keeping the collecting optics close to the test section. However, difficulties arise in keeping the collecting optics aligned with the measuring volume due to the larger distances between the focusing lens and collecting optics. Note: A short effective measuring volume, while important in measuring three-dimensional flows, is not of concern in two-dimensional flows.

AD-A137 019   A STUDY OF ANNULAR DIFFUSER FLOW USING A   2/2
PHOTON-CORRELATING LASER DOPPLER..(U) AIR FORCE INST OF
TECH WRIGHT-PATTERSON AFB OH SCHOOL OF ENGI..
UNCLASSIFIED   J M DIERKSEN DEC 83 AFIT/GAE/AA/83D-6   F/G 20/4   NL

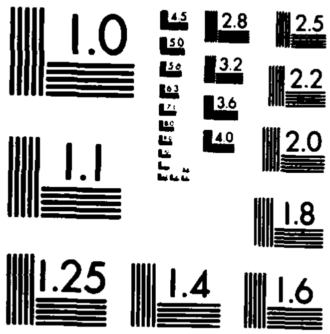

MICROCOPY RESOLUTION TEST CHART
NATIONAL BUREAU OF STANDARDS-1963-A

VI. Conclusions

Well-defined velocity and turbulence intensity profiles for the flow in an annular inlet and diffuser were obtained with a photon-correlating Laser Doppler Anemometer. While the exact point of boundary layer merging cannot be determined, the boundary layers do merge before the flow enters the diffuser. Nevertheless, the flow entering the diffuser is still not fully-developed. Flat plate, turbulent boundary layer predictions over-estimated the actual thickness by approximately 20%. The velocity profiles and static pressure measurements in the diffuser indicate flow which is not separated from the walls.

A non-dimensional velocity may be used to compare profiles of tests which were run at different mass flows. While this method is useful, it does not completely substitute for the comparison of tests at the same mass flow which have the same boundary layer growth rate.

The photon-correlating Laser Doppler Anemometer used in this research is well-suited to study the flow in the ADRF flow handling apparatus. The system, however, has three factors which limit its flexibility in measuring three-dimensional, internal flows. Its limited frequency shifting capability combined with the need to place the collecting optics close to the measuring volume limit it to the measurement of low speed flows. Without a means of filtering the signal caused by background light, the LDA system is limited to steady flow situations and requires long correlation times for each data point.

VII. Recommendations

The following recommendations are made for further studies using the ADRF flow handling apparatus:

1) Make flow studies using different diffuser geometries and higher mass flows, within the limitations of the LDA system.
2) Incorporate an active system to control the mass flow of the air supply.
3) Modify the optical platform to allow the PM assembly to be mounted on the opposite side of the focusing lens. This would allow the collecting optics to avoid laser beam reflections in the diffuser to obtain data points closer to the inner wall.
4) Use test section windows which have an anti-reflective coating for the helium-neon laser wavelength.
5) Incorporate a means of filtering the PM assembly signal to reduce or eliminate the effects of background light.
6) Add a computer-controlled traversing mechanism to the optical platform to move it in the radial direction. This would significantly reduce test times compared to tests requiring manual movement of the measuring volume.
7) Increase the range of phase modulator frequency shifting.

8) Investigate the effects on turbulence intensity of the method of flow seeding used in this study.

Bibliography

1. Kelley, J. V. Design, Fabrication and Testing of an Axisymmetric, Annular, Subsonic Diffuser and Associated Instrumentation Systems. MS Thesis. School of Engineering, Air Force Institute of Technology (AU), Wright-Patterson AFB OH, December 1981.

2. Moore, R. M. Design, Fabrication and Instrumentation of an Annular Diffuser Research Facility. MS Thesis. School of Engineering, Air Force Institute of Technology (AU), Wright-Patterson AFB OH, December 1982.

3. Crawford, M. E. and Kays, W. M. Convective Heat and Mass Transfer. New York: McGraw-Hill Book Company, 1980.

4. Schlichting, H. Boundary-Layer Theory. New York: McGraw-Hill Book Company, 1979.

5. Abbiss, J. B. et al. "Laser Doppler Anemometry," Optics and Laser Technology, 6: 249-261 (December 1974).

6. Malvern Instruments, Ltd., Laser Photon Correlation Velocimeter System: Operating and Installation Manual, Spring Lane Trading Estate, Malvern Link, Worcestershire WR14 1AL, England.

7. TSI LDV-879-23M-2MBRI. Laser Velocimetry Systems. Product Brochure and Technical Summary. Thermo-Systems, Inc., St. Paul MN, 1979.

8. Schulz-DuBois, E. O. "High Resolution Intensity Interferometry by Photon Correlation," Photon Correlation Techniques in Fluid Mechanics, edited by E. O. Schulz-DuBois. New York: Springer-Verlag Berlin Heidelberg, 1983.

9. Birch, A. D. et al. "Photon Correlation Spectroscopy and Its Application to the Measurement of Turbulence Parameters in Fluid Flows," Journal of Physics D: Applied Physics, 8: 438-447 (March 11, 1975).

10. Foord, R. et al. "A Solid-State Electro-optic Phase Modulator for Laser Doppler Anemometry," Journal of Physics D: Applied Physics, 7: L36-L39 (January 21, 1974).

11. Walterick, R. E. An Experimental Investigation of the Near Wake of a Circular Cylinder. MS Thesis. School of Engineering, Air Force Institute of Technology (AU), Wright-Patterson AFB OH, September 1980.

12. Neyland, D. L. Hardware and Software Integration for Concurrent Data Acquisition and Reduction of Photon Correlated Laser Doppler Velocimetry. MS Thesis. School of Engineering, Air Force Institute of Technology (AU), Wright-Patterson AFB OH, December 1981.

13. Stephens, D. G. Turbulence Measurement in an Ejector Wing Flow Field Using Photon Correlated Laser Doppler Velocimetry. MS Thesis. School of Engineering, Air Force Institute of Technology (AU), Wright-Patterson AFB OH, December 1981.

Appendix A:

Measuring Volume Size

The actual size of the measuring volume is defined by the $1/e^2$ intensity contour and may be calculated using Eqs (19) and (20)

$$d_m = \frac{2\lambda f}{\pi r_o \cos\left(\frac{\theta}{2}\right)} \tag{19}$$

$$l_m = \frac{2\lambda f}{\pi r_o \sin\left(\frac{\theta}{2}\right)} \tag{20}$$

where d_m is the measuring volume diameter, l_m is the measuring volume length along the major axis of the ellipsoid, and r_o is the unfocused $1/e^2$ beam radius (7:97). The number of fringes in the measuring volume can be calculated using Eq (21).

$$N = \frac{d_m}{d_f} \tag{21}$$

The collecting optics, however, determine the effective measuring volume size because they may only collect scattered light from a portion of the actual measuring volume. The geometry of the collecting optics is shown in Figure 44. This figure shows the collecting optics to be in the same plane as the two laser beams, but this does not have to be the case. The effective measuring volume length can be calculated using Eq (22)

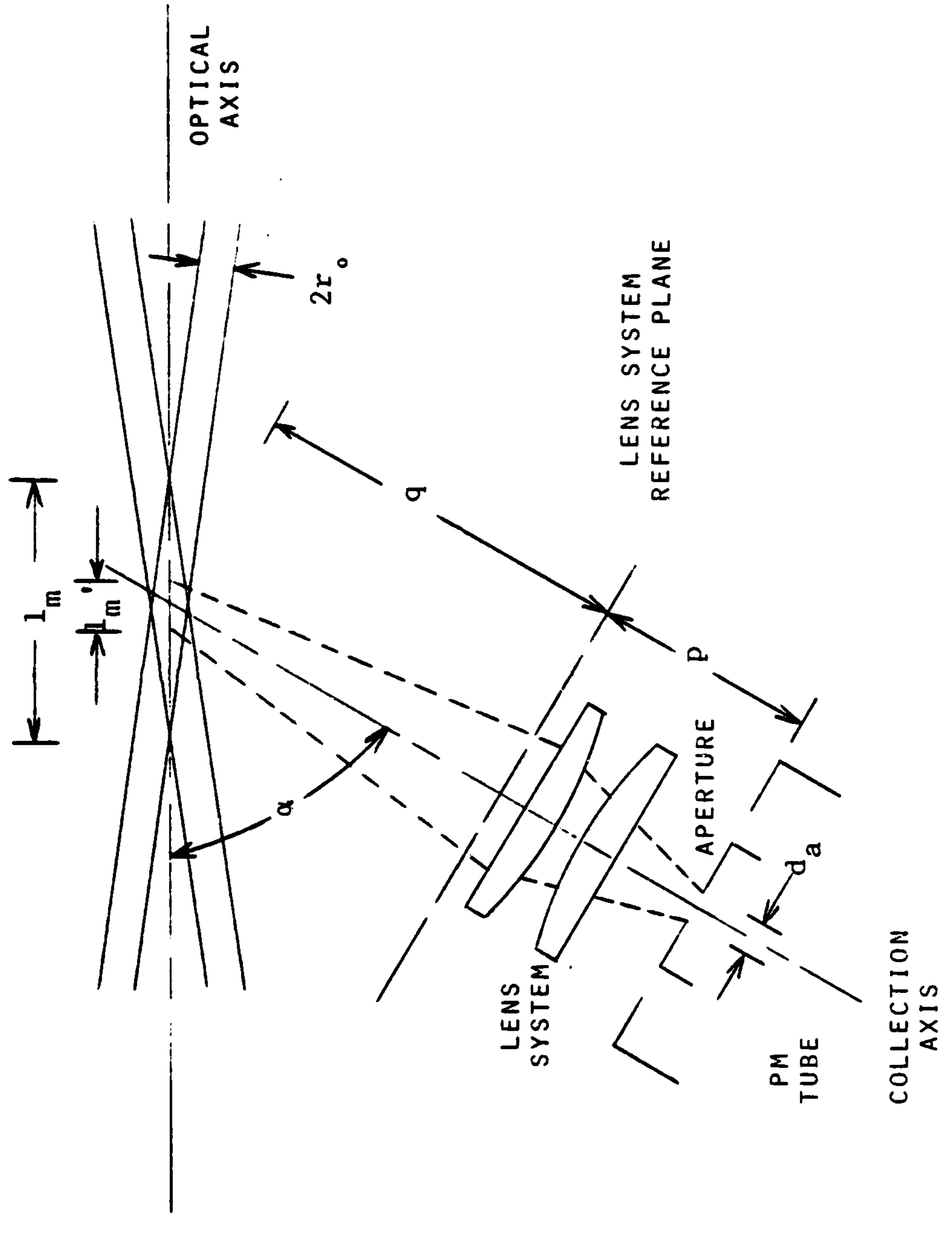

FIG. 44. COLLECTING OPTICS GEOMETRY

$$l_m' = d_a \frac{q}{p \sin \alpha} \tag{22}$$

where α is the angle between the optical axis and the collection axis (7:98). The effective measuring volume length will be the lesser of l_m and l_m' since it can never be larger than l_m. A similar method can be used to calculate the effective vertical dimension of the measuring volume by replacing sin α with the cosine of the angle (β) between the collection axis and the plane of the two intersecting beams.

$$d_m' = d_a \frac{q}{p \cos \beta} \tag{23}$$

Likewise, the effective vertical dimension will be the lesser of d_m and d_m'. Lastly, the effective horizontal dimension (perpendicular to the fringe planes) will be the lesser of d_m and d_m'' where d_m'' is defined by Eq (24).

$$d_m'' = d_a \frac{q}{p \cos \alpha} \tag{24}$$

The following are the applicable dimensions for the optical geometry of the LDA system used in this research.

$\lambda = 6328\ (10^{-10})$ m	$p = 205$ mm
$f = 250$ mm	$q = 211$ mm
$r_o = 0.55$ mm	$\alpha = 16.9°$
$\theta = 4.58°$	$\beta = 1.7°$
$d_m = 183\ \mu m$	$l_m' = 354\ \mu m$
$l_m = 4581\ \mu m$	$d_m' = 103\ \mu m$
$d_a = 100\ \mu m$	$d_m'' = 108\ \mu m$

Appendix B:

LDA Optical Alignment Procedure

The first step in the procedure involves mounting and aligning the laser/beamsplitter and phase modulator on the steel mounting channel. When the laser is on during the alignment procedure, protective goggles should be worn, not only for safety reasons, but because they reduce the reflected laser light from surfaces and give a more accurate indication of the beam center. The beamsplitter is adjusted so the two laser beams are parallel and 20 mm apart. The laser is mounted to the steel mounting channel so the plane of the beams is parallel to the mounting surface and at the correct height for the phase modulator. After the beams and phase modulator are aligned as specified in the system operating manual (reference 6), the final adjustment of the beamsplitter is made to ensure the beams are parallel and 20 mm apart. This is done to correct for any possible flaws in the phase modulator optics which could affect the parallel nature or 20 mm separation of the beams. The laser, beamsplitter, and phase modulator can now be treated as a single unit which can be aligned with the remaining optics using the four adjustable legs on the mounting channel.

The second unit in the alignment process is the optical platform which contains the remainder of the transmitting and collecting optics. The optical platform is mounted on the laboratory bench so it translates in a direction perpendicular to the bench rails and is leveled in the horizontal plane. The beams are then aligned on the lower periscope mirror so as the optical platform is translated, the beams always project to the same points on a screen fixed to the platform. With the beams projecting on a screen attached to the annular inlet test section window, the periscope mirrors are adjusted to keep the beam projections stationary as the platform is translated. [illegible] focusing lens is placed in its holder and an alignment mask i[illegible] serted into the lens. The mask is an aluminum disk which sn[illegible] slides into one side of the lens. It has two 0.75 millimeter (0.03 in) diameter holes, each 10 millimeters (0.39 in) from the center along the same diameter. Scribe marks on the mask are aligned with marks on the lens holder to ensure the alignment holes are horizontal. The focusing lens can then be positioned so the beams pass through the alignment holes. This aligns the center of the lens with the optical axis. As the platform is translated, the beams can be rechecked to ensure they always pass through the alignment mask holes. The beams are then focused on the test section centerbody and the PM assembly positioned so the image is centered and focused on the aperture. Gross focusing adjustments are made by moving the PM assembly on the optical platform while fine focusing is done with the collecting lens. The PM assembly is aligned with the laser beams focused on the test section centerbody to account for the effects of beam refraction through the test section windows. The optical platform is positioned in the vertical direction to place the measuring volume in the horizontal plane passing through the test section centerbody axis. This plane is centered between two IGV blades upstream of the annular inlet test section. Finally, with the beams focused on the centerbody, the laboratory bench is positioned so the beams remain focused as the bench is translated.

Appendix C:

LDA Velocity and Turbulence Calculations

The velocity and turbulence measurements of the photon-correlating LDA are based on the intensity autocorrelation function. This function is simply a time correlation of the scattered light intensity which highlights the periodic nature of the signal. The periodicity is due to the ordered motion of the particles transiting the measuring volume. In other words, most particles are moving in the same direction with the same velocity. For these reasons, the time between $\tau = 0$ and the value of τ where the next peak of the autocorrelation function occurs is a measure of the average time it takes the particles to travel a specified distance. This distance, using the fringe model, is the fringe spacing and the velocity may be calculated with Eq (25)

$$u = \frac{d_f}{(Pk2-3)\ t_s} \tag{25}$$

where Pk2 is the channel number (value of τ) at which the autocorrelation function reaches its first peak after the first valley (see Figure 45) (6:6-5).

Turbulence in the flow is indicated by damping of the correlation function. Due to flow turbulence, the velocity of every particle is a function of time so some of the particles in a fringe at any specified time will not reach the next fringe

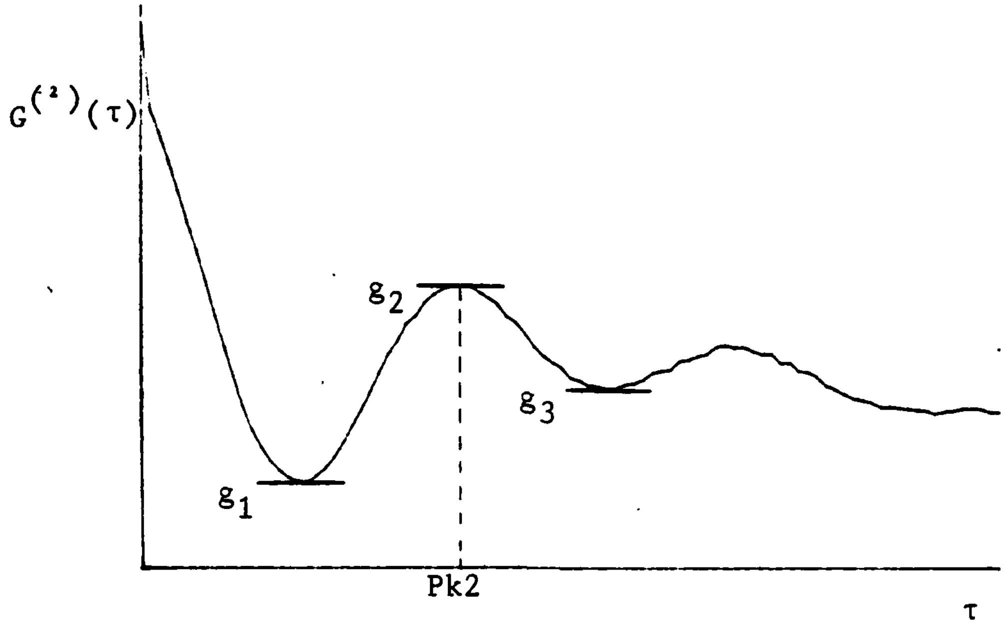

FIG. 45. CORRELATION FUNCTION: VELOCITY AND TURBULENCE INFORMATION

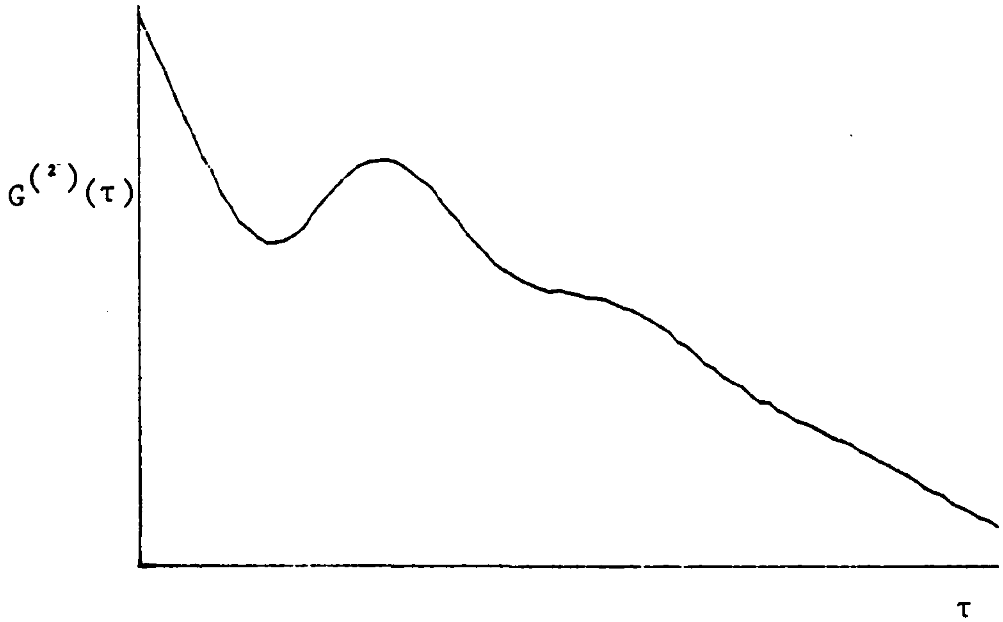

FIG. 46. SKEWED CORRELATION FUNCTION

at the same time in the future as the other particles. This results in less time correlation in the signal for increasing values of τ. The result is a damped autocorrelation function. The turbulence intensity may be calculated from the correlation function using Eqs (26) and (27)

$$R = \frac{g_2 - g_1}{g_2 - g_3} \tag{26}$$

$$\eta = \frac{1}{\pi}\left(\frac{1}{2}(R-1) + \frac{2}{N^2}\right)^{\frac{1}{2}} \tag{27}$$

where g_1, g_2, and g_3 are the values of the correlation function at the first valley, the next peak, and the second valley respectively (see Figure 45) (6:6-6). Also, N is the number of fringes in the $1/e^2$ radius of the measuring volume and η is the turbulence intensity.

The correlation function may be skewed due to an insufficient number of fringes in the control volume or the detection of background light (see Figure 46) (13:91). This skewedness must be removed from the correlation function before the information for velocity and turbulence calculations is extracted. The method used to do this is described by Stephens (reference 13). A brief summary is included here.

A mean line from which the correlation function can be unskewed must first be determined. A least-squares polynomial curvefit through the local maxima (peaks) and another curvefit through the local minima (valleys) is determined. A mean line is then calculated at each correlator channel by averaging the value of the two curves at that channel. The unskewed correlation function is the difference between the skewed function and the mean function. It is from the unskewed correlation function that the values of g_1, g_2, g_3, and Pk2 are taken.

The equations discussed earlier are strictly for use when phase modulation of the laser beams is not employed. They are, however, the basis of the equations used to calculate average velocity and turbulence intensity when phase modulation is in use. Figure 47 shows the effects of phase modulation (frequency shifting) on the correlation function in measuring the same point in a flow. With positive frequency shifting (DRIVE mode), the fringes move in the direction of the flow component being measured. On the other hand, the fringes move in the opposite direction with negative frequency shifting (INVERT mode). Thus, the correlation function contains velocity and turbulence information of the particles with respect to the reference frame of the fringes. To calculate the particle velocity with respect to the laboratory reference frame, Eq (28) is used.

$$u = u^{*} + \Delta F(d_f) \tag{28}$$

In this equation, u^* is the velocity of the particle with respect to the fringes and is calculated from the unskewed correlation function. A velocity is first calculated from the unskewed correlation function and then adjusted for frequency shifting.

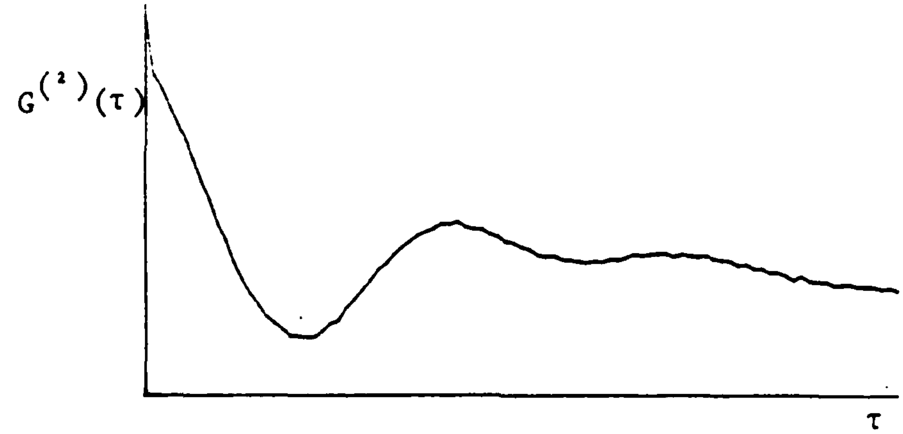

(A) POSITIVE FREQUENCY SHIFTING

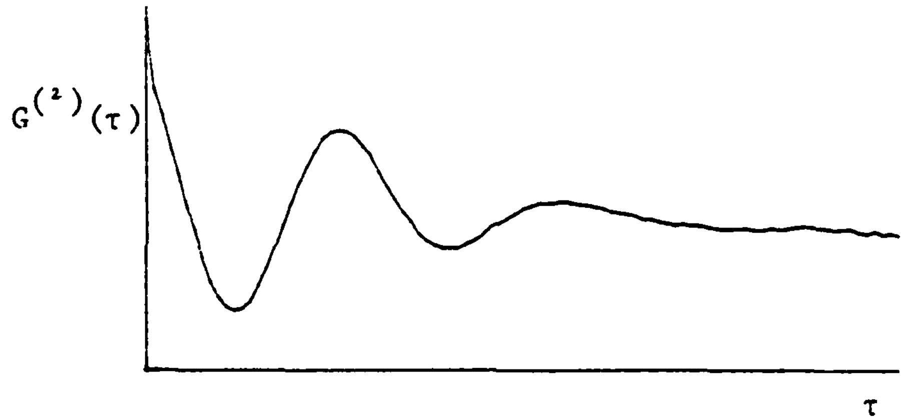

(B) ZERO FREQUENCY SHIFTING

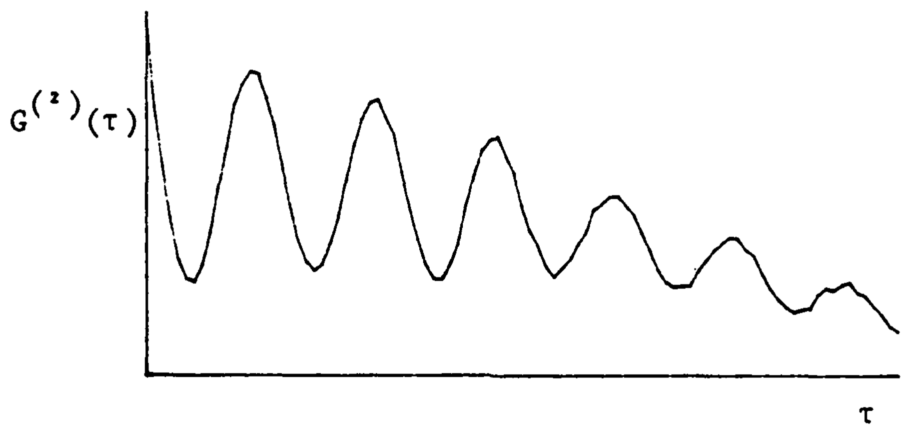

(C) NEGATIVE FREQUENCY SHIFTING

FIG. 47. EFFECTS OF FREQUENCY SHIFTING ON CORRELATION FUNCTION

The equation for calculating the turbulence intensity with frequency shifting is also slightly different than Eq (27) and may be developed in the following way. The turbulence intensity is defined by Eq (29)

$$\eta = \frac{\left(\frac{\sum_{i=1}^{n} (u_i - u)^2}{n}\right)^{\frac{1}{2}}}{u} \tag{29}$$

where u_i is the instantaneous absolute velocity, u is the average absolute velocity, and n is the number of velocity samples taken. Eq (30) may be inferred from Eq (28)

$$u_i = u_i^* + \Delta F(d_f) \tag{30}$$

where u_i^* is the instantaneous velocity of the particle with respect to the fringes. Substituting Eqs (28) and (30) into Eq (29) yields

$$\eta = \frac{\left(\frac{\sum_{i=1}^{n} [u_i^* + \Delta F\ d_f - (u^* + \Delta F\ d_f)]^2}{n}\right)^{\frac{1}{2}}}{u}$$

$$= \frac{\left(\frac{\sum_{i=1}^{n} (u_i^* - u^*)^2}{n}\right)^{\frac{1}{2}}}{u} \tag{31}$$

The turbulence intensity of the particles with respect to the fringes (η^*) may be defined by Eq (32).

$$\eta^* = \frac{\left(\frac{\sum_{i=1}^{n} (u_i^* - u^*)^2}{n} \right)^{1/2}}{u^*} \tag{32}$$

Eq (33) results from the combination of Eqs (31) and (32).

$$\eta u = \eta^* u^* \tag{33}$$

This equation may be rewritten as such

$$\eta = \eta^* \frac{u^*}{u} \tag{34}$$

Eq (34) is the equation needed to calculate the absolute turbulence intensity of the flow when frequency shifting is used. Note: Eq (25) is used to calculate u^* and Eq (27) is used for η^*. Without frequency shifting, u equals u^* and hence η equals η^*.

Appendix D:

Laser Doppler Anemometer Data

DATE: SEPTEMBER 20,1983 PAGE NO. 1

AXIAL POSITION FROM IGV TRAILING EDGE: 34.3mm

RADIAL POSITION (mm)	SAMPLE TIME (nsec)	FREQUENCY SHIFT (KHz)	Pk2	G1	G2	G3	R	TURBULENCE INTENSITY (%)	AVERAGE VELOCITY (m/sec)
-13.0	50	-200.0	31	129748	165486	148277	2.07671	32.5	4.07
-12.7	50	-200.0	31	215147	273453	242284	1.87064	29.3	4.07
-12.2	50	-200.0	29	237287	301551	266624	1.83995	28.0	4.50
-11.7	50	-200.0	28	415101	501179	449588	1.66848	24.7	4.75
-11.2	50	+0.0	33	263109	332643	294728	1.83395	20.6	5.27
-10.7	50	+0.0	32	253346	332249	282937	1.60005	17.5	5.46
-10.2	50	+0.0	30	256471	325068	273635	1.47734	15.7	5.86
-9.7	50	+0.0	31	276040	349816	296968	1.39599	14.3	5.65
-9.1	50	+200.0	39	231950	295092	253006	1.50033	11.8	5.93
-8.6	50	+200.0	38	253846	330069	276543	1.42404	11.0	6.10
-8.1	50	+200.0	38	211493	280330	230279	1.37532	10.3	6.10
-7.6	50	+200.0	37	211786	282973	228568	1.30845	9.4	6.23
-7.1	50	+200.0	37	198681	269164	213218	1.25985	8.7	6.23
-6.6	50	+200.0	37	192882	264212	206840	1.24330	8.4	6.23
-6.1	50	+200.0	37	238695	323764	254422	1.22680	8.1	6.23
-5.6	50	+200.0	36	232886	318001	247312	1.20407	7.8	6.33
-5.1	50	+200.0	37	196597	271457	208933	1.19730	7.6	6.23
-4.6	50	+200.0	36	198183	272798	209791	1.18424	7.4	6.33
-4.1	50	+200.0	35	223589	306047	236222	1.18092	7.4	6.53
-3.6	50	+200.0	35	353269	430965	365596	1.20704	7.9	6.53
-3.0	50	+200.0	35	372788	454804	386105	1.19386	7.7	6.53
-2.5	50	+200.0	36	337833	420565	351591	1.19947	7.7	6.33
-2.0	50	+200.0	35	373119	464382	387463	1.18655	7.5	6.53
-1.5	50	+200.0	36	328171	418930	341067	1.16562	7.0	6.33
-1.0	50	+200.0	36	299649	379733	312274	1.18715	7.5	6.33
-.5	50	+200.0	35	262057	337654	274958	1.20578	7.9	6.53
0.0	50	+200.0	36	243351	312691	254487	1.19132	7.5	6.33

DATE: SEPTEMBER 20,1983 PAGE NO. 2

AXIAL POSITION FROM IGV TRAILING EDGE: 34.3mm

RADIAL POSITION (mm)	SAMPLE TIME (nsec)	FREQUENCY SHIFT (KHz)	Pk2	G1	G2	G3	R	TURBULENCE INTENSITY (%)	AVERAGE VELOCITY (m/sec)
.5	50	+200.0	36	244020	316567	255535	1.18868	7.5	6.33
1.0	50	+200.0	36	238937	308357	250909	1.20841	7.9	6.33
1.5	50	+200.0	36	69728	97496	74884	1.22802	8.2	6.33
2.0	50	+200.0	36	45279	77250	50500	1.19520	7.6	6.33
2.5	50	+200.0	36	44717	74615	49616	1.19596	7.6	6.33
3.0	50	+200.0	37	39903	66639	44876	1.22854	8.2	6.23
3.6	50	+200.0	36	300195	393392	317276	1.22441	8.1	6.33
4.1	50	+200.0	37	252527	328254	268559	1.26855	8.8	6.23
4.6	50	+200.0	38	255219	337829	272784	1.27004	8.8	6.10
5.1	50	+200.0	38	219622	286060	234830	1.29686	9.2	6.10
5.6	50	+200.0	39	219708	286222	237774	1.37288	10.2	5.93
6.1	50	+200.0	39	231086	294450	250492	1.44149	11.1	5.98
6.6	50	+200.0	39	261047	329808	283969	1.50005	11.8	5.93
7.1	50	+200.0	40	188851	235587	206271	1.59423	12.7	5.86
7.6	50	+200.0	42	213723	258264	233811	1.82149	14.7	5.64
8.1	50	+200.0	44	81557	104325	92862	1.98624	15.9	5.44
8.6	50	+200.0	46	92900	114492	105638	2.43851	18.9	5.20
9.1	50	+0.0	35	88708	115607	103592	2.23871	25.1	4.94
9.7	50	+0.0	37	88364	109339	102074	2.88708	31.0	4.65
10.2	50	-200.0	31	107921	149297	133469	2.61408	39.8	4.07
10.7	50	-500.0	25	91543	130949	106232	1.59433	33.8	3.24
11.2	50	-500.0	26	94252	137392	108809	1.50931	38.1	2.92
11.7	50	-500.0	27	106415	152904	120718	1.44438	37.8	2.64
12.2	50	-500.0	27	96924	139129	109385	1.41894	36.7	2.64
12.7	50	-500.0	28	153799	193755	167865	1.54326	44.5	2.37
13.2	50	-500.0	29	208509	247161	226422	1.66375	60.0	2.13

DATE: SEPTEMBER 17,1983 PAGE NO. 1

AXIAL POSITION FROM IGV TRAILING EDGE: 48.8mm

RADIAL POSITION (mm)	SAMPLE TIME (nsec)	FREQUENCY SHIFT (KHz)	Pk2	G1	G2	G3	R	TURBULENCE INTENSITY (%)	AVERAGE VELOCITY (m/sec)
-13.5	50	-200.0	34	294087	343771	321236	2.20471	35.9	3.52
-13.2	50	-200.0	32	158763	206261	179851	1.79845	28.5	3.87
-12.7	50	-200.0	30	120733	165356	138338	1.65161	25.0	4.28
-12.2	50	-200.0	29	138275	179444	153416	1.58174	23.3	4.50
-11.7	50	-200.0	28	133691	179009	149863	1.55489	22.5	4.75
-11.2	50	+0.0	35	156882	212586	182285	1.83832	20.7	4.94
-10.7	50	+0.0	32	190188	250260	213937	1.65384	18.3	5.46
-10.2	50	+0.0	32	160884	215748	180599	1.56091	17.0	5.46
-9.7	50	+0.0	31	143413	199317	161069	1.46164	15.4	5.65
-9.1	50	+200.0	40	132503	181906	150447	1.57040	12.5	5.86
-8.6	50	+200.0	40	131580	183926	147945	1.45482	11.2	5.86
-8.1	50	+200.0	38	143331	202861	160219	1.39603	10.6	6.10
-7.6	50	+200.0	38	174302	247147	191605	1.31152	9.4	6.10
-7.1	50	+200.0	37	141384	203955	155837	1.30038	9.3	6.23
-6.6	50	+200.0	37	137984	200250	150894	1.26155	8.7	6.23
-6.1	50	+200.0	37	134638	195466	146634	1.24565	8.5	6.23
-5.6	50	+200.0	36	141454	204315	153217	1.23019	8.2	6.38
-5.1	50	+200.0	36	139642	197717	149235	1.19787	7.7	6.33
-4.6	50	+200.0	36	118550	171912	127431	1.19964	7.7	6.38
-4.1	50	+200.0	37	132134	184350	140974	1.20380	7.7	6.23
-3.6	50	+200.0	36	125779	182674	134698	1.18591	7.4	6.38
-3.0	50	+200.0	35	124999	179480	133800	1.19268	7.6	6.53
-2.5	50	+200.0	36	130904	186054	139621	1.18772	7.5	6.33
-2.0	50	+200.0	35	107138	154263	114954	1.19384	7.7	6.53
-1.5	50	+200.0	35	124182	174995	132504	1.19536	7.7	6.53
-1.0	50	+200.0	35	123838	173284	131010	1.16966	7.2	6.53
-.5	50	+200.0	36	115295	161952	122393	1.17960	7.3	6.38
0.0	50	+200.0	37	108655	154214	115385	1.17331	7.1	6.23

DATE: SEPTEMBER 17,1983 PAGE NO. 2

AXIAL POSITION FROM IGV TRAILING EDGE: 48.8mm

RADIAL POSITION (mm)	SAMPLE TIME (nsec)	FREQUENCY SHIFT (KHz)	Pk2	G1	G2	G3	R	TURBULENCE INTENSITY (%)	AVERAGE VELOCITY (m/sec)
.5	50	+200.0	37	115538	165107	123207	1.18303	7.3	6.23
1.0	50	+200.0	36	123634	171891	130591	1.16845	7.1	6.38
1.5	50	+200.0	37	159593	214010	168741	1.20208	7.7	6.23
2.0	50	+200.0	37	133929	189796	142453	1.18005	7.3	6.23
2.5	50	+200.0	36	121426	176005	129713	1.17903	7.3	6.33
3.0	50	+200.0	36	129454	187860	138893	1.19289	7.6	6.33
3.6	50	+200.0	36	109613	159951	118167	1.20472	7.8	6.38
4.1	50	+200.0	37	132046	190890	142981	1.22824	8.2	6.23
4.6	50	+200.0	36	117356	169812	127552	1.24126	8.4	6.38
5.1	50	+200.0	38	113792	163249	124500	1.27636	8.9	6.10
5.6	50	+200.0	38	114362	161316	126052	1.33147	9.7	6.10
6.1	50	+200.0	39	165616	205458	177609	1.43063	11.0	5.93
6.6	50	+200.0	38	37763	55603	44231	1.56873	12.7	6.10
7.1	50	+200.0	39	174138	201263	188089	2.05896	17.1	5.93
7.6	50	+200.0	39	41190	56986	48397	1.83909	15.2	5.93
8.1	50	+200.0	42	236685	271007	256016	2.28948	18.4	5.64
8.6	50	+200.0	42	72908	94163	85177	2.36541	19.0	5.64
9.1	50	+0.0	34	198937	250996	226537	2.12838	24.0	5.10
9.7	50	+0.0	36	287138	357833	330793	2.61495	28.7	4.79
10.2	50	-200.0	29	132135	184689	154065	1.71613	25.9	4.50
10.7	50	-200.0	30	150730	212198	175931	1.69489	25.8	4.28
11.2	50	-200.0	31	63394	95230	76296	1.68143	25.9	4.07
11.7	50	-200.0	31	50439	78151	60811	1.59813	24.3	4.07
12.2	50	-200.0	33	40072	64093	49655	1.66373	26.3	3.69
12.7	50	-200.0	33	47780	75879	58509	1.61769	25.4	3.69
13.2	50	-200.0	34	50303	74848	61487	1.83702	30.0	3.52
13.5	50	-200.0	38	110590	138894	126876	2.35516	40.4	2.91

DATE: SEPTEMBER 20, 1983

AXIAL POSITION FROM IGV TRAILING EDGE: 110.0mm

RADIAL POSITION (mm)	SAMPLE TIME (nsec)	FREQUENCY SHIFT (KHz)	Pk2	G1	G2	G3	R	TURBULENCE INTENSITY (%)	AVERAGE VELOCITY (m/sec)
-13.0	50	-200.0	30	55026	78027	62383	1.51887	22.4	4.28
-12.7	50	-200.0	29	48742	71725	56193	1.47968	21.2	4.50
-12.2	50	-200.0	28	45442	62027	50713	1.46588	20.6	4.75
-11.7	50	-200.0	27	90641	112059	97667	1.48819	20.8	5.01
-11.2	50	-200.0	27	49084	73158	54941	1.32155	17.0	5.01
-10.7	50	+0.0	33	49075	72937	56946	1.49222	15.9	5.27
-10.2	50	+0.0	33	120324	172902	135862	1.41950	14.7	5.27
-9.7	50	+0.0	32	98941	151023	113589	1.39130	14.2	5.46
-9.1	50	+0.0	31	161275	219151	177267	1.38182	14.0	5.55
-8.6	50	+200.0	42	125993	163561	143637	1.70789	13.7	5.64
-8.1	50	+200.0	41	116044	159194	131913	1.58171	12.5	5.75
-7.6	50	+200.0	40	112631	159897	129319	1.54576	12.2	5.80
-7.1	50	+200.0	41	219119	231523	238900	1.46407	11.2	5.75
-6.6	50	+200.0	39	200722	266248	220461	1.43109	11.3	5.98
-6.1	50	+200.0	39	185329	247633	204031	1.42892	10.9	5.98
-5.6	50	+200.0	39	203964	274630	222334	1.35127	9.9	5.98
-5.1	50	+200.0	38	189659	259525	206752	1.32389	9.6	6.10
-4.6	50	+200.0	37	188924	261559	206863	1.32796	9.7	6.23
-4.1	50	+200.0	38	190269	263190	207146	1.30114	9.3	6.10
-3.6	50	+200.0	38	227113	315146	245860	1.27056	8.8	6.10
-3.0	50	+200.0	37	188247	260878	204159	1.23055	9.0	6.23
-2.5	50	+200.0	37	191431	264146	206986	1.27215	8.9	6.23
-2.0	50	+200.0	37	189318	267262	206165	1.27574	8.9	6.23
-1.5	50	+200.0	37	181832	257908	197477	1.25388	8.7	6.23
-1.0	50	+200.0	38	174879	250044	190693	1.26645	8.7	6.10
-.5	50	+200.0	37	173570	247225	188940	1.26370	8.7	6.23
0.0	50	+200.0	37	171656	247414	188075	1.27669	9.0	6.23

DATE: SEPTEMBER 20,1983

AXIAL POSITION FROM IGV TRAILING EDGE: 110.0mm

RADIAL POSITION (mm)	SAMPLE TIME (nsec)	FREQUENCY SHIFT (KHz)	Pk2	G1	G2	G3	R	TURBULENCE INTENSITY (%)	AVERAGE VELOCITY (m/sec)
.5	50	+200.0	38	170273	244047	186251	1.27645	8.9	6.10
1.0	50	+200.0	37	186109	264726	203129	1.27633	8.9	6.23
1.5	50	+200.0	38	235011	310885	253016	1.31113	9.4	6.10
2.0	50	+200.0	39	178861	253695	196661	1.31210	9.4	5.98
2.5	50	+200.0	38	186430	263313	205930	1.33983	9.8	6.10
3.0	50	+200.0	40	174244	246644	193591	1.36467	10.0	5.86
3.6	50	+200.0	39	169437	238577	189733	1.41555	10.8	5.98
4.1	50	+200.0	40	185436	259457	208253	1.44561	11.1	5.86
4.6	50	+200.0	41	173218	242079	196126	1.49851	11.6	5.75
5.1	50	+200.0	41	179390	250186	204241	1.54086	12.1	5.75
5.6	50	+200.0	42	179616	247579	205513	1.61564	12.8	5.54
6.1	50	+200.0	42	718308	793516	752605	1.83832	14.9	5.64
7.1	50	+200.0	43	168181	196567	183364	2.14997	17.3	5.54
7.6	50	+200.0	45	43617	65351	53741	1.87199	14.9	5.35
8.1	50	+0.0	33	40735	69460	49373	1.43006	14.9	5.27
8.6	50	+0.0	34	83084	135695	93806	1.42620	14.8	5.10
9.1	50	+0.0	34	76669	123973	91273	1.44655	15.2	5.10
9.7	50	+0.0	34	151040	217198	171944	1.46192	15.4	5.10
10.2	50	+0.0	36	116262	177865	136538	1.49060	15.9	4.79
10.7	50	+0.0	36	118002	180528	139305	1.51678	16.3	4.79
11.2	50	+0.0	38	125330	137881	146538	1.51298	16.2	4.52
11.7	50	+0.0	37	132253	195969	155347	1.53809	17.4	4.55
12.2	50	-200.0	30	143511	220366	165473	1.40007	19.7	4.23
12.7	50	-200.0	31	92746	141779	111043	1.59529	24.3	4.07
13.2	50	-200.0	35	157472	200360	185374	2.86178	45.3	3.35

DATE: SEPTEMBER 21,1983 PAGE NO. 1

AXIAL POSITION FROM IGV TRAILING EDGE: 215.4mm

RADIAL POSITION (mm)	SAMPLE TIME (nsec)	FREQUENCY SHIFT (KHz)	Pk2	G1	G2	G3	R	TURBULENCE INTENSITY (%)	AVERAGE VELOCITY (m/sec)
-12.7	50	-200.0	30	718476	762962	741230	2.04708	31.7	4.28
-12.2	50	-200.0	29	220309	252918	231253	1.50511	21.8	4.50
-11.7	50	-200.0	28	194469	228380	203530	1.36465	18.3	4.75
-11.2	50	+0.0	38	268480	307560	284546	1.69812	18.9	4.52
-10.7	50	+0.0	35	107658	129663	115264	1.52822	16.5	4.94
-10.2	50	+0.0	36	170750	204432	181616	1.47627	15.7	4.79
-9.7	50	+0.0	36	173423	202506	184477	1.61315	17.7	4.79
-9.1	50	+0.0	35	818010	913980	848625	1.46844	15.5	4.94
-8.6	50	+0.0	35	819038	916316	848147	1.42701	14.8	4.94
-8.1	50	+0.0	34	1170503	1263319	1201985	1.51327	16.2	5.10
-7.6	50	+0.0	34	1201864	1300779	1232889	1.45699	15.3	5.10
-7.1	50	+0.0	33	1036022	1129870	1064776	1.44172	15.1	5.27
-6.6	50	+0.0	33	769514	863705	793870	1.34877	13.4	5.27
-6.1	50	+200.0	44	606165	675902	631067	1.55539	12.0	5.44
-5.6	50	+200.0	44	796423	897014	830304	1.50789	11.5	5.44
-5.1	50	+200.0	45	762903	862942	796304	1.50123	11.3	5.35
-4.6	50	+200.0	43	710311	808383	739841	1.43082	10.6	5.54
-4.1	50	+200.0	43	646758	737249	675110	1.45628	10.9	5.54
-3.6	50	+200.0	44	859605	973902	894222	1.43446	10.6	5.44
-3.0	50	+200.0	44	764314	869786	795576	1.42127	10.5	5.44
-2.5	50	+200.0	43	816618	927440	849924	1.42967	10.6	5.54
-2.0	50	+200.0	42	803705	911383	835822	1.42505	10.6	5.54
-1.5	50	+200.0	43	789746	901239	822861	1.42251	10.5	5.54
-1.0	50	+200.0	43	724748	826565	754346	1.40983	10.4	5.54
-.5	50	+200.0	42	848258	932174	884551	1.37177	10.0	5.54
0.0	50	+200.0	44	908595	1047938	949125	1.41017	10.3	5.44
.5	50	+200.0	43	866117	1006716	904712	1.37836	10.0	5.54
1.0	50	+200.0	44	853094	986865	891121	1.39718	10.2	5.44

DATE: SEPTEMBER 21,1983 PAGE NO. 2

AXIAL POSITION FROM IGV TRAILING EDGE: 215.4mm

RADIAL POSITION (mm)	SAMPLE TIME (nsec)	FREQUENCY SHIFT (KHz)	Pk2	G1	G2	G3	R	TURBULENCE INTENSITY (%)	AVERAGE VELOCITY (m/sec)
1.5	50	+200.0	44	854754	987293	893615	1.41484	10.4	5.44
2.0	50	+200.0	44	929535	1076425	973608	1.42866	10.5	5.44
2.5	50	+200.0	44	764464	887449	802375	1.44562	10.7	5.44
3.0	50	+200.0	44	855196	988724	896669	1.45053	10.8	5.44
3.6	50	+200.0	45	838651	967787	881268	1.49257	11.2	5.35
4.1	50	+200.0	46	924934	1060707	968563	1.47349	10.9	5.26
4.6	50	+200.0	45	916123	1050204	963008	1.53770	11.7	5.35
5.1	50	+200.0	47	922401	1050464	969279	1.57743	12.0	5.18
5.6	50	+200.0	46	759666	872325	801867	1.59896	12.3	5.26
6.1	50	+200.0	47	752684	871258	798459	1.62877	12.5	5.18
6.6	50	+200.0	47	760889	879437	807022	1.63705	12.5	5.18
7.1	50	+200.0	47	822182	951567	872712	1.64080	12.6	5.18
7.6	50	+0.0	35	746951	879520	779469	1.32503	13.0	4.94
8.1	50	+0.0	35	828524	975462	867527	1.36135	13.7	4.94
8.6	50	+0.0	36	756547	892791	793781	1.37607	13.9	4.79
9.1	50	+0.0	36	738255	867969	774437	1.38685	14.1	4.79
9.7	50	+0.0	37	824351	961387	862848	1.39068	14.2	4.65
10.2	50	+0.0	37	856983	1004732	902344	1.44303	15.1	4.65
10.7	50	+0.0	38	881984	1017608	924243	1.45262	15.3	4.52
11.2	50	+0.0	38	747397	872499	789775	1.51227	16.2	4.52
11.7	50	+0.0	39	695417	807527	735802	1.56304	17.0	4.39
12.2	50	+0.0	40	764416	888554	811054	1.60179	17.5	4.23
12.7	50	+0.0	40	694536	808109	741000	1.69164	18.8	4.26
13.2	50	-200.0	31	681792	801545	719560	1.46066	21.4	4.07
13.7	50	-200.0	32	770057	889988	816678	1.63593	25.4	3.67
14.2	50	-200.0	34	843777	940309	891569	1.98055	32.4	3.52
14.7	50	-500.0	26	359511	409768	382883	1.86933	49.6	2.92

DATE: SEPTEMBER 25,1983 PAGE NO. 1

AXIAL POSITION FROM IGV TRAILING EDGE: 240.0mm

RADIAL POSITION (mm)	SAMPLE TIME (nsec)	FREQUENCY SHIFT (KHz)	Pk2	G1	G2	G3	R	TURBULENCE INTENSITY (%)	AVERAGE VELOCITY (m/sec)
-16.8	50	-500.0	30	733261	784044	764928	2.65662	89.3	1.90
-15.7	50	-500.0	26	156083	190055	167020	1.47475	36.8	2.92
-15.2	50	-200.0	35	122343	153103	135939	1.79844	29.7	3.36
-14.7	50	-200.0	34	261401	318026	284159	1.67198	26.9	3.52
-14.2	50	-200.0	33	252430	310704	273123	1.55065	24.0	3.69
-13.7	50	-200.0	33	278583	346265	300788	1.48824	22.6	3.69
-13.2	50	-200.0	33	282228	342899	301265	1.45727	21.9	3.69
-12.7	50	-200.0	33	346753	396765	363208	1.49035	22.7	3.59
-12.2	50	-200.0	31	218155	266788	230792	1.35110	18.7	4.07
-11.7	50	-200.0	32	159041	203426	169542	1.30992	17.9	3.87
-11.2	50	-200.0	32	109911	143943	116627	1.24588	16.0	3.87
-10.7	50	+0.0	42	144024	184024	155891	1.42181	14.7	4.06
-10.2	50	+0.0	41	409795	472980	430071	1.47255	15.6	4.16
-9.7	50	+0.0	41	92191	120709	99493	1.34418	13.3	4.16
-9.1	50	+0.0	40	83021	109556	90303	1.37822	14.0	4.28
-8.6	50	+0.0	39	124333	164207	133968	1.31865	12.9	4.39
-8.1	50	+0.0	39	130938	172508	140843	1.31282	12.7	4.39
-7.6	50	+0.0	38	136553	179941	146671	1.30411	12.6	4.52
-7.1	50	+0.0	38	203114	266271	215525	1.24459	11.3	4.52
-6.6	50	+0.0	38	191839	250913	203523	1.24654	11.3	4.52
-6.1	50	+0.0	38	197958	259220	210810	1.26550	11.8	4.52
-5.5	50	+0.0	37	172951	225334	182711	1.22897	10.9	4.65
-5.1	50	+0.0	37	221644	292063	234464	1.22257	10.8	4.65
-4.6	50	+0.0	37	209949	279049	222533	1.22267	10.8	4.65
-4.1	50	+100.0	43	193322	254049	207516	1.30504	10.5	4.75

DATE: SEPTEMBER 25,1983 PAGE NO. 2

AXIAL POSITION FROM IGV TRAILING EDGE: 240.0mm

RADIAL POSITION (mm)	SAMPLE TIME (nsec)	FREQUENCY SHIFT (KHz)	Pk2	G1	G2	G3	R	TURBULENCE INTENSITY (%)	AVERAGE VELOCITY (m/sec)
-3.5	50	+100.0	42	193675	255042	207830	1.29982	10.4	4.85
-3.0	50	+100.0	44	262383	345819	280749	1.28225	10.1	4.65
-2.5	50	+100.0	44	218654	289099	233648	1.27039	9.8	4.65
-2.0	50	+100.0	44	239787	310095	255435	1.28628	10.1	4.65
-1.5	50	+100.0	44	217687	281089	231949	1.29023	10.2	4.65
-1.0	50	+100.0	43	290723	378764	310423	1.28827	10.2	4.75
-.5	50	+100.0	43	240672	313679	256883	1.28542	10.2	4.75
0.0	50	+100.0	43	209914	274886	224828	1.29795	10.4	4.75
.5	50	+100.0	44	193228	254558	207263	1.29677	10.3	4.65
1.0	50	+100.0	43	182604	231974	195064	1.33756	11.0	4.75
1.5	50	+100.0	44	269440	339952	287153	1.33547	10.9	4.65
2.0	50	+100.0	44	286062	363335	305382	1.33338	10.9	4.65
2.5	50	+100.0	45	286679	362246	306093	1.34585	11.1	4.56
3.0	50	+100.0	45	255268	323709	273290	1.35746	11.2	4.56
3.6	50	+100.0	44	271663	345239	291543	1.37024	11.5	4.65
4.1	50	+100.0	46	233855	297829	252075	1.39822	11.8	4.47
4.6	50	+100.0	46	388815	495639	420186	1.41576	12.1	4.47
5.1	50	+100.0	45	449804	564609	484958	1.44135	12.5	4.56
5.6	50	+100.0	47	348614	440988	375514	1.41086	11.9	4.30
6.1	50	+100.0	46	415635	523393	448735	1.44335	12.4	4.47
6.6	50	+100.0	47	388658	491246	422534	1.49302	13.1	4.30
7.1	50	+0.0	40	385931	494483	413521	1.34078	13.3	4.23
7.6	50	+0.0	40	343279	437766	369120	1.37644	13.9	4.28
8.1	50	+0.0	42	326406	417598	352045	1.39112	14.2	4.06
8.6	50	+0.0	41	315528	404731	341790	1.41724	14.7	4.16

DATE: SEPTEMBER 25,1983 PAGE NO. 3

AXIAL POSITION FROM IGV TRAILING EDGE: 240.0mm

RADIAL POSITION (mm)	SAMPLE TIME (nsec)	FREQUENCY SHIFT (KHz)	Pk2	G1	G2	G3	R	TURBULENCE INTENSITY (%)	AVERAGE VELOCITY (m/sec)
9.1	50	+0.0	42	309989	393014	335908	1.45386	15.3	4.06
9.7	50	+0.0	41	347747	443183	378188	1.46837	15.5	4.16
10.2	50	+0.0	42	311740	397121	340436	1.50623	16.1	4.06
10.7	50	+0.0	44	368796	469292	403321	1.52334	16.4	3.[illegible]
11.2	50	+0.0	45	435865	548937	477182	1.57581	17.2	3.77
11.7	50	-100.0	38	366421	470039	397594	1.43030	18.1	3.73
12.2	50	-100.0	39	366212	466203	400134	1.51342	19.8	3.60
12.7	50	-100.0	40	403284	505902	442197	1.61083	21.7	3.48
13.2	50	-100.0	41	393808	487673	431888	1.68262	23.1	3.37
13.7	50	-100.0	41	330030	407576	365771	1.85492	25.8	3.37
14.2	50	-200.0	37	362917	448023	400501	1.79087	30.5	3.07
14.7	50	-200.0	38	231208	290487	260113	1.95166	33.9	2.94
15.2	50	-200.0	40	297443	365980	335544	2.25184	40.1	2.69
15.7	50	-500.0	28	273648	351738	299013	1.48109	42.0	2.37
16.3	50	-500.0	29	292503	371450	317866	1.47334	44.6	2.13
16.8	50	-500.0	30	142840	188385	157427	1.47119	47.9	1.90
17.3	50	-500.0	31	141364	184442	154678	1.44731	50.6	1.70
17.8	50	-500.0	33	225400	288468	246159	1.49065	63.5	1.32
18.0	50	-500.0	34	277883	338761	301325	1.62616	79.6	1.15

DATE: SEPTEMBER 16,1983 PAGE NO. 1

AXIAL POSITION FROM IGV TRAILING EDGE: 262.4mm

RADIAL POSITION (mm)	SAMPLE TIME (nsec)	FREQUENCY SHIFT (KHz)	Pk2	G1	G2	G3	R	TURBULENCE INTENSITY (%)	AVERAGE VELOCITY (m/sec)
-18.8	50	-500.0	28	1333559	1386426	1359988	1.99963	60.2	2.37
-18.3	50	-500.0	28	592181	638503	610874	1.67656	49.6	2.37
-17.8	50	-500.0	27	176018	219994	187408	1.34955	33.6	2.64
-17.3	50	-500.0	26	85611	127462	94143	1.25606	27.2	2.92
-16.8	50	-200.0	35	89727	132050	106745	1.67253	27.3	3.36
-16.3	50	-200.0	34	746554	827380	781406	1.75807	28.5	3.52
-15.7	50	-200.0	34	544087	624781	575173	1.62662	26.0	3.52
-15.2	50	-200.0	34	469352	533967	493698	1.60457	25.5	3.52
-14.7	50	-200.0	32	274112	341040	295155	1.45863	21.6	3.67
-14.2	50	-200.0	33	273736	333313	290564	1.39365	20.4	3.69
-13.7	50	-200.0	32	437038	496200	455633	1.46018	21.7	3.87
-13.2	50	-200.0	31	316435	377710	332308	1.34959	18.7	4.07
-12.7	50	+0.0	40	577690	644519	605129	1.69659	18.9	4.28
-12.2	50	+0.0	41	561660	623166	585370	1.62734	17.9	4.16
-11.7	50	+0.0	40	496472	563100	520943	1.58050	17.3	4.28
-11.2	50	+0.0	39	396438	461849	417130	1.46436	15.5	4.39
-10.7	50	+0.0	39	172551	228206	137530	1.36993	13.8	4.39
-10.2	50	+0.0	39	162906	214370	176796	1.36965	13.8	4.39
-9.7	50	+0.0	38	104851	144072	114992	1.34875	13.4	4.52
-9.1	50	+0.0	38	92859	129465	100997	1.28586	12.2	4.52
-8.6	50	+0.0	37	106997	150107	117199	1.31004	12.7	4.65
-8.1	50	+0.0	37	94768	133381	103459	1.29046	12.3	4.65
-7.6	50	+0.0	37	147343	198867	158661	1.28148	12.1	4.65
-7.1	50	+0.0	36	109764	164750	121106	1.25988	11.6	4.79
-6.6	50	+0.0	36	94067	147429	103935	1.22688	10.9	4.79
-6.1	50	+100.0	42	76379	116818	36468	1.31596	10.7	4.85

DATE: SEPTEMBER 16,1983

AXIAL POSITION FROM IGV TRAILING EDGE: 262.4mm

RADIAL POSITION (mm)	SAMPLE TIME (nsec)	FREQUENCY SHIFT (KHz)	Pk2	G1	G2	G3	R	TURBULENCE INTENSITY (%)	AVERAGE VELOCITY (m/sec)
-5.6	50	+100.0	42	69501	107989	78399	1.30071	10.5	4.85
-5.1	50	+100.0	42	68571	109385	77768	1.29090	10.3	4.85
-4.6	50	+100.0	42	75044	119550	84777	1.27990	10.1	4.85
-4.1	50	+100.0	41	72230	115190	81232	1.26510	9.9	4.95
-3.6	50	+100.0	41	69457	114105	79077	1.27464	10.0	4.95
-3.0	50	+100.0	42	69136	112447	78892	1.29072	10.3	4.85
-2.5	50	+100.0	41	68005	111707	77500	1.27757	10.1	4.95
-2.0	50	+100.0	42	116273	178197	130086	1.28712	10.2	4.85
-1.5	50	+100.0	42	110776	170038	123842	1.28284	10.1	4.85
-1.0	50	+100.0	42	118908	181499	132724	1.28326	10.2	4.85
-.5	50	+100.0	42	111939	174370	125966	1.28981	10.3	4.85
0.0	50	+100.0	43	106749	166169	119786	1.28109	10.1	4.75
.5	50	+100.0	43	100222	154844	113742	1.32895	10.9	4.75
1.0	50	+100.0	44	96528	149187	109855	1.33917	11.0	4.65
1.5	50	+100.0	44	87882	136267	100651	1.35851	11.3	4.65
2.0	50	+100.0	43	84663	130170	97082	1.37534	11.6	4.75
2.5	50	+100.0	44	112726	172481	129100	1.37744	11.6	4.65
3.0	50	+100.0	45	125270	187856	143568	1.41317	12.1	4.56
3.6	50	+100.0	45	104581	157740	120881	1.44221	12.5	4.56
4.1	50	+100.0	46	94595	142149	110491	1.50214	13.2	4.47
4.6	50	+100.0	47	85396	128241	99452	1.48823	13.0	4.39
5.1	50	+100.0	47	111330	166218	130460	1.53496	13.6	4.39
5.6	50	+100.0	47	102699	152669	120670	1.56162	13.9	4.39
6.1	50	+100.0	47	96412	142823	113823	1.60067	14.4	4.39
6.6	50	+0.0	41	85165	134612	99132	1.39367	14.3	4.16
7.1	50	+0.0	42	104221	161941	121850	1.43972	15.1	4.06

DATE: SEPTEMBER 16,1983 PAGE NO. 3

AXIAL POSITION FROM IGV TRAILING EDGE: 262.4mm

RADIAL POSITION (mm)	SAMPLE TIME (nsec)	FREQUENCY SHIFT (KHz)	Pk2	G1	G2	G3	R	TURBULENCE INTENSITY (%)	AVERAGE VELOCITY (m/sec)
7.6	50	+0.0	41	85184	131808	100075	1.46924	15.5	4.16
7.6	50	+0.0	42	83495	129536	97651	1.44396	15.1	4.06
8.1	50	+0.0	41	79622	124606	93302	1.43702	15.0	4.16
8.6	50	+0.0	43	79457	122268	93656	1.49630	16.0	3.96
9.1	50	-100.0	36	81819	130618	95446	1.38743	16.9	4.00
9.7	50	-100.0	37	80905	125530	94070	1.41847	17.7	3.86
10.2	50	-100.0	37	79375	123970	92225	1.40475	17.4	3.86
10.7	50	-100.0	39	84554	131605	100163	1.49644	19.5	3.60
11.2	50	-100.0	39	81427	123700	96913	1.57809	21.0	3.60
11.7	50	-100.0	40	77166	114448	91755	1.64289	22.3	3.43
12.2	50	-100.0	40	77515	114132	93400	1.76623	24.3	3.43
12.7	50	-100.0	41	77481	111889	93179	1.83908	25.6	3.37
13.2	50	-100.0	41	84730	122230	101656	1.82270	25.3	3.37
13.7	50	-200.0	37	63100	94082	76617	1.77395	30.1	3.07
14.2	50	-200.0	38	80925	117586	97083	1.78806	30.9	2.94
14.7	50	-200.0	39	86036	123696	104619	1.97417	34.8	2.51
15.2	50	-200.0	39	56949	83235	69634	1.93259	34.1	2.81
15.7	50	-200.0	42	45919	66792	56978	2.12675	39.3	2.47
16.3	50	-500.0	29	49695	74471	56294	1.36308	39.1	2.13
16.8	50	-500.0	30	54944	83664	63125	1.39833	44.1	1.90
17.3	50	-500.0	30	22366	33701	25560	1.39228	43.8	1.90
17.8	50	-500.0	30	12998	19188	14442	1.30424	38.7	1.90
18.3	50	-500.0	30	13390	19887	15243	1.39897	44.2	1.90
18.8	50	-500.0	31	15811	23558	17922	1.37442	46.4	1.70
19.3	50	-500.0	32	5418	7880	6225	1.48782	57.6	1.50
19.8	50	-500.0	34	6833	9697	7757	1.47632	69.6	1.15

Appendix E:

Velocity Resolution of Photon-correlating LDA Measurements

The autocorrelation function determined by a digital correlator, such as the Malvern Type K7023, is defined only at discrete values of τ, the correlator time delay. These values of τ are represented by the correlator channels. Since the velocity measurements are a function of the peak channel number, Pk2, and since Pk2 has discrete values, the velocity will also have discrete values. In comparing a continuous correlation function with its digital representation, it is evident that a peak of the continuous function may occur anywhere within a $\pm\frac{1}{2}$ channel interval of the peak of its digital form. While the value of τ at which a peak occurs can be estimated from a digital correlation function (i.e. estimating fractional channels), the estimated peak will vary among experimenters so that the $\pm\frac{1}{2}$ channel interval is still a useful means of determining the range of velocities represented by a photon-correlating LDA measurement.

The absolute velocity can be calculated using Eq (35).

$$u = \frac{d_f}{(Pk2-3)t_s} + \Delta F\ d_f \tag{35}$$

The rate of change in velocity with respect to a change in the peak channel number, Pk2, is given by Eq (36).

$$\frac{du}{d(Pk2)} = \frac{-d_f}{(Pk2-3)^2 t_s} \tag{36}$$

Two more useful forms of Eq (36) are Eqs (37) and (38).

$$\frac{du}{d(Pk2)} = \frac{-(u^*)^2 \; t_s}{d_f} \tag{37}$$

$$\frac{du}{d(Pk2)} = \frac{-(u - \Delta F d_f)^2 \; t_s}{d_f} \tag{38}$$

The absolute value of du/d(Pk2) is the velocity resolution of the LDA system in measuring a given flow. Bear in mind that u, ΔF, t_s and d_f cannot assume any combination of values because the correlator is limited by the number of channels used to represent the correlation function. The value of Pk2 is limited to the range of 5 to 99 by the Malvern K7023; however, in practical applications, it should be limited to the range of 10 to 95. Thus, combinations of the variables in Eqs (37) and (38) may be checked for reasonableness by using Eq (35) and the above limitation on Pk2.

The value of du/d(Pk2) is also a measure of the accuracy of the digital representation of the correlation function. Since an actual peak of the function occurs within a $\pm\frac{1}{2}$ channel interval of the digital representation's peak, the accuracy of the measurement will be $\pm\frac{1}{2}|du/d(Pk2)|$.

VITA

Jeffrey M. Dierksen was born on September 13, 1955 in Alameda, California. He graduated from Proviso West High School in Hillside, Illinois in 1973 and continued his education at the United States Air Force Academy in Colorado Springs, Colorado. Upon graduation in 1977, he received a Bachelor of Science degree in aeronautical engineering and a commission as a Second Lieutenant. His first assignment in the Air Force was as a Minuteman ICBM Missile Launch Officer at Francis E. Warren AFB in Cheyenne, Wyoming. He also served there as an Emergency War Order Instructor. He entered the Air Force Institute of Technology, School of Engineering in June of 1982.

Permanent Address: 1700 Pinto Lane
Cheyenne, Wyoming 82007

UNCLASSIFIED

SECURITY CLASSIFICATION OF THIS PAGE

REPORT DOCUMENTATION PAGE

1a. REPORT SECURITY CLASSIFICATION: Unclassified	1b. RESTRICTIVE MARKINGS
2a. SECURITY CLASSIFICATION AUTHORITY	3. DISTRIBUTION/AVAILABILITY OF REPORT: Approved for public release; distribution unlimited.
2b. DECLASSIFICATION/DOWNGRADING SCHEDULE	
4. PERFORMING ORGANIZATION REPORT NUMBER(S): AFIT/GAE/AA/83D-6	5. MONITORING ORGANIZATION REPORT NUMBER(S)
6a. NAME OF PERFORMING ORGANIZATION: School of Engineering, Air Force Institute of Technology — 6b. OFFICE SYMBOL (If applicable): AFIT/EN	7a. NAME OF MONITORING ORGANIZATION
6c. ADDRESS (City, State and ZIP Code): Wright-Patterson AFB, Ohio 45433	7b. ADDRESS (City, State and ZIP Code)
8a. NAME OF FUNDING/SPONSORING ORGANIZATION: Air Force Aero-Propulsion Laboratory — 8b. OFFICE SYMBOL (If applicable): AFWAL/POTC	9. PROCUREMENT INSTRUMENT IDENTIFICATION NUMBER
8c. ADDRESS (City, State and ZIP Code): Wright-Patterson AFB, Ohio 45433	10. SOURCE OF FUNDING NOS.: PROGRAM ELEMENT NO. / PROJECT NO. / TASK NO. / WORK UNIT NO.
11. TITLE (Include Security Classification): See Box 19	

12. PERSONAL AUTHOR(S): Jeffrey M. Dierksen, Capt, USAF

13a. TYPE OF REPORT	13b. TIME COVERED	14. DATE OF REPORT (Yr., Mo., Day)	15. PAGE COUNT
MS Thesis	FROM ____ TO ____	1983 December	131

16. SUPPLEMENTARY NOTATION

Approved for public release: IAW AFR 190-17.
LYNN E. WOLAVER
Dean for Research and Professional Development
Air Force Institute of Technology (AIC)
Wright-Patterson AFB OH 45433
[illegible]

17. COSATI CODES		
FIELD	GROUP	SUB. GR.
21	1	

18. SUBJECT TERMS (Continue on reverse if necessary and identify by block number): Diffusers, Lasers, Doppler Systems, Velocimeters

19. ABSTRACT (Continue on reverse if necessary and identify by block number)

TITLE: A STUDY OF ANNULAR DIFFUSER FLOW USING A PHOTON-CORRELATING LASER DOPPLER ANEMOMETER

THESIS CHAIRMAN: Dr. William C. Elrod

20. DISTRIBUTION/AVAILABILITY OF ABSTRACT: UNCLASSIFIED/UNLIMITED ☒ SAME AS RPT. ☐ DTIC USERS ☐	21. ABSTRACT SECURITY CLASSIFICATION: Unclassified

22a. NAME OF RESPONSIBLE INDIVIDUAL	22b. TELEPHONE NUMBER (Include Area Code)	22c. OFFICE SYMBOL
Dr. William C. Elrod	513-255-3517	AFIT/ENY

DD FORM 1473, 83 APR — EDITION OF 1 JAN 73 IS OBSOLETE.

UNCLASSIFIED

SECURITY CLASSIFICATION OF THIS PAGE

An experimental investigation of air flow in an annular inlet and diffuser was conducted using a photon-correlating Laser Doppler Anemometer. The inlet has an inside wall radius of 22.9 centimeters (9.0 in) and a cross-sectional area of 0.0426 sq meters (0.4583 sq ft). The diffuser walls have a divergence half-angle of seven degrees. Flow rates in the vicinity of 0.25 kg/sec (0.55 lbm/sec) were studied. The Reynolds number in the annular inlet was 18,300. The flow in the annulus was turbulent and the boundary layer growth was approximately 20% less than that predicted using flat plate boundary layer assumptions, The laser anemometer measurements are compared to hot film anemometer measurements. Good comparison was obtained except in the annular inlet. The difference is probably due to the differing boundary layer growth rates between the laser and hot film anemometer tests since they were conducted with different mass flow rates. The photon-correlating Laser Doppler Anemometer is evaluated in this application. The flexibility of a laser anemometer system in measuring three-dimensional, internal flows is determined by two factors: the system's frequency shifting capability and the geometry of its optics. Reflected background light is inherent in measuring internal flows. Without a means of reducing the signal caused by this light, long measurement times are necessary for each data point.

END

FILMED

2-84

DTIC